

# Flotation of Extreme Particle Sizes

Jack Leland

Thesis submitted to the faculty of the  
Virginia Polytechnic Institute and State University  
in partial fulfillment of the requirements for the degree of

Master of Science

In

Mechanical Engineering

Roe-Hoan Yoon, Chair

Mohit Gupta

Rui Qiao

February 16, 2026

Blacksburg, Virginia

Keywords: Flotation, Coarse Particle Flotation, Ultrafine Particles, Dewatering, Coal Waste, Chalcopyrite

# Flotation of Extreme Particle Sizes

Jack Leland

## Academic Abstract

Flotation is effective over a narrow particle size range. As particle sizes increase above  $\sim 150 \mu\text{m}$ , body detachment forces overcome surface attachment forces, while, at the same time, mineral liberation decreases, reducing attachment force increasing the detachment probability. As particle sizes decrease below  $\sim 20 \mu\text{m}$ , the collision probabilities between bubbles and particles decrease because fine particles follow streamlines around bubbles due to their low inertia. In this work, Jig Flotation and Two Liquid Flotation (TLF) are developed to extend the maximum and minimum particle size of flotation, respectively.

The Jig Flotation process reduces detachment probabilities using an intermittent fluidized bed instead of a mechanically agitated flotation cell for bubble-particle collision. The pulsion and suction cycles creating the intermittent fluidization allow for the formation of a froth phase, allowing Jig Flotation to be selective for both fine and coarse particles. The jiggling mechanism allows particles to be separated by density independent of particle size. This mechanism is enabled by the attachment of bubbles to selectively hydrophobized minerals, reducing their apparent density and enhancing their density difference with gangue minerals. In the present work, several Jig Flotation cells have been designed and tested, and encouraging results achieved on chalcopyrite ore.

The TLF process uses recyclable oils instead of air bubbles to recover ultrafine coal particles. Oil, having higher contact angles than air bubbles, enhances the recovery of ultrafine particles. The TLF process has produced coal with below 5% ash and below 2% moisture with recoveries greater than 80% from fine coal wastes.

# Flotation of Extreme Particle Sizes

Jack Leland

## General Audience Abstract

Flotation is effective for only some particle sizes. As particle sizes increase above  $\sim 150\ \mu\text{m}$ , particles are more likely to detach from bubbles due to their lower area of exposed minerals. As particle sizes decrease below  $\sim 20\ \mu\text{m}$ , particles tend to flow around bubbles due to their low mass, making them more difficult to recover. In this work, Jig Flotation and Two Liquid Flotation (TLF) are developed to overcome the challenges for small and large particles, respectively.

The Jig Flotation process reduces detachment probabilities using an alternately upward and downward flow of fluid instead of mixing as used in traditional flotation cells for bubble-particle collision. The alternating upward and downward flow allows froth to collect at the top of the cell, keeping unwanted fine particles from being recovered. The jiggling mechanism allows particles to be separated by density independent of particle size. This mechanism is enabled by the attachment of bubbles to selectively the desired particles, reducing their apparent density and enhancing their density difference with undesired minerals. In the present work, several Jig Flotation cells have been designed and tested, and encouraging results achieved on copper ore.

The TLF process uses recyclable oils instead of air bubbles to recover small coal particles. Oil attracts and attaches to target particles more strongly than air bubbles, enhancing the recovery of small particles. The TLF process has produced coal with below 5% impurity and below 2% moisture with recoveries greater than 80% from fine coal wastes.

## **Acknowledgments**

Mohit Gupta and Ashwin Srinivasan performed much of this work with me. The work presented in this thesis, specifically Chapters 3 and 4, are as much theirs as mine. Additionally, Roe-Hoan Yoon's guidance was vital to the success of this work. I also want to thank James Grubb and Rachel Layman as they made the research presented in this work possible. Finally, this work would not have been possible without the kindness and support of my friends and colleagues.

## Table Of Contents

Chapter 1:Introduction and Theory.....	1
1.1 Introduction.....	1
1.2 Theory.....	2
1.2.1 Flotation Theory.....	2
1.2.2 Jigging Theory.....	10
1.3 Conclusion.....	12
References:.....	14
Chapter 2:Coarse Particle Flotation Technologies.....	23
2.1 HydroFloat™.....	23
2.2 NovaCell™.....	25
2.3 Reflux™ Flotation Cell.....	26
2.4 CoarseAIR™.....	28
2.5 Froth Feeding.....	29
2.6 Hybrid Jig.....	30
2.7 Jig Flotation.....	31
2.8 Conclusion.....	31
References:.....	33
Chapter 3:Jig Flotation Scale Up.....	39
3.1 Introduction.....	39
3.2 Modelling Jig Flotation.....	41
3.3 Test Work.....	44
3.3.1 Two Inch Jig Flotation Cell.....	45
3.3.2 Continuous 8x2 Inch Jig Flotation Cell.....	46

3.3.3 Pilot Scale Jig.....	50
3.3.4 Modified Conventional Jig.....	53
3.4 Conclusion .....	54
References:.....	55
Chapter 4:Continuous Two Liquid Flotation Process Demonstration .....	57
4.1 Introduction.....	57
4.2 Theory .....	58
4.3 Experimental .....	60
4.3.1 UCC Thickener underflow.....	60
4.3.2 Itmann TUF Sample.....	62
4.3.3 UCC Wellmore #8.....	63
4.4 Conclusion .....	65
References:.....	66
Chapter 5:Conclusion.....	68
5.1 Introduction.....	68
5.2 Future Work .....	69
5.2.1 Jig Flotation .....	70
5.2.2 Two Liquid Flotation .....	71
5.3 Final thoughts.....	71
References:.....	73

## List of Figures

Figure 1.1: Elephant curve showing the effect of particle size on recovery of sulphide minerals [10]. .....	3
Figure 1.2: Particle following streamlines around a bubble the under hydrodynamic model of bubble particle attachment [16]. .....	5
Figure 1.3: Detachment forces shown as a function of particle size.....	7
Figure 1.4: Pulsion cycle in a Jig. ....	10
Figure 1.5: Movement of three particles A, A', and B during initial settling.....	11
Figure 1.6: Mechanisms governing separation in a jig [37].....	12
Figure 2.1: Schematic of HydroFloat™ [1]. .....	23
Figure 2.2: Schematic of NovaCell™ [10]. .....	25
Figure 2.3: Schematic of Reflux™ Flotation Cell [14].....	27
Figure 2.4: Schematic of CoarsAir flotation cell [21].....	28
Figure 2.5: Schematic of Metso's Froth Feeding CPF [23]. .....	29
Figure 2.6: Schematic of a batch Hybrid Jig [25]. .....	30
Figure 2.7: Schematic of a batch Jig Flotation cell [27]. .....	31
Figure 3.1: Movement of a bubble particle aggregate (blue) and the pulp froth interface (red) in a Jig Flotation cell showing the aggregate moving upward relative the pulp froth interface.....	40
Figure 3.2: Force balance on a particle in the presence of upward fluidization. ....	41
Figure 3.3: Analytical (blue) and numerical (red) simulation of the movement of a bubble particle aggregate in a Jig Flotation cell. ....	44
Figure 3.4: Schematic of 2inch batch Jig Flotation cell.....	45
Figure 3.5 Jig Flotation test results based on 210-425 μm copper-quartz composite particles from a copper flotation plant operating in Australia. ....	45
Figure 3.6:a) showing the schematic of a 8x2" continuous Jig Flotation Cell. b) showing a photo of a 8x2" Jig Flotation cell in operation. c) showing the process flow diagram for a continuous Jig Flotation cell. .	47

Figure 3.7: Grade vs. recovery for several continuous Jig Flotation tests on by-zero porphyry copper sample. ....	47
Figure 3.8: a) Recovery by particle size for monosize samples for DenverCell flotation without super collector (red) with super collector (blue), and with super collector and Jig Flotation (green). b) Recovery by particle size with unclassified feed with DenverCell and KAX (red), DenverCell and super collector (blue), and Jig Flotation and super collector (green). ....	48
Figure 3.9: a) Copper recovery with Denver cell and single Jig Flotation tests conducted at different grind sizes represented by d80. b) Grade vs. recovery obtained with two stage Jig Flotation and DenverCell at a several grind sizes represented by d80.....	49
Figure 3.10: a) Modified Jig Morganizer for pilot scale Jig Flotation tests. b) Process flow of acontinuous pilot scale Jig Flotation tests. ....	50
Figure 3.11: Upgrade vs. recovery for several preliminary continuous pilot scale Jig Flotation tests with feed ground to various d80s.....	51
Figure 3.12: Copper recovery, particle yield, water recovery, and upgrade ratio a) with varying stroke, b) with varying diffuser air flow rate, and c) with varying frequencies. Note that the secondary vertical axis b) has a different scale than a) and c).....	52
Figure 3.13: Conventional jig modified for Jig Flotation. ....	53
Figure 4.1: Continuous Two Liquid Flotation process shown schematically.....	58
Figure 4.2: Flow sheet of continuous Two-Liquid Flotation process.....	59
Figure 4.3: Two-Liquid Flotation Process Demonstration Unit.....	60
Figure 4.4 Phase separator upgrade. ....	61
Figure 4.5: Extended Jig Morganizer with visible phase separation.....	63
Figure 4.6: Combustible Recovery vs. Feed % solids at two different feed to solvent ratios. 1:1 shown in blue and 2:1 shown in red. ....	64

## List of Tables

Table 3.1: Recovery and upgrade ratio at different particle size ranges using Jig Flotation.....	48
Table 3.2: Comparison of size-by-size grade and recovery obtained with Jig Flotation cell and DenverCell both using super collector. ....	49
Table 4.1: UCC Bailey TUF results obtained with and without phase separator. ....	61
Table 4.2: Results obtained with TLF pilot plant with Itmann TUF feed - 250 $\mu$ m. ....	62
Table 4.3: Size-by-size coal ash and recovery obtained on Itmann TUF. ....	63
Table 4.4: Increased throughput obtained on Wellmore #8 sample. ....	64

# Chapter 1: Introduction and Theory

## 1.1 Introduction

Flotation, patented by Sulman and Kirkpatrick-Picard in 1905 [1], is used to produce practically all metals humans use today and is regarded as the best available method of separating mineral fines. Flotation is effective over a relatively narrow particle size range, of 20-150  $\mu\text{m}$  [2]. Outside of this range, coarse particles ( $+150 \mu\text{m}$ ) are lost due to detachment and low liberation, and ultrafine particles ( $-20 \mu\text{m}$ ) are lost due to low collision probability. According to Elshkaki et al., 42% of the energy required for producing primary copper is used in processing [3], and according to O'Connor, up to 70% of the total mineral processing cost has been associated with comminution to achieve the optimum particle size range for flotation [4]. As ore grade decreases, more energy is spent on comminution in part because lower-grade ores tend to be fine-grained, requiring finer grinding to achieve the necessary liberation [5], and for low-grade ores, the bulk of the energy put into comminution is consumed grinding gangue minerals [6]. This increasing cost can be mitigated by increasing the grind size and reducing the volume being ground using preconcentration.

Below the optimum particle size range, ultrafine particles are lost and report to the tails in large quantities. Waste streams containing these fine particles are difficult to dewater as they remain suspended and form small capillaries requiring higher pressure for filtration. These waste streams are disposed of in impoundments, causing serious environmental issues and the potential for large disasters [7]. Along with the hazards these tailings pose, they are a potential source of high-grade materials. In the case of coal, about 4 billion tons of coal fines have been discarded into numerous impoundments in the U.S., mostly in the Central Appalachian coalfields [7]. In the case of thickener underflows, which make up the bulk of these tailings, the coal content is as high as 50%. A 2025 survey [8] of mining byproducts not currently being recovered found that critical minerals found in tailings could account for annual US imports and would be a major portion of global production of critical minerals if there were a way to recover them [8]. In both cases, these particles are already well liberated; therefore, a costly comminution circuit is not necessary for their recovery.

With the ongoing global energy transition, the demand for various materials, including copper, is increasing sharply at a time as declining ore grades [9]. At the same time, the cost of producing copper is on the rise due to the decline in the ore grades. New technologies to decrease the cost of processing and recovering particles typically lost to tailings are needed. These technologies must address the particle size limitations of flotation. In this work, the development of two technologies (Jig Flotation and Two Liquid Flotation) will be discussed for the concentration of extreme particle sizes to address these needs. First, the relevant theory will be discussed for Flotation and Jigging, as they are relevant to the discussions in this work. Emphasis will be placed on the limitations of flotation at extreme particle sizes and the fundamental reasons for these limitations. In the discussion of the theory of jigging, emphasis will be placed on its advantages for coarse particle recovery. In Chapter 2, a literature review of existing coarse particle flotation technologies will be presented to provide a reference for the new coarse particle flotation technology, Jig Flotation, introduced in Chapter 3. Chapter 3 will cover the theory governing Jig flotation and its scale-up. In Chapter 4, the development of a process flow sheet for an ultrafine coal recovery technology, i.e., TLF, will be presented. Finally, in Chapter 5, a summary of the results and implications of this work is presented, along with recommendations for future research.

## **1.2 Theory**

### **1.2.1 Flotation Theory**

In traditional flotation, the collection of particles in the pulp phase occurs in three subprocesses. First, collision occurs between a bubble and a particle. During collision, attachment occurs, producing a bubble particle aggregate. Once the bubble-particle aggregate is formed, it must remain stable long enough for buoyancy to carry the aggregate to the froth phase. Each of these steps has a probability of success assuming the previous step has occurred. These probabilities can be used to calculate the probability of a particle reporting to the froth phase. The equation of particle collection probability is given by

$$P_{col} = P_c P_a (1 - P_d) \tag{1.1}$$

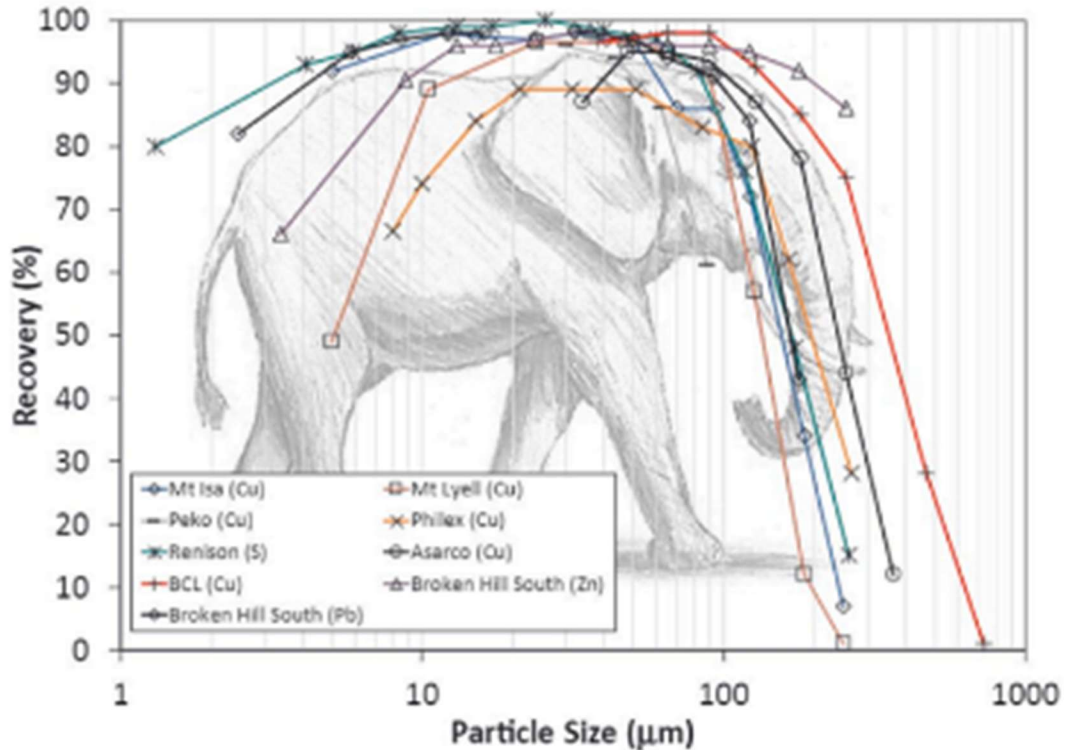


Figure 1.1: Elephant curve showing the effect of particle size on recovery of sulphide minerals [10].

where  $P_c$  is the probability of bubble particle collision,  $P_a$  is the probability of attachment during collision, and  $P_d$  is the probability of detachment [11]. Once in the froth phase, detachment must still be avoided. The probability of detachment in the froth phase can be considered part of the probability of detachment in Equation 1.1, and Equation 1.1 used to calculate the probability of particle recovery in both the pulp and froth phases. However, the mechanisms of detachment and subsequent reattachment in the froth phase are very different than those in the pulp [12].

These subprocesses are highly dependent on particle size. Figure 1.1 shows the oft-referenced ‘elephant curve’ showing how recovery varies with particle size for various sulphide minerals [10]. Flotation recovery peaks between 10 and 100 µm, dropping off sharply at the ‘tail’ and ‘trunk’ of the elephant [10]. These will be referred to as ultrafine and coarse particles, respectively. As will be explained in the next sections, the drop in recovery for ultrafine particles is due to low collision probability, while the drop in recovery for coarse particles is due to high detachment probability. The basics of each of these subprocesses will be discussed individually in the following sections with emphasis on how they are affected by particle size.

#### Collision:

As a bubble moves through the pulp, the fluid will follow streamlines around the bubble. Fine particles with lower inertia will tend to follow these streamlines around the bubble and therefore must be closer to the center line of the bubble in order to make contact with the bubble [13]. Particles can be diverted from these streamlines by inertial and surface forces, allowing them to be further from the centreline of the bubble and still make contact [14], [15], [16]. This distance to the centreline creates an area that is swept out as a bubble moves through the pulp. The bubble collides with particles in the swept-out volume, and therefore the density of particles and bubbles in the pulp influences the frequency of collisions [13], [14]. Additionally, increasing the relative velocity between the bubbles and particles increases the rate of collisions due to a higher volume swept over time, and the higher relative momentum of particles increasing their ability to divert from streamlines [13]. Typically, in flotation, these higher velocities are generated by increasing the agitation and therefore the turbulence in the cell [17].

The increase in collision probability with particle size has been observed in several studies [15], [17], [18]. Darabi et al. [17] found that collision frequencies were 10-12 times higher in turbulent zones as compared to the quiescent zones of a mechanically agitated flotation cell, and that other contacting mechanisms were negligible for fine particles; however, gravitational, inertial, and interceptional mechanisms were effective for coarse particles. Reis et al. [18] observed an increase in flotation rate with decreasing bubble size in part due to the increased number density of bubbles for the same air flow rate, therefore increasing the frequency of collision.

#### Attachment:

Under the Dobby Finch model [19], attachment occurs when the time for the thin liquid film to thin between the bubble and particle (induction time) is shorter than the time the particle slides across the particle's surface (sliding time). Increasing the sliding time or decreasing the induction time both increase the probability of attachment. Yoon and Luttrell developed a hydrodynamic model of bubble particle attachment in which bubble particle attachment occurs when the particle passes within the critical thickness at which the thin film ruptures, as shown in Figure 1.2. Under both of these models, attachment decreases

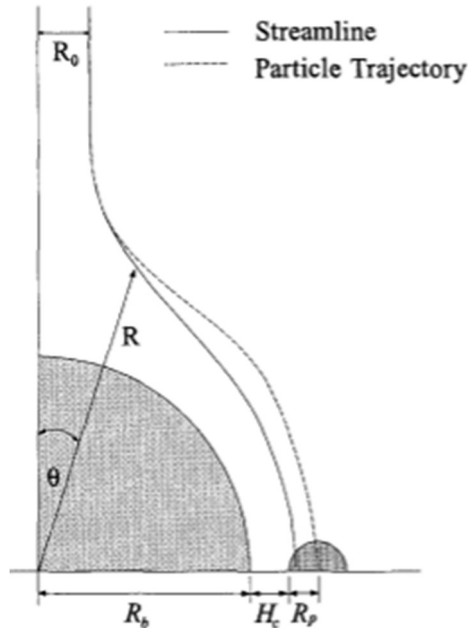


Figure 1.2: Particle following streamlines around a bubble under the hydrodynamic model of bubble particle attachment [16]. with increasing particle and bubble size and increasing hydrophobicity [19]. Dai et al. [20] found good agreement with these predictions experimentally with quartz of varying size and hydrophobicity. It was found that attachment efficiency decreased with increasing particle size, decreased with increasing bubble size, and increased with contact angle.

Bubble size impacts attachment in several ways. There is less distance for particles to slide on smaller bubbles, resulting in lower sliding times and therefore a lower probability of attachment. On the other hand, larger bubbles will have a thicker film, causing increased induction times [16]. Fine bubbles rise more slowly through the pulp, giving rise to smaller relative velocities and longer sliding times [21]. Overall, several studies have shown an inverse relationship between bubble size and bubble particle attachment efficiency [20], [22], [23].

Mao and Yoon [24] developed a model for predicting flotation rate constant using extended DLVO theory, including hydrophobic force as the driving force of attachment for flotation, showing that induction time would decrease with hydrophobicity. Under the model developed by Yoon and Luttrell [16], increased hydrophobicity decreases the critical thickness for film rupture, increasing attachment efficiency. Similarly, under the Dobby Finch model, attachment efficiency increases with increased contact angle due to a decrease in the induction time [20].

Detachment:

Three types of detachment have been identified. Detachment due to body forces, detachment due to deceleration at the pulp froth interface, and detachment due to bubble coalescence. All of these detachment mechanisms are important for the flotation of coarse particles due to their low attachment due to low liberation and higher body forces due to higher volume.

*Body forces:*

The sum of the forces acting on a particle attached to a bubble during flotation is given as

$$\sum F_{particle} = F_{g,particle} + F_{b,particle} + F_{d,particle} + F_c + F_\omega \quad 1.2$$

where  $F_g$  is the gravity force,  $F_b$  is the buoyancy force,  $F_d$  is the drag force,  $F_c$  is the centrifugal force generated by bubble particle aggregates rotating in small vortices generated in turbulent mechanical cells [25], and  $F_\omega$  is the bubble particle attachment force. For the bubble, the gravitational force and centrifugal force can be neglected, since the bubble's mass is negligible. Therefore, the equation for the sum of forces on a bubble is given by

$$\sum F_{bubble} = F_{b,bubble} + F_{d,bubble} - F_\omega \quad 1.3$$

Detachment will occur when the attachment force is equal to or less than the difference in net force between the bubble and particle. The difference in force between the bubble and particle is given by

$$\Delta F = F_{g,particle} + \Delta F_b + \Delta F_d + F_{c,particle} \quad 1.4$$

assuming the worst case, where all three differences are in the same direction. Both  $F_g$  and  $F_c$ , being body forces, increase with the cube of the diameter of the particle.  $\Delta F_b$  increases with the cube of the difference in diameters between the bubble and particle.  $\Delta F_d$  increases linearly or with the square of the difference between bubble and particle diameter, depending on the flow regime.

These detachment forces must be counteracted by the attachment force to prevent detachment. The capillary force due to the three-phase contact line at the bubble particle water interface is given by

$$F_{cap} = \pi d_p \sigma \sin(\alpha) \sin(\theta + \alpha) \quad 1.5$$

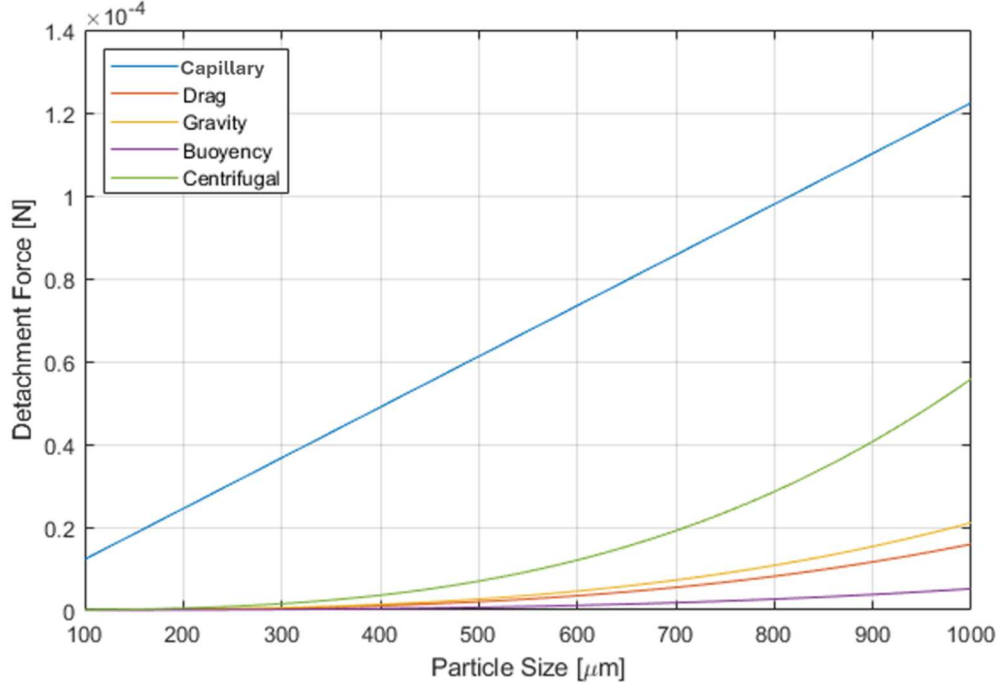


Figure 1.3: Detachment forces shown as a function of particle size.

where  $d_p$  is the particle diameter,  $\sigma$  is the liquid gas surface tension,  $\alpha$  is the surface angle of contact for the particle, and  $\theta$  is the surface contact angle [25], [26]. Equation 1.5 shows that this attachment force grows linearly with particle diameter. On the other hand, the primary detachment forces grow with the cube of particle size. This means that as particle size increases, the detachment forces will rapidly outweigh the attachment force. Further, the work of adhesion decreases with increasing particle size due to decreasing liberation. The work of adhesion is given by,

$$W_a = \gamma_{LV} \pi r_1 (1 - \cos \theta)^2 \quad 1.6$$

in which  $\gamma_{LV}$  is the surface tension of water,  $r_1$  is the radius of the mineral (e.g., chalcopyrite) grain exposed on the surface of a composite particle, and  $\theta$  is the contact angle [24]. As particle size increases, the exposed grain radius will decrease as liberation decreases, further decreasing attachment.

An example calculation is shown in Figure 1.3 illustrating how body detachment forces are more important for coarse particles. The acceleration in a vortex formed in a mechanically agitated cell can be calculated as

$$a_c = 3.75 \frac{\varepsilon^{2/3}}{d_b^{1/3}} \quad 1.7$$

where  $\varepsilon$  is the energy dissipation rate per unit mass of the medium and  $d_b$  is the bubble diameter [25]. For a typical mechanically agitated cell, the energy dissipation is on the order of  $1 \text{ kW/m}^3$  [25]. Figure 1.3 shows the magnitude of various detachment forces calculated as a function of particle size, assuming Stokes' drag, a particle SG of 2.6, a bubble diameter of  $3000 \mu\text{m}$ , and a contact angle of  $80^\circ$ . The greatest detachment force is the centrifugal force, which grows with particle size as does detachment by the gravity force. This makes sense as both are the result of a mass in a uniform acceleration field, and mass increases with the cube of particle size. The acceleration field created by turbulence is greater than that of gravity, and therefore, the centrifugal force is greater. Decreasing the centrifugal force and, therefore, turbulence is critical for the recovery of coarse particles.

*Detachment at the interface:*

Several studies have found evidence that detachment occurs at the pulp froth interface [27], [28]. Falutsu and Dobby [27] developed a column that measures froth zone recovery and drop back directly. It was found that recovery did not depend on froth height, indicating that detachment was occurring at the interface before particles entered the froth phase and not in the froth due to coalescence. Seaman et al. [28] developed a device for measuring the froth zone recovery. They found a difference in grade between particles on the pulp froth interface and in the concentrate, indicating that particles selectively enter the froth phase by hydrophobicity.

Falutsu [29] developed a thermodynamic explanation of interface detachment in which the kinetic energy of the bubble particle aggregate is dissipated when it reaches the pulp froth interface, and if higher than the work of adhesion, would cause detachment. Ireland and Jameson 2014 [31] tested the kinetic energy hypothesis experimentally and found, through high-speed imagery, that particles move from the bottom of the bubble to the top of the bubble and back down upon arriving at the interface. The kinetic energy was dissipated by friction forces and deformation of the bubble. This is likely why detachment was not observed even when there was sufficient kinetic energy to exceed the work of adhesion of the bubble particle aggregate. Tests were not conducted at different chemistries or particle sizes, however. These factors could make detachment at the pulp froth interface more prevalent. The major detachment force in

this arrangement would be centrifugal force, as the particles move along the bubble surface. This would grow cubically with particle size; therefore, this would be a larger factor for coarse particles. This shows that there are factors that mitigate the interface detachment problem, and kinetic energy alone cannot predict detachment at the froth interface [31]. Another possible mechanism was observed by Jameson and Emer [30]. It was observed that coarse particles attached to bubbles did not have sufficient buoyancy to enter the froth phase and would therefore remain below the froth phase without being recovered but not necessarily detach immediately upon reaching the froth phase [30].

#### *Detachment in the froth*

Detachment also occurs in the froth phase due to coalescence. This has been more consistently measured and explained than interface detachment. Ata and Jameson [32] found that the froth recovery increased with decreasing froth depth, indicating that coalescence in the froth phase was a significant detachment source. Detachment in the froth phase occurs when bubbles coalesce to form larger bubbles [33]. When coalescence occurs, the total bubble volume can remain constant, but the surface area for particle attachment decreases. Additionally, the coalescence produces oscillations that can detach particles. In the case of fully coated bubbles, particles detach due to reduced surface area; however, in the case of a few weakly attached particles, detachment occurs due to oscillations caused by coalescence. The latter is more important for coarse particle flotation as it involves smaller numbers of weakly attached particles, which will be susceptible to oscillations [33]. Yoon et al. 2016 [34], developed a froth recovery model based on the coarsening of bubbles as the limitation of froth recovery. This model in conjunction with a pulp recovery model was able to predict flotation recovery and rate constant using artificial sample from 35 to 119  $\mu\text{m}$  in size based on surface chemistry and hydrodynamic parameters [34].

Minimizing coalescence will therefore minimize detachment in the froth. Froth stability is an important factor in minimizing coalescence in the froth zone. Awatey et al. [35] found that the presence of fines (-106  $\mu\text{m}$ ) stabilized the froth and led to increased coarse particle recovery on coarse chalcopyrite and galena in batch DenverCell tests. Fang et al. found a similar result that fine particles stabilized the froth phase and that contact angles ranging from 60 to 70° were optimal for froth phase stabilization [36].

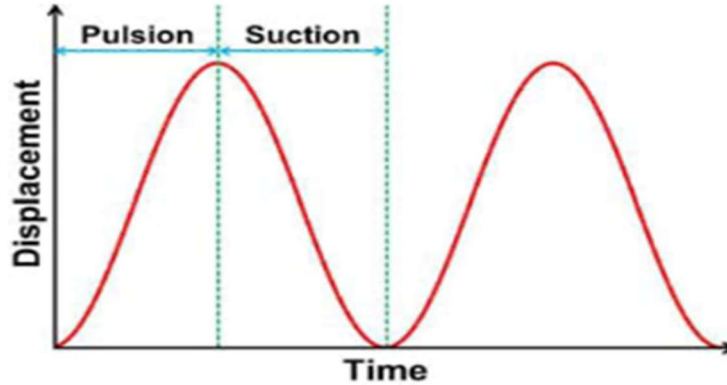


Figure 1.4: Pulsion cycle in a Jig.

### 1.2.2 Jigging Theory

Where flotation is a separation technique based on surface properties, Jigging is a separation technology based on volumetric properties. As particle size increases, the importance of volumetric properties will increase with  $d_p^3$ , while the importance of surface properties will rise with  $d_p^2$ . It follows, therefore, that jigging action will be more efficient at coarser particle sizes.

Jigging operates as an intermittent fluidized bed with a pulsion stroke where fluidization water is upward, and a suction stroke where fluidization is downward, as shown in Figure 1.4. This allows jigging to separate based on three mechanisms: hindered settling, differential initial acceleration, and consolidation trickling [37]. Combined, these mechanisms separate particles by density, independent of particle size, where a fluidized bed, based only on hindered settling, separates by both size and density.

A fluidized bed, which many CPF technologies are based on, separates particles by differences in settling velocity. Particles settle against an upward flow of water. Particles with a faster settling velocity than the fluidization velocity report to the underflow, while particles with a slower settling velocity than the fluidization velocity report to the overflow. Assuming Stokes' drag settling velocity is given by

$$u_s = \frac{gd_p^2(\rho_p - \rho_m)}{18} \quad 1.8$$

where  $\rho_p$  is the particle density, and  $\rho_m$  is the density of the medium. By Equation 1.8, hindered settling will separate particles by both size and density.

When the particle begins settling, the particle's motion relative to the fluid is zero, meaning the drag force can be ignored. The initial acceleration of the settling particle can be given by

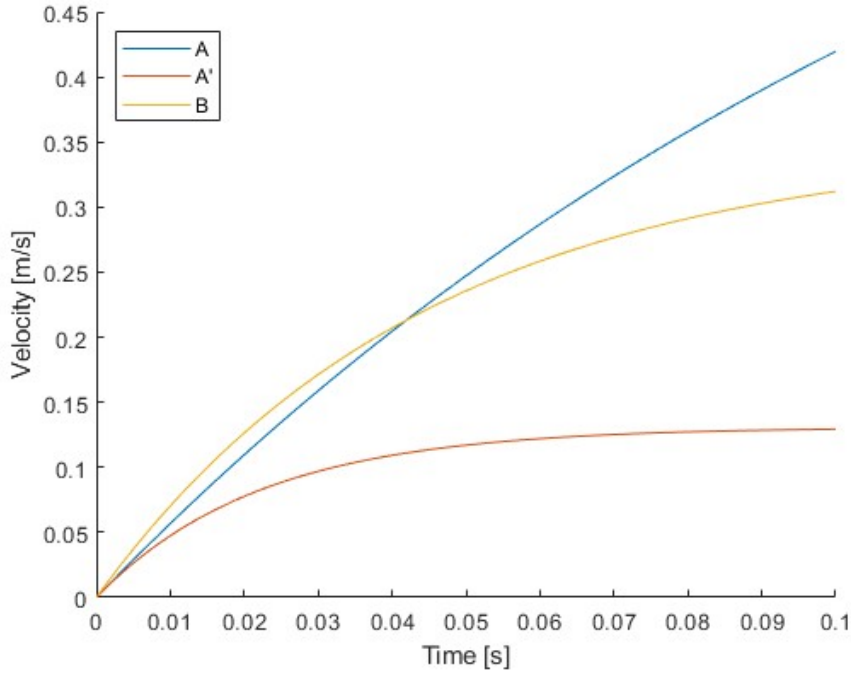


Figure 1.5: Movement of three particles A, A', and B during initial settling.

$$\frac{du}{dt} = \left(1 - \frac{\rho_m}{\rho_p} g\right) \quad 1.9$$

In Equation 1.9 acceleration is only dependent on  $\rho_p$ , and therefore separation based on initial acceleration is by density.

An example can be used to illustrate this separation mechanism. Given 3 particles A, B, and A', where A and A' are silica particles with SGs of 2.5 and diameters of 1000 and 400  $\mu\text{m}$ , respectively, and B is a chalcopyrite particle with an SG of 4.1 and a diameter of 400  $\mu\text{m}$ , the downward velocity of these particles as they settle is shown in Figure 1.5. Initially, particle B settles faster than both silica particles due to higher initial acceleration. By  $\sim 0.06$  seconds, particles B and A have travelled the same distance. In a jig, this means that if the period of the pulsion cycle is less than 0.06 seconds, these particles would have sorted with A' on top, A in the middle, and B on the bottom, and thus these particles are stratified by density. If the pulsion cycle is longer than 0.06 seconds, sorting by particle size becomes a factor, and particle B is between particles A and A'. Therefore, the intermittent nature of fluidization in jigging enables the differential initial acceleration mechanism, which eliminates the dependence on particles for separation. With sufficiently high jigging frequencies, separation by density is possible.

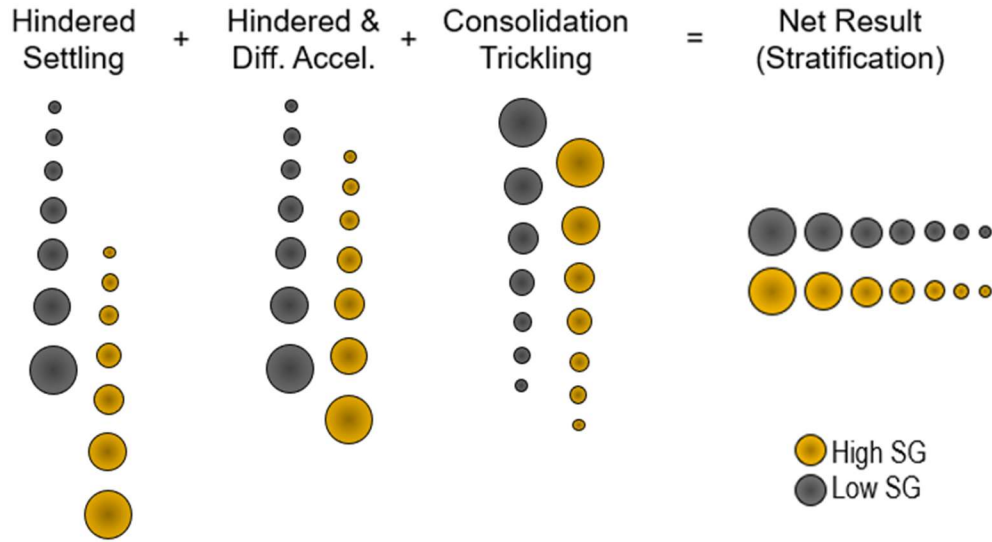


Figure 1.6: Mechanisms governing separation in a jig [37].

With a large range in particle size, there will inevitably be some mixing of the coarsest light particles and the finest heavy particles. Consolidation trickling during the suction stroke mitigates this by allowing heavier fine particles to trickle down through voids between coarser particles. An illustration of these combined mechanisms is given in Figure 1.6. Hindered settling separates particles by both density and size, with lighter, smaller particles on top and heavier, larger particles on the bottom. The addition of differential initial acceleration makes this separation primarily by particle density. Finally, consolidated trickling allows small dense particles that mixed with large low-density particles to trickle lower into the bed. The result of these combined mechanisms is separation by density [37].

### 1.3 Conclusion

Flotation is effective only in a narrow particle size range, typically 20-150  $\mu\text{m}$ , as the subprocesses governing flotation, collision, attachment, and detachment are highly size dependent. For ultrafine particles (<20  $\mu\text{m}$ ), flotation is limited by the collision subprocess due to low inertia, making particles less likely to divert from streamlines around bubbles and collide with bubbles. The collision probability for fine particles can be increased by increasing the number density of bubbles, using fine bubbles to increase the frequency of collisions, using high shear agitation to increase bubble particle interactions, and increasing hydrophobicity to reduce the induction time and critical film thickness to promote bubble particle attachment.

Coarse particle flotation is primarily limited by the detachment subprocess. Body forces such as gravity, buoyancy, and centrifugal forces grow in significance cubically with particle size, rapidly overcoming surface attachment forces, which increase with the square of particle size. The centrifugal force is especially important as mechanically agitated flotation cells produce high acceleration fields within the pulp. Detachment in the froth phase is also important for coarse particles, which tend to be less hydrophobic due to lower liberation. The presence of fine particles in the froth phase can help to reduce bubble coalescence and, therefore, detachment in the froth phase. The inclusion of these particles can also increase the density of the froth phase, mitigating the buoyancy problem for coarse particles in the froth phase. Coarse particle flotation requires quiescent conditions to minimize detachment in the pulp and a stable froth to minimize detachment in the froth.

Another separation technology, jigging, is explored theoretically. Jigging is a highly effective technology for coarse particles. By combining hindered settling, differential initial acceleration, and consolidation trickling, jigging is capable of separating particles by density independent of particle size. Jigging typically operates at coarser size ranges as compared with flotation. These advantages make it appealing as a basis for coarse particle flotation.

The conditions necessary for fine and coarse particle flotation are contradictory. Fine particle flotation requires turbulent conditions to promote bubble particle collision and enhanced kinetics to increase the frequency of collision. The following chapter explores the existing coarse particle flotation technologies, which attempt to mitigate the issues of detachment for coarse particles.

## References:

- [1] H. F. K.-P. J. B. Henry Livingston Sulman, "Ore concentration," US835479A, 1906
- [2] B. A. Wills and J. A. Finch, "Chapter 12 - Froth Flotation," in *Wills' Mineral Processing Technology (Eighth Edition)*, Eighth Edition., B. A. Wills and J. A. Finch, Eds., Boston: Butterworth-Heinemann, 2016, pp. 265–380. doi: <https://doi.org/10.1016/B978-0-08-097053-0.00012-1>.
- [3] A. Elshkaki, T. E. Graedel, L. Ciacci, and B. Reck, "Copper demand, supply, and associated energy use to 2050," *Global Environmental Change*, vol. 39, pp. 305–315, Jul. 2016, doi: [10.1016/J.GLOENVCHA.2016.06.006](https://doi.org/10.1016/J.GLOENVCHA.2016.06.006).
- [4] C O'Connor, "Global Challenges Facing the Minerals Processing Industry," in *IMPC Eurasia*, 2019, pp. 1–10.
- [5] T. Norgate and S. Jahanshahi, "Energy and greenhouse gas implications of deteriorating quality ore reserves," Nov. 2006.
- [6] M. Gupta and R. H. Yoon, "Maximizing the recovery and throughput of a rougher flotation bank by improving the recovery of composite particles," *Miner. Eng.*, vol. 207, p. 108545, Feb. 2024, doi: [10.1016/j.mineng.2023.108545](https://doi.org/10.1016/j.mineng.2023.108545).
- [7] Committee on Coal Waste Impoundments *et al.*, "Coal waste impoundments: Risks, responses and alternatives," in *Coal waste impoundments: Risks*, 2002, p. 10212. doi: [10.17226/10212](https://doi.org/10.17226/10212).
- [8] E. A. Holley, K. M. Hadden, D. Hammerling, R. Eggert, D. E. Spiller, and P. P. Nelson, "By-product recovery from US metal mines could reduce import reliance for critical minerals," *Science (1979)*., vol. 389, no. 6767, pp. 1325–1331, Sep. 2025, doi: [10.1126/science.adw8997](https://doi.org/10.1126/science.adw8997).
- [9] S. Northey, S. Mohr, G. M. Mudd, Z. Weng, and D. Giurco, "Modelling future copper ore grade decline based on a detailed assessment of copper resources and mining," *Resour. Conserv. Recycl.*, vol. 83, pp. 190–201, Feb. 2014, doi: [10.1016/J.RESCONREC.2013.10.005](https://doi.org/10.1016/J.RESCONREC.2013.10.005).
- [10] J. N. Kohmuench, M. J. Mankosa, H. Thanasekaran, and A. Hobert, "Improving coarse particle flotation using the HydroFloat™ (raising the trunk of the elephant curve)," *Miner. Eng.*, vol. 121, 2018, doi: [10.1016/j.mineng.2018.03.004](https://doi.org/10.1016/j.mineng.2018.03.004).

- [11] B. V. Derjaguin, S. S. Dukhin, and N. N. Rulyov, “Kinetic Theory of Flotation of Small Particles,” in *Surface and Colloid Science*, vol. 13, E. Matijevic and R. Good, Eds., New York: Plenum Press, 1984, ch. 2, pp. 71–110.
- [12] S. Ata, “Phenomena in the froth phase of flotation — A review,” *Int. J. Miner. Process.*, vol. 102–103, pp. 1–12, Jan. 2012, doi: 10.1016/J.MINPRO.2011.09.008.
- [13] K. L. Sutherland, “Physical Chemistry of Flotation. XI. Kinetics of the Flotation Process,” *J. Phys. Colloid Chem.*, vol. 52, no. 2, pp. 394–425, 1948, doi: 10.1021/j150458a013.
- [14] Z. Dai, D. Fornasiero, and J. Ralston, “Particle–bubble collision models — a review,” *Adv. Colloid Interface Sci.*, vol. 85, no. 2, pp. 231–256, 2000, doi: [https://doi.org/10.1016/S0001-8686\(99\)00030-5](https://doi.org/10.1016/S0001-8686(99)00030-5).
- [15] S. Farrokhpay, L. Filippov, and D. Fornasiero, “Flotation of Fine Particles: A Review,” *Mineral Processing and Extractive Metallurgy Review*, vol. 42, no. 7, pp. 473–483, 2021, doi: 10.1080/08827508.2020.1793140.
- [16] G. H. Luttrell and R.-H. Yoon, “A hydrodynamic model for bubble—particle attachment,” *J. Colloid Interface Sci.*, vol. 154, no. 1, pp. 129–137, 1992, doi: [https://doi.org/10.1016/0021-9797\(92\)90085-Z](https://doi.org/10.1016/0021-9797(92)90085-Z).
- [17] H. Darabi, S. M. J. Koleini, D. Deglon, B. Rezai, and M. Abdollahy, “Investigation of bubble-particle interactions in a mechanical flotation cell, part 1: Collision frequencies and efficiencies,” *Miner. Eng.*, vol. 134, pp. 54–64, 2019, doi: <https://doi.org/10.1016/j.mineng.2019.01.012>.
- [18] A. S. Reis, A. M. Reis Filho, L. R. Demuner, and M. A. S. Barrozo, “Effect of bubble size on the performance flotation of fine particles of a low-grade Brazilian apatite ore,” *Powder Technol.*, vol. 356, pp. 884–891, 2019, doi: <https://doi.org/10.1016/j.powtec.2019.09.029>.
- [19] G. S. Dobby and J. A. Finch, “Particle size dependence in flotation derived from a fundamental model of the capture process,” *Int. J. Miner. Process.*, vol. 21, no. 3, pp. 241–260, 1987, doi: [https://doi.org/10.1016/0301-7516\(87\)90057-3](https://doi.org/10.1016/0301-7516(87)90057-3).

- [20] Z. Dai, D. Fornasiero, and J. Ralston, "Particle–Bubble Attachment in Mineral Flotation," *J. Colloid Interface Sci.*, vol. 217, no. 1, pp. 70–76, 1999, doi: <https://doi.org/10.1006/jcis.1999.6319>.
- [21] S. Janishar Anzoom, G. Bournival, and S. Ata, "Coarse particle flotation: A review," *Miner. Eng.*, vol. 206, p. 108499, 2024, doi: <https://doi.org/10.1016/j.mineng.2023.108499>.
- [22] H. Darabi, S. M. J. Koleini, D. Deglon, B. Rezai, and M. Abdollahy, "Investigation of bubble-particle attachment, detachment and collection efficiencies in a mechanical flotation cell," *Powder Technol.*, vol. 375, pp. 109–123, 2020, doi: <https://doi.org/10.1016/j.powtec.2020.07.085>.
- [23] V. Chipakwe, R. Jolsterå, and S. C. Chelgani, "Nanobubble-Assisted Flotation of Apatite Tailings: Insights on Beneficiation Options," *ACS Omega*, vol. 6, no. 21, pp. 13888–13894, 2021, doi: [10.1021/acsomega.1c01551](https://doi.org/10.1021/acsomega.1c01551).
- [24] L. Mao and R.-H. Yoon, "Predicting flotation rates using a rate equation derived from first principles," *Int. J. Miner. Process.*, vol. 51, no. 1, pp. 171–181, 1997, doi: [https://doi.org/10.1016/S0301-7516\(97\)00025-2](https://doi.org/10.1016/S0301-7516(97)00025-2).
- [25] S. Goel and G. J. Jameson, "Detachment of particles from bubbles in an agitated vessel," *Miner. Eng.*, vol. 36–38, pp. 324–330, 2012, doi: <https://doi.org/10.1016/j.mineng.2012.08.001>.
- [26] D. Xu, I. Ametov, and S. R. Grano, "Detachment of coarse particles from oscillating bubbles—The effect of particle contact angle, shape and medium viscosity," *Int. J. Miner. Process.*, vol. 101, no. 1, pp. 50–57, 2011, doi: <https://doi.org/10.1016/j.minpro.2011.07.003>.
- [27] M. Falutsu and G. S. Dobby, "Direct measurement of froth drop back and collection zone recovery in a laboratory flotation column," *Miner. Eng.*, vol. 2, no. 3, pp. 377–386, 1989, doi: [https://doi.org/10.1016/0892-6875\(89\)90006-X](https://doi.org/10.1016/0892-6875(89)90006-X).
- [28] D. R. Seaman, J.-P. Franzidis, and E. V Manlapig, "Bubble load measurement in the pulp zone of industrial flotation machines—a new device for determining the froth recovery of attached particles," *Int. J. Miner. Process.*, vol. 74, no. 1, pp. 1–13, 2004, doi: <https://doi.org/10.1016/j.minpro.2004.04.001>.

- [29] M. Falutsu, “Column flotation froth characteristics — stability of the bubble-particle system,” *Int. J. Miner. Process.*, vol. 40, no. 3, pp. 225–243, 1994, doi: [https://doi.org/10.1016/0301-7516\(94\)90045-0](https://doi.org/10.1016/0301-7516(94)90045-0).
- [30] G. J. Jameson and C. Emer, “Effect of bubble loading on the recovery of coarse mineral particles by flotation,” *Miner. Eng.*, vol. 215, p. 108788, 2024, doi: <https://doi.org/10.1016/j.mineng.2024.108788>.
- [31] P. M. Ireland and G. J. Jameson, “Collision of a rising bubble–particle aggregate with a gas–liquid interface,” *Int. J. Miner. Process.*, vol. 130, pp. 1–7, 2014, doi: <https://doi.org/10.1016/j.minpro.2014.05.002>.
- [32] S. Ata and G. J. Jameson, “Recovery of coarse particles in the froth phase – A case study,” *Miner. Eng.*, vol. 45, pp. 121–127, May 2013, doi: [10.1016/J.MINENG.2013.02.006](https://doi.org/10.1016/J.MINENG.2013.02.006).
- [33] S. Ata, “The detachment of particles from coalescing bubble pairs,” *J. Colloid Interface Sci.*, vol. 338, no. 2, pp. 558–565, Oct. 2009, doi: [10.1016/J.JCIS.2009.07.003](https://doi.org/10.1016/J.JCIS.2009.07.003).
- [34] R. H. Yoon, G. Soni, K. Huang, S. Park, and L. Pan, “Development of a turbulent flotation model from first principles and its validation,” *Int. J. Miner. Process.*, vol. 156, no. 2, pp. 43–51, Nov. 2016, doi: [10.1016/j.minpro.2016.05.009](https://doi.org/10.1016/j.minpro.2016.05.009).
- [35] B. Awatey, W. Skinner, and M. Zanin, “Effect of particle size distribution on recovery of coarse chalcopyrite and galena in Denver flotation cell,” *Canadian Metallurgical Quarterly*, vol. 52, no. 4, pp. 465–472, 2013, doi: [10.1179/1879139513Y.0000000085](https://doi.org/10.1179/1879139513Y.0000000085).
- [36] J. Fang, Y. Ge, and J. Yu, “Effects of particle size and wettability on froth stability in a collophane flotation system,” *Powder Technol.*, vol. 379, pp. 576–584, Feb. 2021, doi: [10.1016/J.POWTEC.2020.11.028](https://doi.org/10.1016/J.POWTEC.2020.11.028).
- [37] A. Gaudin, *Principles\_of\_Mineral\_Dressing*. McGraw-Hill Book Company, 1939.
- [38] I. Achaye, J. Wiese, and B. McFadzean, “Effect of mineral particle size on froth stability,” *Mineral Processing and Extractive Metallurgy*, vol. 130, no. 3, pp. 253–261, 2021, doi: [10.1080/25726641.2019.1606147](https://doi.org/10.1080/25726641.2019.1606147).

- [39] N. Ahmed and G. J. Jameson, “The effect of bubble size on the rate of flotation of fine particles,” *Int. J. Miner. Process.*, vol. 14, no. 3, pp. 195–215, Apr. 1985, doi: 10.1016/0301-7516(85)90003-1.
- [40] Z. Aktas, J. J. Cilliers, and A. W. Banford, “Dynamic froth stability: Particle size, airflow rate and conditioning time effects,” *Int. J. Miner. Process.*, vol. 87, no. 1–2, pp. 65–71, Apr. 2008, doi: 10.1016/J.MINPRO.2008.02.001.
- [41] W. M. Ambrós, “Jigging: A Review of Fundamentals and Future Directions,” *Minerals*, vol. 10, no. 11, 2020, doi: 10.3390/min10110998.
- [42] A. V. Nguyen, J. Ralston, and H. J. Schulze, “On modelling of bubble–particle attachment probability in flotation,” *Int. J. Miner. Process.*, vol. 53, no. 4, pp. 225–249, May 1998, doi: 10.1016/S0301-7516(97)00073-2.
- [43] G. Bournival, S. Ata, and G. J. Jameson, “The influence of submicron particles and salt on the recovery of coarse particles,” *Miner. Eng.*, vol. 69, pp. 146–153, Dec. 2014, doi: 10.1016/J.MINENG.2014.07.003.
- [44] K. Changunda, M. Harris, and D. A. Deglon, “Investigating the effect of energy input on flotation kinetics in an oscillating grid flotation cell,” *Miner. Eng.*, vol. 21, no. 12–14, pp. 924–929, Nov. 2008, doi: 10.1016/J.MINENG.2008.03.015.
- [45] John A. Christopherson, “Recent Deister Flotaire Column Flotation Cell Developments,” *Resources Processing*, vol. 35, no. 4, pp. 207–225, 1988.
- [46] John A. Christophersen and Adolf J. Jonaitis, “Deister Flotaire Column Flotation Cell - Plant Experience,” *Society for Mining, Metallurgy & Exploration*, 1989.
- [47] K. C. Corin, B. J. McFadzean, N. J. Shackleton, and C. T. O’Connor, “Challenges Related to the Processing of Fines in the Recovery of Platinum Group Minerals (PGMs),” *Minerals*, vol. 11, no. 5, 2021, doi: 10.3390/min11050533.
- [48] R. Crawford and J. Ralston, “The influence of particle size and contact angle in mineral flotation,” *Int. J. Miner. Process.*, vol. 23, no. 1–2, pp. 1–24, May 1988, doi: 10.1016/0301-7516(88)90002-6.

- [49] J. A. Curry, M. J. L. Ismay, and G. J. Jameson, "Mine operating costs and the potential impacts of energy and grinding," *Miner. Eng.*, vol. 56, pp. 70–80, Feb. 2014, doi: 10.1016/J.MINENG.2013.10.020.
- [50] Z. Dai, S. Dukhin, D. Fornasiero, and J. Ralston, "The Inertial Hydrodynamic Interaction of Particles and Rising Bubbles with Mobile Surfaces," *J. Colloid Interface Sci.*, vol. 197, no. 2, pp. 275–292, Jan. 1998, doi: 10.1006/JCIS.1997.5280.
- [51] J. B. Dankwah, R. K. Asamoah, M. Zanin, and W. Skinner, "Dense liquid flotation: Can coarse particle flotation performance be enhanced by controlling fluid density?," *Miner. Eng.*, vol. 180, p. 107513, Apr. 2022, doi: 10.1016/J.MINENG.2022.107513.
- [52] J. B. Dankwah, R. K. Asamoah, M. Zanin, W. Skinner, and G. 30/07/2022–01/08/2022 7th UMaT Biennial International Mining and Mineral Conference Tarkwa, *A simple analysis showing the limits of coarse particle flotation*. in Future Industries Institute. Ghana: UMat, 2022.
- [53] N. D. Denkov, K. G. Marinova, and S. S. Tcholakova, "Mechanistic understanding of the modes of action of foam control agents," *Adv. Colloid Interface Sci.*, vol. 206, pp. 57–67, Apr. 2014, doi: 10.1016/J.CIS.2013.08.004.
- [54] A. Dippenaar, "The destabilization of froth by solids. II. The rate-determining step," *Int. J. Miner. Process.*, vol. 9, no. 1, pp. 15–22, Jan. 1982, doi: 10.1016/0301-7516(82)90003-5.
- [55] A. Dippenaar, "The destabilization of froth by solids. I. The mechanism of film rupture," *Int. J. Miner. Process.*, vol. 9, no. 1, pp. 1–14, Jan. 1982, doi: 10.1016/0301-7516(82)90002-3.
- [56] M. FAN, D. TAO, R. HONAKER, and Z. LUO, "Nanobubble generation and its application in froth flotation (part I): nanobubble generation and its effects on properties of microbubble and millimeter scale bubble solutions," *Mining Science and Technology (China)*, vol. 20, no. 1, pp. 1–19, Jan. 2010, doi: 10.1016/S1674-5264(09)60154-X.
- [57] S. Farrokhpay and D. Fornasiero, "Flotation of coarse composite particles: Effect of mineral liberation and phase distribution," *Advanced Powder Technology*, vol. 28, no. 8, pp. 1849–1854, Aug. 2017, doi: 10.1016/J.APT.2017.03.012.

- [58] D. Fornasiero and L. O. Filippov, “Innovations in the flotation of fine and coarse particles,” *J. Phys. Conf. Ser.*, vol. 879, no. 1, p. 012002, 2017, doi: 10.1088/1742-6596/879/1/012002.
- [59] K. P. Galvin, S. J. Pratten, N. Lambert, A. M. Callen, and J. Lui, “Influence of a jiggging action on the gravity separation achieved in a teetered bed separator,” *Miner. Eng.*, vol. 15, no. 12, pp. 1199–1202, Dec. 2002, doi: 10.1016/S0892-6875(02)00211-X.
- [60] H. J. Schulze, “Dimensionless number and approximate calculation of the upper particle size of floatability in flotation machines,” *Int. J. Miner. Process.*, vol. 9, no. 4, pp. 321–328, Oct. 1982, doi: 10.1016/0301-7516(82)90038-2.
- [61] C. Gontijo, D. Fornasiero, and J. Ralston, “The Limits of Fine and Coarse Particle Flotation,” *Can. J. Chem. Eng.*, vol. 85, pp. 739–747, Oct. 2008, doi: 10.1002/cjce.5450850519.
- [62] R. B. Gordon, “Production residues in copper technological cycles,” *Resour. Conserv. Recycl.*, vol. 36, no. 2, pp. 87–106, Aug. 2002, doi: 10.1016/S0921-3449(02)00019-8.
- [63] H. and N. A. and Y. R.-H. Gupta Mohit and Lim, “Optimizing Flotation Circuit Using a Model that Can Predict Both Grade and Recoveries,” in *12th International Copper Conference*, Cham: Springer Nature Switzerland, 2025, pp. 1669–1674.
- [64] K. Huang and R.-H. Yoon, “Surface Forces in the Thin Liquid Films (TLFs) of Water Confined between n-Alkane Drops and Hydrophobic Gold Surfaces,” *Langmuir*, vol. 35, no. 48, pp. 15681–15691, Dec. 2019, doi: 10.1021/acs.langmuir.9b02102.
- [65] G. J. Jameson, “New directions in flotation machine design,” *Miner. Eng.*, vol. 23, no. 11–13, pp. 835–841, Oct. 2010, doi: 10.1016/J.MINENG.2010.04.001.
- [66] G. J. Jameson, “Advances in Fine and Coarse Particle Flotation,” *Canadian Metallurgical Quarterly*, vol. 49, no. 4, pp. 325–330, Oct. 2010, doi: 10.1179/cmqr.2010.49.4.325.
- [67] M. J. Mankosa, J. N. Kohmuench, L. Christodoulou, and E. S. Yan, “Improving fine particle flotation using the StackCell™ (raising the tail of the elephant curve),” *Miner. Eng.*, vol. 121, pp. 83–89, Jun. 2018, doi: 10.1016/J.MINENG.2018.03.012.

- [68] Mike Mankosa, “A New Paradigm in Sulphide Processing,” *Engineering and Mining Journal*, pp. 56–61, 2017.
- [69] M. J. Mankosa, J. N. Kohmuench, L. Christodoulou, and G. H. Luttrell, “RECOVERY OF VALUES FROM A PORPHORY COPPER TAILINGS STREAM,” 2016. [Online]. Available: <https://api.semanticscholar.org/CorpusID:7172689>
- [70] B. K. Mishra and S. P. Mehrotra, “Modelling of particle stratification in jigs by the discrete element method,” *Miner. Eng.*, vol. 11, no. 6, pp. 511–522, Jun. 1998, doi: 10.1016/S0892-6875(98)00033-8.
- [71] S. Nazari, S. Z. Shafaei, M. Gharabaghi, R. Ahmadi, B. Shahbazi, and F. Maoming, “Effects of nanobubble and hydrodynamic parameters on coarse quartz flotation,” *Int. J. Min. Sci. Technol.*, vol. 29, no. 2, pp. 289–295, Mar. 2019, doi: 10.1016/J.IJMST.2018.08.011.
- [72] R. M. Rahman, S. Ata, and G. J. Jameson, “Froth recovery measurements in an industrial flotation cell,” *Miner. Eng.*, vol. 53, pp. 193–202, Nov. 2013, doi: 10.1016/J.MINENG.2013.08.003.
- [73] S. Gautam and G. J. Jameson, “The detachment of particles from bubbles at various locations in a turbulent flotation cell,” *Miner. Eng.*, vol. 132, pp. 316–325, Mar. 2019, doi: 10.1016/J.MINENG.2018.06.004.
- [74] G. Bournival, L. de Oliveira e Souza, S. Ata, and E. J. Wanless, “Effect of alcohol frothing agents on the coalescence of bubbles coated with hydrophobized silica particles,” *Chem. Eng. Sci.*, vol. 131, pp. 1–11, Jul. 2015, doi: 10.1016/J.CES.2015.03.036.
- [75] H. J. Schulze, “New theoretical and experimental investigations on stability of bubble/particle aggregates in flotation: A theory on the upper particle size of floatability,” *Int. J. Miner. Process.*, vol. 4, no. 3, pp. 241–259, Sep. 1977, doi: 10.1016/0301-7516(77)90005-9.
- [76] H. J. Steiner, “A contribution to the theory of jigging, Part I: Similarity criteria of the motion of jig layers,” *Miner. Eng.*, vol. 9, no. 6, pp. 675–686, Jun. 1996, doi: 10.1016/0892-6875(96)00055-6.
- [77] Eric Bain Wasmund, “Flotation technology for coarse and fine particle recovery,” *I Congreso Internacional De Flotacion De Minerales*, 2014.

- [78] E. Wingate and J. Kohmuench, “An optimized approach to phosphate recovery,” *Beneficiation of Phosphates: Comprehensive Extraction, Technology Innovations, Advanced Reagents*, vol. 43, 2016.

## Chapter 2: Coarse particle Flotation Technologies

In the previous chapter, it was shown that the flotation of coarse particles is limited by detachment. In mechanically agitated cells, detachment is primarily due to turbulence. Several technologies have been developed to extend the top size of flotation by minimizing detachment. In the following sections, an overview of each of these technologies, their mechanisms, advantages, and some results that illustrate their performance are presented. Emphasis will be placed on results on copper-bearing minerals and coal, as these have been tested on many of the technologies and therefore give a basis for comparison.

### 2.1 HydroFloat™

HydroFloat™, shown in Figure 2.1, consists of a lower dewatering cone and an upper separation chamber [2]. Above the lower dewatering cone, aerated fluidization water is added. This creates a teeter bed within the separation chamber. Feed is added to the top of the teeter bed and settles against the fluidization water. Fluidization water spills over the top of the separation chamber into a concentrate launder [1]. Tails are taken from the bottom of the dewatering cone.

HydroFloat™ is based on the Eriez CrossFlow™ classifier, which operates as a fluidized bed to separate particles by size. Fluidized beds separate particles by differences in settling velocity. Particles having a settling velocity lower than the fluidization velocity (fine and/or low-density particles) are elutriated to the overflow, while those with a higher terminal velocity than the fluidization velocity (coarse

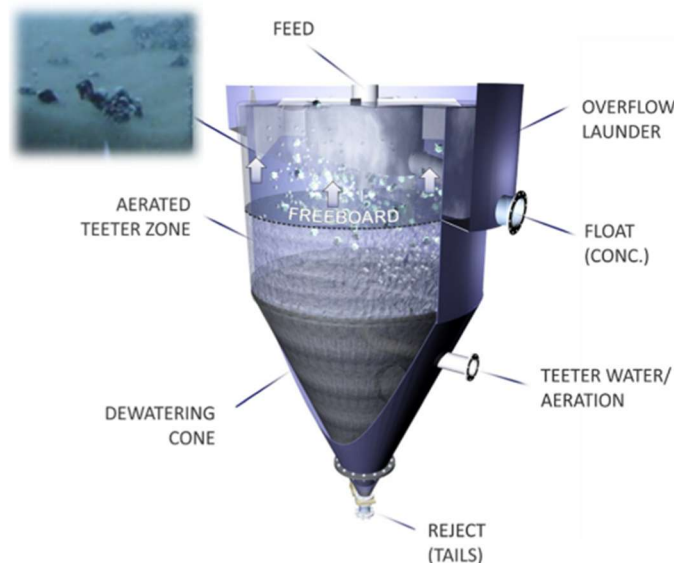


Figure 2.1: Schematic of HydroFloat™ [1].

and/or high-density particles) settle to the underflow. HydroFloat™ enhances the density difference by aerating the fluidized bed with microbubbles generated using a Cav Tube or a high shear circuit [2], [3]. These microbubbles selectively attach to the hydrophobic species, lowering the apparent density of the particles. The settling velocity of the resulting bubble particle aggregate is lower than the fluidization velocity, and the aggregate rises to the concentrate launder.

The teeter bed formed increases the apparent density of the medium. Low-density coarse particles remain on top of the dense teeter bed. The teeter bed also enhances bubble particle collision by compressing the streamlines around bubbles and increasing the density of particles for interaction. The hindered settling conditions reduce the relative velocity of bubbles and particles, increasing the sliding time between bubbles and particles, increasing the probability of attachment. Hindered settling also increases the residence time of particles, making more efficient use of cell volume [2].

The major advantage of the fluidized bed is the reduced turbulence in the cell, reducing detachment. This is vital for coarse particle flotation. Because of the quiescent conditions, there is very little axial mixing; this means HydroFloat™ acts as a plug flow reactor. Another advantage for coarse particle flotation is that the recovery of particles is not dependent on buoyancy. With sufficiently high fluidization velocities, particles and bubble particle aggregates that have SGs greater than 1 can be recovered. The constant fluidization water flow precludes the formation of a froth phase. Coarse particles do not need to rise through a froth phase to be recovered. This is advantageous in that detachment at the pulp froth interface and due to coalescence is avoided. However, this means that HydroFloat™ cannot take advantage of froth cleaning [2].

The major disadvantage of HydroFloat™ is the need for pre-classification. Fine particles with low settling velocities will unselectively report to the concentrate launder. This means that a HydroFloat™ cell requires pre-classified feed to remove these fine fractions. The HydroFloat™ separator can handle a maximum top-to-bottom size ratio of 5:1 [4].

HydroFloat™ was initially applied for coal and phosphate recovery [2], [5]. In lab testing of phosphate feed between 500 and 3000 µm, 95% recovery at a BPL of 67% was achieved [6]. In pilot testing

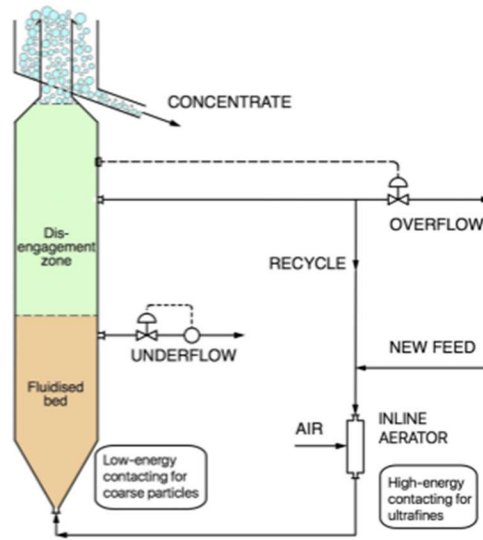


Figure 2.2: Schematic of NovaCell™ [10].

of feed between 500 and 1190  $\mu\text{m}$ , 85% recovery was achieved, and 60% recovery was achieved in the +1190  $\mu\text{m}$  feed fraction [6]. It was later found that aeration was sufficient to reverse the density difference for metals where the density difference between gangue and desired metal is not favourable [7], [8]. In testing with copper ore recoveries as high as 89% were achieved with particle sizes ranging from 180  $\mu\text{m}$  to 850  $\mu\text{m}$  [7]. This was achieved at upgrade ratios between 4 and 24 and with mass yields between 4% and 15%. HydroFloat™ has demonstrated the capacity for complete recovery down to 1.5% liberated sulfide minerals in testing with gold, with a top size of 850  $\mu\text{m}$  [9].

## 2.2 NovaCell™

The NovaCell™ shown schematically in Figure 2.2 consists of a Lower fluidized bed, a disengagement zone where flotation occurs, and a froth zone [10]. Like HydroFloat™, the NovaCell™ is based on a fluidized bed. Unlike HydroFloat™, the NovaCell™ aims to process coarse and fine particles simultaneously in a single unit. It achieves this using different mechanisms for fine and coarse particles, recovering coarse particles by fluidization and recovering fine particles by flotation through a froth phase. These separate mechanisms produce two product streams and two tails streams. Slurry is taken from the top portion of the cell below the froth phase to prevent overflow and recover coarse particles unable to enter the froth. This overflow stream consists of lifted coarse particles unable to enter the froth phase and fine particles lifted by the fluidization water. Because of the unselective lifting of fine particles, this recycled

stream must be classified in an internal classification circuit. The coarse section is taken as a product. Part of the fine portion leaves as tails, while part is recycled and mixed with new feed. This increases the residence time in the cell. The resulting stream goes through a pressurized downcomer to generate fine bubbles. This high shear environment increases the collection of fine particles. This stream is injected at the bottom of the cell as both feed and fluidization water. A second tails stream is taken at the bottom of the dewatering cone, consisting of unfluidized particles [10].

The NovaCell™ is capable of treating both fine and coarse particles in a single unit without the need for preclassification. This is achieved using separate recovery and collection regions for each within the cell. Coarse particles are attached to air bubbles in the quiescent fluidized bed zone and selectively lifted to the drop back cone, where they are separated from fine particles in a classification circuit. Fine particles are attached to air bubbles in a high shear downcomer, improving kinetics, and float to the top of the cell where they selectively move through the froth phase. This arrangement allows for fine particles to be recovered by buoyancy, as in a traditional flotation cell, and coarse particles to be recovered by settling velocity as in a fluidized bed. The NovaCell™ also increases the residence time of particles by using a fluidized bed and recycling a portion of the tails.

Morgan and Jameson [11] performed batch tests using NovaCell™ on 0x600 µm copper feed with a grade of .47%. After 10 minutes of flotation, 89.5% recovery was achieved with an upgrade ratio of 8.38 times and a mass pull of 10.8%. Continuous testing on a coal feed with a top size of 2000 µm and a feed ash of 20.6% resulted in an average recovery of 94.2%, an average yield of 86.3%, and an average product ash of 12.4%. The residence time in this cell was reported as 1.7 minutes [12].

### **2.3 Reflux™ Flotation Cell**

The Reflux™ Flotation Cell, shown schematically in Figure 2.3, is based on the Reflux™ Classifier [13]. Similar to the NovaCell™, the Reflux™ Flotation Cell aims to treat both fine and coarse particles in a single unit. The Reflux™ Flotation Cell achieves this without a classification circuit. The Reflux™ Flotation Cell consists of an upper reversed fluidized with downward wash water instead of upward

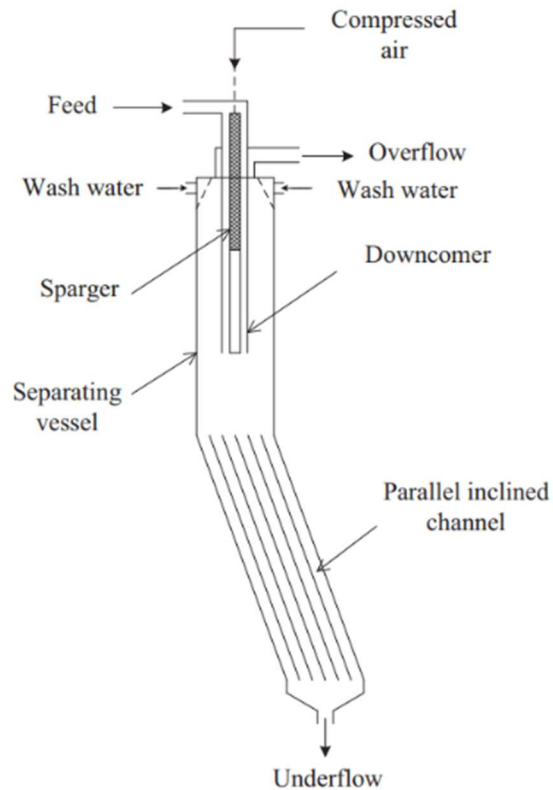


Figure 2.3: Schematic of Reflux™ Flotation Cell [14].

fluidization water. Below the fluidization chamber is a chamber with parallel, equally spaced inclined channels, below which tails are taken. Feed is added through the downcomer above the inclined channels. The downcomer creates high shear to generate fine bubbles and contact them with fine particles [13], [15], [16]. Exiting the downcomer, the feed enters the reverse fluidized bed. Bubbles and bubble particle aggregates rise against the flow of wash water from the top of the cell, forming a bubbly zone. This makes the Reflux™ Flotation Cell excellent at desliming, allowing it to treat the entire size range, including slimes, selectively [16]. The Reflux™ Flotation Cell operates without a true froth zone; instead, it has a zone of downwardly fluidized bubbles. This reduces the detachment by deceleration when particles reach the froth zone that is seen in other flotation cells [17]. Bubble particle aggregates are prevented from reporting to the tails by inclined channels at the bottom of the cell before the dewatering cone [13], [15], [16]. This is the Reflux™ mechanism. These particles are lifted to the top of these channels by the boycott effect [18], [19]. The downward fluidization requires particles to be buoyant to report to the concentrate launder [13], [15], [16].

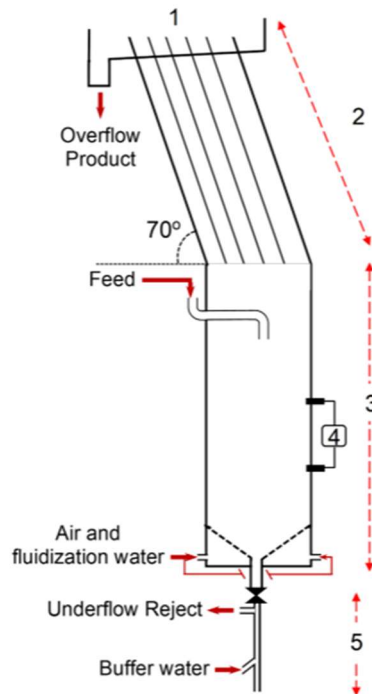


Figure 2.4: Schematic of CoarseAIR™ flotation cell [21].

Sutherland et al. [20] conducted continuous flotation using a Reflux™ Flotation cell on coal slurry with a top size of 2000  $\mu\text{m}$ . Across four tests, an 86.8% recovery was achieved, and a high recovery of +80% was maintained at the coarsest fraction. Wash water was shown to lower the ash at the finest fraction from 34.7% to 14.6% without affecting recovery [20].

## 2.4 CoarseAIR™

The CoarseAIR™ flotation cell, shown in Figure 2.4, is based on the Reflux™ Classifier. It operates with an upward-flowing fluidized bed. Aerated water with fine bubbles, typically less than 500  $\mu\text{m}$ , is used to fluidize the feed [22]. Inclined channels at the top of the unit reject coarse gangue particles via the boycott effect [18]. Feed enters just below the inclined channels [22]. The aim of this technology is high recovery instead of a high upgrade ratio. The yield can be adjusted by increasing or decreasing the channel spacing to reduce the lift, thus reducing the amount of solids reporting to the concentrate. Because of the upward fluidization water, all fines report to the concentrate, requiring post-classification of the product with the coarse particles going to regrinding and fines going to further flotation. Because of the high recovery, the CoarseAIR™ can operate as a rougher stage to increase the mill grind size by recovering coarse particles and rejecting some fine gangue [21].

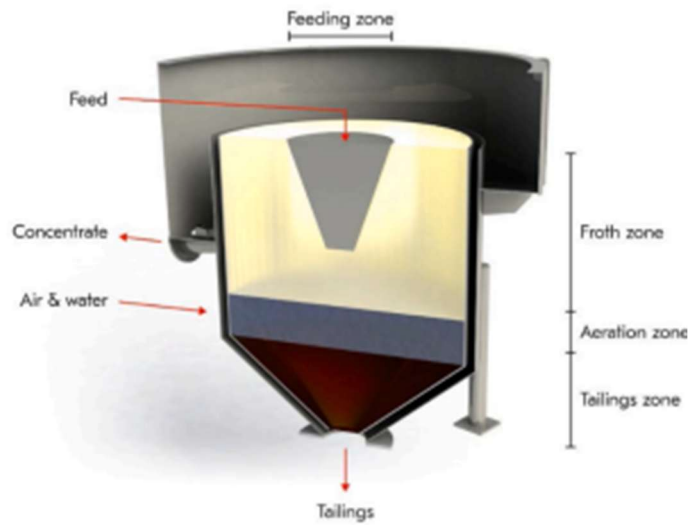


Figure 2.5: Schematic of Metso's Froth Feeding CPF [23].

Crompton et al. [21] performed tests on low-grade chalcopyrite feed with a top size of 530  $\mu\text{m}$  fed continuously to a CoarseAIR™ unit. 90% overall recovery was achieved at a mass pull of 40%. High upgrade around 5x was achieved between 100 and 400  $\mu\text{m}$ , dropping off above 500  $\mu\text{m}$ , and dropping sharply below 100  $\mu\text{m}$  due to entrainment. In a separate study, Crompton et al. [22] conducted tests with low-grade chalcopyrite ore screened to a top size of 530  $\mu\text{m}$ . These tests were performed at almost double the throughput as in the previous study [21]. An overall recovery of 84% was achieved. In the coarse particle fraction (+90  $\mu\text{m}$ ), 73% recovery of Cu at a yield of 19.1% was achieved, while in the fine particle fraction (-90  $\mu\text{m}$ ), a Cu recovery of 99.1% at a yield of 75% was achieved [22].

## 2.5 Froth Feeding

Recently, Metso has developed a new CPF technology [23]. Unlike the other CPF technologies discussed, it is not based on a fluidized bed. It has not been officially named and will be referred to as Froth Feeding CPF for clarity in this paper. The cell shown schematically in Figure 2.5 consists of a large upper froth zone, a smaller aeration zone, and a conical tailings zone at the bottom of the cell. Unlike typical flotation technologies, feed is introduced directly to the froth rather than the pulp. By feeding particles directly into the froth phase, detachment due to turbulence in the pulp phase and detachment during crossing the pulp froth barrier is avoided. Another advantage of Froth Feeding CPF is that it uses less water than CPF technologies based on fluidized beds because it does not require upward fluidization water [23].

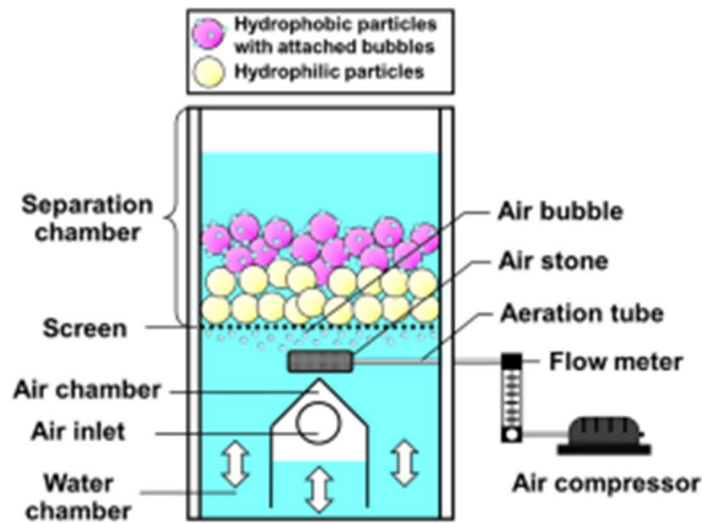


Figure 2.6: Schematic of a batch Hybrid Jig [25].

A laboratory unit of this cell has been tested in a continuous manner using copper ore with a  $d_{80}$  of  $360\ \mu\text{m}$  and a Cu grade of 0.83% [23]. High overall recovery of 89.6% was achieved at 58.9% yield with 81.9% recovery in the  $+150\ \mu\text{m}$  portion [23]. Pilot-scale testing was performed with the cell operating as a tails scavenger on tails with a  $d_{80}$  of  $166\ \mu\text{m}$  [24]. 63.4% recovery was achieved without classification at 59% mass pull and a recovery of 61.5% in the  $+125\ \mu\text{m}$  portion. The majority of the mass pull was in the  $-125\ \mu\text{m}$  portion, so testing was performed with classified feed scalped to above  $125\ \mu\text{m}$ . With the scalped feed, 67% recovery was achieved with the same  $+125\ \mu\text{m}$  recovery of 61.5% and a lower mass pull of 45%. The yield for the coarse portion remained similar between the scalped and unscalped feed tests [24].

## 2.6 Hybrid Jig

Most of the flotation units described above are based on fluidized beds, which separate particles by settling velocity and therefore based on particle density and size. Jigging is a technology that separates particles exclusively by density. It achieves this by intermittent fluidization that causes particles to accelerate differentially based on their density instead of their diameter or cross-section. Hori et al 2009 [26] developed a jig capable of separating plastic particles with similar and even equal SGs, shown in Figure 2.6. By selectively attaching bubbles, the density difference between particles in the jig is enhanced. Batch tests were performed in this jig with 2-3mm plastic particles. 99.9% purity of hydrophobic particles was possible even for plastics of the same SG but different surface hydrophobicities [26]. Ito et al [25] conducted

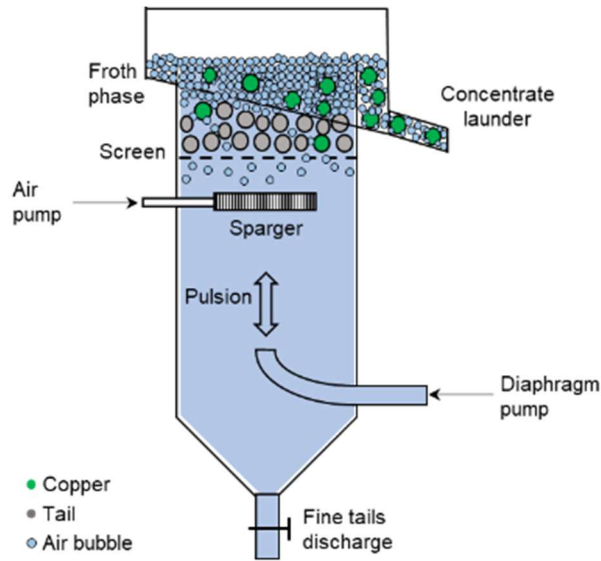


Figure 2.7: Schematic of a batch Jig Flotation cell [27].

tests using a continuous hybrid jig to separate 2-10mm PVC and PET particles. With the continuous hybrid jig, 50% recovery of PVC at 99% purity and 26% recovery of PET with 85% purity was achieved [25].

## 2.7 Jig Flotation

Similar to the hybrid Jig, Gupta and Yoon [27] developed a separation technique based on jiggling and flotation dubbed Jig Flotation for processing minerals, shown in Figure 2.7. Where the hybrid jig operates like a classical jig with a stratified bed that is split to take particles of different densities, Jig Flotation combines jiggling and flotation. Particles are preconcentrated by jiggling and recovered, through a froth by flotation. Particles must be buoyant to be recovered though heavier particles are rejected first.

In batch tests, particles were subjected to jiggling motion by water pulsation on top of a screen in a 1" diameter tube [27]. Below the screen, air bubbles were introduced via a diffuser. The cell was operated with a thin froth phase. Batch tests were performed on 212-600  $\mu\text{m}$  low-grade porphyry ore. 73.6% recovery and 10x upgrade were achieved.

## 2.8 Conclusion

The coarse particle flotation technologies reviewed in this chapter aim to mitigate bubble particle detachment, the main limitation for coarse particle recovery. The most common mechanism used in these technologies is an aerated fluidized bed in the case of HydroFloat™, NovaCell™, Reflux™ Flotation Cell, and CoarseAIR™. The advantage of the fluidized bed is that it suspends particles under quiescent

conditions, minimizing detachment; however, the particles can only be fluidized selectively at a narrow size range, so these technologies require a classification step. HydroFloat™ is able to float coarse particles and eliminates the buoyancy and froth recovery restrictions for coarse particles using an aerated fluidized bed, though it requires classification of feed. The NovaCell™ is able to float fine and coarse particles in a single unit by using two attachment zones, high shear for fine particles and low shear for coarse particles, and two recovery methods, froth flotation for fine particles and a drop back collection cone for coarse particles. This requires an internal classification circuit to separate the drawback product from unselectively lifted fines. The Reflux™ Flotation Cell uses downward fluidization to suspend bubbles instead of particles, creating a bubbly zone that minimizes froth phase detachment. Inclined channels at the base of the cell prevent loss of coarse low SG particles. The Reflux™ Flotation Cell is capable of rejecting fine particles with downward fluidization. This, however, requires higher buoyancy for recovery, and therefore, high SG minerals cannot be treated by the Reflux™ Flotation Cell. CoarseAIR™ uses an aerated fluidized bed and inclined channels to reject entrained fine gangue particles. The CoarseAIR™ can treat the full particle size range in feed, but due to reduced selectivity for fine particles, the product stream requires classification. The Froth Feeding CPF is not based on an aerated fluidized bed; instead, feed is introduced directly into the froth phase, eliminating the detachment due to turbulence in the pulp. Using Froth Feeding CPF, high recovery is achieved; however, like CoarseAIR™, selectivity is low at the fine fractions.

These technologies show great strides for coarse particle flotation. Recoveries of 80-90% for copper ores up to 850 µm have been achieved. There is room for improvement, particularly with regard to selectivity over a wide particle size range on mineral ores. Jig Flotation, an emerging technology, has shown promising results by combining the advantages of fluidized beds, jiggling, and flotation. With the incorporation of jiggling, it will be possible to treat a wider range of particle sizes selectively. The following chapter will report work done on the scale-up of this technology from lab-scale batch testing to pilot-scale continuous units.

## References:

- [1] M. J. Mankosa, J. N. Kohmuench, L. Christodoulou, and G. H. Luttrell, "RECOVERY OF VALUES FROM A PORPHORY COPPER TAILINGS STREAM," 2016. [Online]. Available: <https://api.semanticscholar.org/CorpusID:7172689>
- [2] J. N. Kohmuench, G. H. Luttrell, and M. J. Mankosa, "Coarse particle concentration using the HydroFloat Separator," *Min. Metall. Explor.*, vol. 18, no. 2, pp. 61–67, 2001, doi: 10.1007/BF03402873.
- [3] L. Vollert, B. Akerstrom, B. Seaman, and J. Kohmuench, "NEWCREST'S INDUSTRY FIRST APPLICATION OF ERIEZ HYDROFLOAT™ TECHNOLOGY FOR COPPER RECOVERY FROM TAILINGS AT CADIA VALLEY OPERATIONS," Vancouver, Aug. 2019.
- [4] B. Awatey, H. Thanasekaran, J. N. Kohmuench, W. Skinner, and M. Zanin, "Critical contact angle for coarse sphalerite flotation in a fluidised-bed separator vs. a mechanically agitated cell," *Miner. Eng.*, vol. 60, pp. 51–59, Jun. 2014, doi: 10.1016/J.MINENG.2014.02.009.
- [5] M. J. Mankosa, J. N. Kohmuench, P. Investigators, and E. Magnetics, "IN-PLANT TESTING OF THE HYDROFLOAT SEPARATOR FOR COARSE PHOSPHATE RECOVERY FINAL REPORT," 2002. [Online]. Available: <https://api.semanticscholar.org/CorpusID:55055389>
- [6] J. N. Kohmuench, M. J. Mankosa, D. G. Kennedy, J. L. Yasalonis, G. B. Taylor, and G. H. Luttrell, "Implementation of the HydroFloat technology at the South Fort Meade Mine," *Min. Metall. Explor.*, vol. 24, no. 4, pp. 264–270, 2007, doi: 10.1007/BF03403375.
- [7] J. N. Kohmuench, M. J. Mankosa, H. Thanasekaran, and A. Hobert, "Improving coarse particle flotation using the HydroFloat™ (raising the trunk of the elephant curve)," *Miner. Eng.*, vol. 121, 2018, doi: 10.1016/j.mineng.2018.03.004.
- [8] B. Awatey, H. Thanasekaran, J. N. Kohmuench, W. Skinner, and M. Zanin, "Optimization of operating parameters for coarse sphalerite flotation in the HydroFloat fluidised-bed separator," *Miner. Eng.*, vol. 50–51, pp. 99–105, Sep. 2013, doi: 10.1016/J.MINENG.2013.06.015.

- [9] J. D. Miller, C. L. Lin, Y. Wang, M. J. Mankosa, J. N. Kohmuench, and G. H. Luttrell, “SIGNIFICANCE OF EXPOSED GRAIN SURFACE AREA IN COARSE PARTICLE FLOTATION OF LOW-GRADE GOLD ORE WITH THE HYDROFLOAT™ TECHNOLOGY,” 2016.
- [10] G. J. Jameson and C. Emer, “Coarse chalcopyrite recovery in a universal froth flotation machine,” *Miner. Eng.*, vol. 134, pp. 118–133, Apr. 2019, doi: 10.1016/J.MINENG.2019.01.024.
- [11] S. Morgan and G. J. Jameson, “Improving mill throughputs, with coarse and fine particle flotation in the NovaCell™,” 2022.
- [12] G. J. Jameson, L. Cooper, K. K. Tang, and C. Emer, “Flotation of coarse coal particles in a fluidized bed: The effect of clusters,” *Miner. Eng.*, vol. 146, p. 106099, Jan. 2020, doi: 10.1016/J.MINENG.2019.106099.
- [13] J. E. Dickinson and K. P. Galvin, “Fluidized bed desliming in fine particle flotation – Part I,” *Chem. Eng. Sci.*, vol. 108, pp. 283–298, Apr. 2014, doi: 10.1016/J.CES.2013.11.006.
- [14] K. Jiang, J. E. Dickinson, and K. P. Galvin, “Two-stage fast flotation of coal tailings using reflux flotation,” *Miner. Eng.*, vol. 98, pp. 151–160, Nov. 2016, doi: 10.1016/J.MINENG.2016.08.010.
- [15] K. P. Galvin and J. E. Dickinson, “Fluidized bed desliming in fine particle flotation – Part II: Flotation of a model feed,” *Chem. Eng. Sci.*, vol. 108, pp. 299–309, Apr. 2014, doi: 10.1016/J.CES.2013.11.027.
- [16] K. P. Galvin, N. G. Harvey, and J. E. Dickinson, “Fluidized bed desliming in fine particle flotation – Part III flotation of difficult to clean coal,” *Miner. Eng.*, vol. 66–68, pp. 94–101, Nov. 2014, doi: 10.1016/J.MINENG.2014.02.008.
- [17] J. Chen, W. Chimonyo, and Y. Peng, “Flotation behaviour in reflux flotation cell – A critical review,” *Miner. Eng.*, vol. 181, p. 107519, May 2022, doi: 10.1016/J.MINENG.2022.107519.
- [18] A. E. BOYCOTT, “Sedimentation of Blood Corpuscles,” *Nature*, vol. 104, no. 2621, p. 532, 1920, doi: 10.1038/104532b0.

- [19] K. P. Galvin, J. Zhou, J. E. Dickinson, and H. Ramadhani, “Desliming of dense minerals in fluidized beds,” *Miner. Eng.*, vol. 39, pp. 9–18, Dec. 2012, doi: 10.1016/J.MINENG.2012.06.013.
- [20] J. L. Sutherland, J. E. Dickinson, and K. P. Galvin, “Flotation of coarse coal particles in the Reflux™ Flotation Cell,” *Miner. Eng.*, vol. 149, p. 106224, Apr. 2020, doi: 10.1016/J.MINENG.2020.106224.
- [21] L. J. Crompton, Md. T. Islam, and K. P. Galvin, “Investigation of Internal Classification in Coarse Particle Flotation of Chalcopyrite Using the CoarseAIR™,” *Minerals*, vol. 12, no. 6, 2022, doi: 10.3390/min12060783.
- [22] L. J. Crompton, M. T. Islam, and K. P. Galvin, “Assessment of the partitioning of coarse hydrophobic particles in the product concentrate of the CoarseAIR™ flotation system using a novel mechanical cell reference method,” *Miner. Eng.*, vol. 198, p. 108088, Jul. 2023, doi: 10.1016/J.MINENG.2023.108088.
- [23] M. De Avila Carvalho, I. Sherrell, C. Emer, and A. Rinne, “Enhanced coarse particle flotation: A novel approach,” *Physicochemical Problems of Mineral Processing*, vol. 61, no. 5, p. 211192, 2025, doi: 10.37190/ppmp/211192.
- [24] M. Carvalho *et al.*, “Advancing coarse particles recovery: Pilot trial of a novel flotation cell,” *Chemical Engineering Journal Advances*, vol. 24, p. 100879, Nov. 2025, doi: 10.1016/J.CEJA.2025.100879.
- [25] M. Ito *et al.*, “Development of suitable product recovery systems of continuous hybrid jig for plastic-plastic separation,” *Miner. Eng.*, vol. 141, p. 105839, Sep. 2019, doi: 10.1016/J.MINENG.2019.105839.
- [26] K. Hori, M. Tsunekawa, M. Ueda, N. Hiroyoshi, M. Ito, and H. Okada, “Development of a New Gravity Separator for Plastics—a Hybrid-Jig—,” *Materials Transactions - MATER TRANS*, vol. 50, pp. 2844–2847, Nov. 2009, doi: 10.2320/matertrans.M-M2009825.
- [27] M. Gupta and R.-H. Yoon, “IMPROVING COARSE PARTICLE FLOTATION BY CONTROL OF SURFACE AND HYDRODYNAMIC FORCES ,” *IMPC*, 2024.

- [28] S. Janishar Anzoom, G. Bournival, and S. Ata, “Coarse particle flotation: A review,” *Miner. Eng.*, vol. 206, p. 108499, 2024, doi: <https://doi.org/10.1016/j.mineng.2023.108499>.
- [29] B. Awatey, “Fluidised-bed flotation of coarse sulphide minerals: factors influencing value recovery,” 2015.
- [30] Marly de Availa Carvalho, Ian Michael Sherrell, and Enkhzul Bayarmagnai, “Slurry feeding arrangement,” US20250018404A1, Jan. 16, 2025
- [31] J. E. Dickinson, K. Jiang, and K. P. Galvin, “Fast flotation of coal at low pulp density using the Reflux Flotation Cell,” *Chemical Engineering Research and Design*, vol. 101, pp. 74–81, Sep. 2015, doi: 10.1016/J.CHERD.2015.04.006.
- [32] S. Farrokhpay and D. Fornasiero, “Flotation of coarse composite particles: Effect of mineral liberation and phase distribution,” *Advanced Powder Technology*, vol. 28, no. 8, pp. 1849–1854, Aug. 2017, doi: 10.1016/J.APT.2017.03.012.
- [33] D. Fornasiero and L. O. Filippov, “Innovations in the flotation of fine and coarse particles,” *J. Phys. Conf. Ser.*, vol. 879, no. 1, p. 012002, 2017, doi: 10.1088/1742-6596/879/1/012002.
- [34] Kevin Patrick Galvin, “Reflux classifier,” US6814241B1, 2000
- [35] Kevin Patrick Galving, “METHOD AND APPARATUS FOR SEPARATING LOW DENSITY PARTICLES FROM FEED SLURRIES,” US11981584B2, 2013
- [36] A. Gaudin, *Principles of Mineral Dressing*. McGraw-Hill Book Company, 1939.
- [37] D Gleason, “Newcrest leverages Eriez HydroFloat tech to help boost Cadia output,” *International Mining*.
- [38] M. T. Islam and A. V. Nguyen, “Bed expansion and gas holdup characteristics of bubble–assisted fluidization of liquid–particle suspensions in a HydroFloat cell,” *Miner. Eng.*, vol. 160, p. 106678, Jan. 2021, doi: 10.1016/J.MINENG.2020.106678.
- [39] M. T. Islam and A. V. Nguyen, “Effect of particle size and shape on liquid–solid fluidization in a HydroFloat cell,” *Powder Technol.*, vol. 379, pp. 560–575, Feb. 2021, doi: 10.1016/J.POWTEC.2020.10.080.

- [40] M. Ito *et al.*, “Improvement of hybrid jig separation efficiency using wetting agents for the recycling of mixed-plastic wastes,” *J. Mater. Cycles Waste Manag.*, vol. 21, no. 6, pp. 1376–1383, 2019, doi: 10.1007/s10163-019-00890-w.
- [41] M. Ito *et al.*, “Estimation of hybrid jig separation efficiency using a modified concentration criterion based on apparent densities of plastic particles with attached bubbles,” *J. Mater. Cycles Waste Manag.*, vol. 22, no. 6, pp. 2071–2080, 2020, doi: 10.1007/s10163-020-01090-7.
- [42] G. J. Jameson, “Advances in Fine and Coarse Particle Flotation,” *Canadian Metallurgical Quarterly*, vol. 49, no. 4, pp. 325–330, Oct. 2010, doi: 10.1179/cmqr.2010.49.4.325.
- [43] G. J. Jameson, “New directions in flotation machine design,” *Miner. Eng.*, vol. 23, no. 11–13, pp. 835–841, Oct. 2010, doi: 10.1016/J.MINENG.2010.04.001.
- [44] G. J. Jameson and C. Emer, “Effect of bubble loading on the recovery of coarse mineral particles by flotation,” *Miner. Eng.*, vol. 215, p. 108788, 2024, doi: <https://doi.org/10.1016/j.mineng.2024.108788>.
- [45] J. N. Kohmuench, M. J. Mankosa, G. H. Luttrell, and G. T. Adel, “Process engineering evaluation of the CrossFlow Separator,” *Min. Metall. Explor.*, vol. 19, no. 1, pp. 43–49, 2002, doi: 10.1007/BF03402900.
- [46] Michael J. Mankosa and Gerald H. Luttrell, “Air-assisted density separator device and method,” US 6,425,485 B1, 1999
- [47] M. J. Mankosa, J. N. Kohmuench, G. H. Luttrell, J. A. Herbst, and A. Noble, “SPLIT-FEED CIRCUIT DESIGN FOR PRIMARY SULFIDE RECOVERY \*,” 2016. [Online]. Available: <https://api.semanticscholar.org/CorpusID:108286634>
- [48] Mike Mankosa, “A New Paradigm in Sulphide Processing,” *Engineering and Mining Journal*, pp. 56–61, 2017.
- [49] M. J. Mankosa, J. N. Kohmuench, L. Christodoulou, and E. S. Yan, “Improving fine particle flotation using the StackCell™ (raising the tail of the elephant curve),” *Miner. Eng.*, vol. 121, pp. 83–89, Jun. 2018, doi: 10.1016/J.MINENG.2018.03.012.

- [50] S. Morgan, P. Amelunxen, B. Akerstrom, and L. Cooper, “Pinto Valley Mine, Copper Recovery Study with the NovaCell,” 2023.
- [51] S. Morgan, “283. NovaCell™ - Technology to Meet the World’s Future Copper Demands,” in *XXXI IMPC-International Mineral Processing Congress*, Society for Mining, Metallurgy, and Exploration (SME), 2024. [Online]. Available: <https://app.knovel.com/hotlink/pdf/id:kt01425FT7/impc-international-mineral/novacell-technology-meet>
- [52] Jesse Morton, “Flotation Innovations Increase Throughput, Recovery,” *Engineering and Mining Journal*.
- [53] H. Soto and G. Barbery, “Flotation of coarse particles in a counter-current column cell,” *Min. Metall. Explor.*, vol. 8, no. 1, pp. 16–21, 1991, doi: 10.1007/BF03402925.
- [54] Joshua Leigh Sutherland, “Flotation of coarse particles in the reflux flotation cell,” PHD, University of Newcastle, Newcastle, 2025.
- [55] L. Vollert, C. Haines, and W. Downie, “Coarse Separation - An Enabler for Improving the Sustainability of Ore Processing,” *Proceedings 26th World Mining Conference*, pp. 2891–2903, 2023.
- [56] Eric Bain Wasmund, “Flotation technology for coarse and fine particle recovery,” *I Congreso Internacional De Flotacion De Minerales*, 2014.
- [57] E. Wingate and J. Kohmuench, “An optimized approach to phosphate recovery,” *Beneficiation of Phosphates: Comprehensive Extraction, Technology Innovations, Advanced Reagents*, vol. 43, 2016.
- [58] M. Zanin, E. Chan, and W. Skinner, “Modelling the fluidised bed in HydroFloat™ for improved process control,” *Powder Technol.*, vol. 388, pp. 241–250, Aug. 2021, doi: 10.1016/J.POWTEC.2021.04.089.

## Chapter 3: Jig Flotation Scale Up

### 3.1 Introduction

70% of the energy used in mineral processing is used in comminution [1]. Decreasing the energy needed for comminution requires reducing the volume being ground and or increasing the grind size. CPF technologies can meet both of these needs by increasing the recoverable size range and rejecting gangue at coarser grind sizes before further grinding. Conventional flotation is only effective at a narrow particle size range (20-150  $\mu\text{m}$  for copper) [2]. Recovery drops off significantly as particle size increases above 150  $\mu\text{m}$ . As discussed in Chapter 1, the challenge of floating coarse particles is due to increased detachment probability in the pulp and froth phase due to the turbulence created in mechanically agitated flotation in the former and a combination of low bubble coalescence and buoyancy in the latter.

Flotation depends on surface forces, which gain importance with the square of particle size, while many of the detachment forces (gravity, centrifugal force, and buoyancy) gain importance with the cube of particle size. The difficulty in floating coarse particles arises from the body detachment forces becoming dominant over surface attachment forces holding particles and bubbles together. The two ways to prevent detachment would be to decrease the detachment forces and increase the attachment forces.

The strongest detachment force is centrifugal forces created by vortices created in turbulent cells. As discussed in Chapter 2, many CPF technologies use fluidized beds instead of mechanical agitation to minimize turbulence in the cell and therefore reduce detachment. In many of these methods, bubble particle aggregates move upward because their settling velocity is lower than the fluidization velocity. This, however, means that these cells can only operate at narrow particle size ranges, as settling velocity depends both on density and particle size. Small particles, relative to the target size, will unselectively rise, and very large particles, relative to the target size, will unselectively fall to the tails. Many of these technologies have mitigated this problem using a classification process before feeding in the case of HydroFloat™, within the cell, in the case of NovaCell™, and after processing, in the case of CoarseAIR™. A CPF technology that can process the full range of particle sizes selectively without classification would be ideal, as the

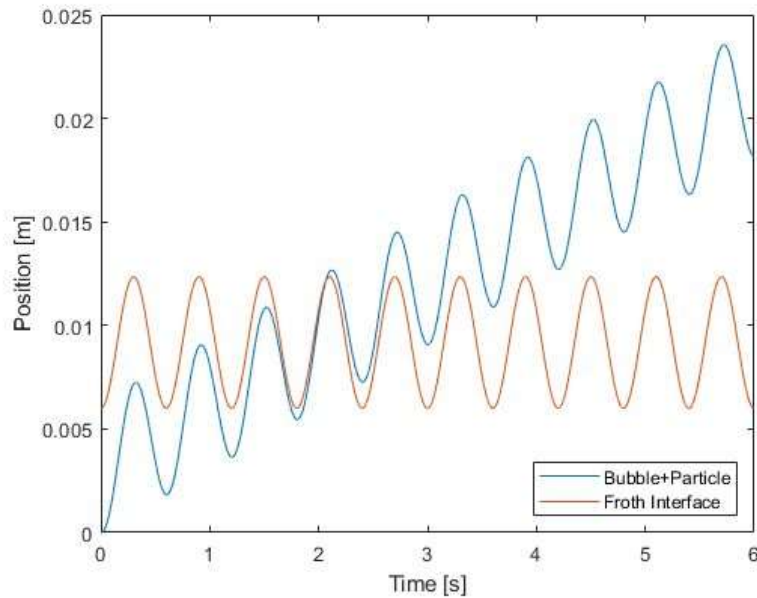


Figure 3.1: Movement of a bubble particle aggregate (blue) and the pulp froth interface (red) in a Jig Flotation cell showing the aggregate moving upward relative the pulp froth interface. requirement for classification increases circuit complexity, and the inefficiency of the classification must be considered when determining the efficiency of the CPF technology.

Jigging is a gravity separation technique that separates particles based on density regardless of particle size. It achieves this using an intermittent fluidized bed in which particles are separated by their initial acceleration, which depends on density and is independent of particle size. Ito et al. developed a hybrid jig for separating plastics with very similar specific gravities by attaching bubbles to the hydrophobic species to enhance the density difference [3].

Similar to the hybrid jig, Gupta and Yoon developed Jig Flotation, a process that combines the advantages of fluidized beds, jigging, and flotation [4]. In Jig Flotation, the jigging mechanism acts as an internal preconcentration within the cell before flotation. The SG of a target mineral (e.g., chalcopyrite with  $SG = 4.1$ ) is reduced to below that of gangue minerals (e.g., quartz with  $SG = 2.6$ ) by selectively adsorbing microbubbles ( $d_b=200-500 \mu\text{m}$ ). The copper-bearing particles segregate to the top of the bed by jigging action. The jigging action also acts as an intermittent fluidized bed with turbulence significantly less than that of a mechanically agitated cell. In tandem with the separation by jigging, particles are separated by flotation. In the flotation step, the apparent density of target mineral bearing particles is further reduced to

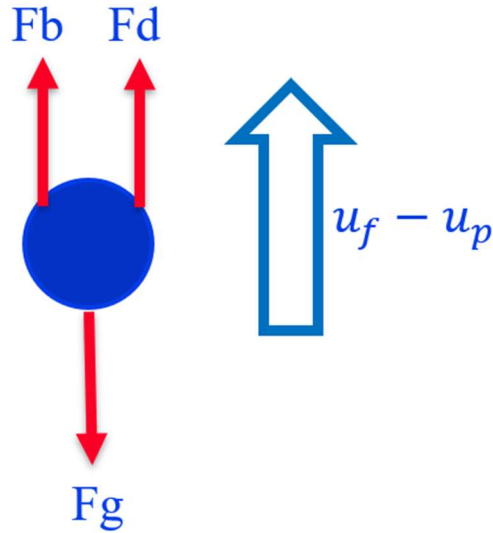


Figure 3.2: Force balance on a particle in the presence of upward fluidization.

below that of the medium using coarse bubbles ( $d_b = 100-3000 \mu\text{m}$ ), rendering them buoyant. Unlike a fluidized bed, liquid does not overflow the concentrate launder; instead, the pulp froth interface oscillates up and down with the jiggling motion. This allows for the formation of a froth phase because the bubble particle aggregate is buoyant and moves upward relative to the pulp froth interface, as shown in Figure 3.1. Maintaining a froth phase is particularly important for maintaining selectivity for fine particles that are easily entrained. The acceleration created during the pulsion cycle allows the bubble-particle aggregates to cross the pulp/froth interface and form a froth phase, in which less hydrophobic particles drop off bubbles to obtain cleaner froth products. Additionally, this higher relative motion leads to particles reporting to the concentrate launder faster than by fluidization, resulting in higher throughput.

### 3.2 Modelling Jig Flotation

The movement of a particle in a jig can be calculated from the force balance shown in Figure 3.2. The equation for the net force on the particle, or bubble particle aggregate treated as a single body, is thus given by

$$m \cdot \frac{du_p}{dt} = Fb - Fg + Fd \quad 3.1$$

where  $m$  is the mass of the particle,  $\frac{du_p}{dt}$  is the acceleration of the particle,  $Fb$  is the buoyancy force,  $Fg$  is the force of gravity, and  $Fd$  is the force of drag, which will be in the direction of flow relative to the particle.

For a bubble particle aggregate, the buoyancy is given by

$$F_b = (V_p + V_b)\rho_f g \quad 3.2$$

where  $V_p$  is the volume of the particle,  $V_b$  is the volume of the bubble,  $\rho_f$  is the density of the medium. For a bubble particle aggregate, the mass of the bubble is negligible; therefore, the force of gravity can be calculated as

$$F_g = mg \quad 3.3$$

assuming Stokes' drag, the drag force on the particle is given as

$$F_d = 3\pi\mu d(u_f(t) - u_p(t)) \quad 3.4$$

where  $\mu$  is the viscosity of the medium,  $d$  is the characteristic length of the particle, which can generally be taken as the diameter of the bubble, as it will generally be significantly larger than the particle,  $u_f$  is the fluid velocity, which in the case of jiggling varies with time, and  $u_p$  is the velocity of the particle. The acceleration of the particle can be solved for in Equation 3.1 using Equation 3.4, resulting in

$$\frac{du_p}{dt} = \frac{F_b - F_g}{m} + \frac{3\pi\mu d}{m}(u_f(t) - u_p(t)) \quad 3.5$$

Equation 3.5 can be converted to a linear ordinary differential equation of the form

$$\frac{du_p}{dt} + C_2 \cdot u_p(t) = C_1 + C_2 u_f(t) \quad 3.6$$

where  $C_1$  and  $C_2$  are

$$C_1 = \frac{F_b - F_g}{m} \quad 3.7$$

$$C_2 = \frac{6\pi\mu d}{m} \quad 3.8$$

respectively. Using the general solution to a linear ordinary differential equation, Equation 3.6 can be solved for the velocity of the particle as

$$u_p = e^{-C_2 t} \left( \int (C_1 + C_2 u_f(t)) \cdot e^{C_2 t} dt + K_1 \right) \quad 3.9$$

where  $K_1$  is an integration constant that depends on the initial velocity of the particle. The pulsation of fluid within the jig can be modelled as a sinusoid, with the position and velocity given as

$$x_f = A \sin(\omega t) \quad 3.10$$

$$u_f = A\omega \cos(\omega t) \quad 3.11$$

respectively, where A is the pulsation amplitude, and  $\omega$  is the angular frequency. Using Equation 3.11, Equation 3.9 can be solved as

$$u_p = \frac{C_1}{C_2} + K_1 e^{-C_2 t} + A\omega C_2 \frac{C_2 \sin(\omega t) - \omega \cos(\omega t)}{C_2^2 + \omega^2} \quad 3.12$$

The terms of Equation 3.12 reveal some aspects of the movement of particles in the jig. The first term is the terminal velocity of the particle in quiescent conditions. The second term is an exponential decay. The first two terms combined are the exponential decay to terminal velocity in quiescent conditions. The third term is the particle's velocity due to the oscillation of the fluidization. The addition of cosine and sine terms indicates that there is a phase offset between the fluidization velocity and particle velocity. This suggests that the motion of the particle in the jig can be thought of conceptually as settling and oscillating components occurring simultaneously.

From Equation 3.12, the acceleration and position of the particle can be calculated as

$$a_p = -C_2 K_1 e^{-C_2 t} + A\omega^2 C_2 \frac{C_2 \cos(\omega t) + \omega \sin(\omega t)}{C_2^2 + \omega^2} \quad 3.13$$

$$x_p = \frac{C_1}{C_2} t - \frac{K_1}{C_2} e^{-C_2 t} - AC_2 \frac{C_2 \cos(\omega t) + \omega \sin(\omega t)}{C_2^2 + \omega^2} + K_2 \quad 3.14$$

respectively. Assuming  $u_p(0)=0$  and  $x_p(0)=0$ , the integration constants are

$$K_1 = -\frac{C_1}{C_2} + A\omega C_2 \frac{\omega}{C_2^2 + \omega^2} \quad 3.15$$

$$K_2 = \frac{K_1}{C_2} + \frac{AC_2^2}{C_2^2 + \omega^2} \quad 3.16$$

Using the analytical solutions in Equations 3.12-3.14, the movement of a particle in Fig Flotation has been graphed in Figure 3.3.

In addition to the analytical model, a numerical model using a forward Euler integration method was used to model the movement of a particle in the Jig Flotation using Equation 3.1 to calculate the acceleration of the particles. Stability was achieved by decreasing the time step size until a stable solution was observed. As shown in Figure 3.3, the result exactly matches the analytical solution.

This model is not a complete description of the mechanisms at play in Jig Flotation. First, only vertical motion has been accounted for. Lateral movement due to turbulence or non-uniform flow within

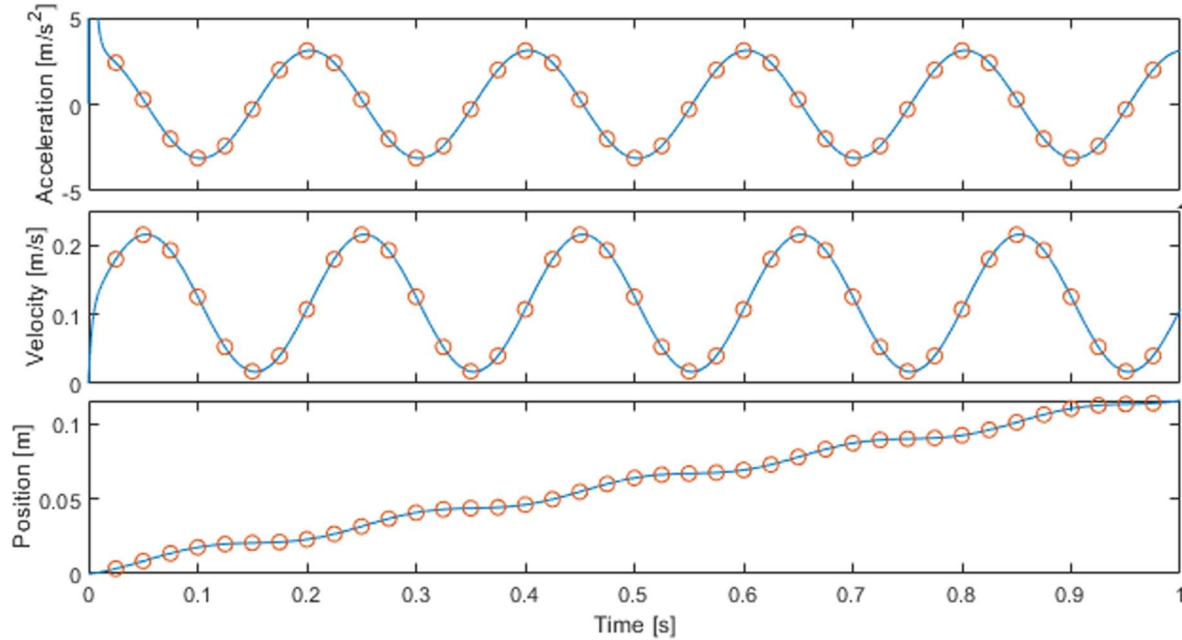


Figure 3.3: Analytical (blue) and numerical (red) simulation of the movement of a bubble particle aggregate in a Jig Flotation cell.

the cell has not been considered. Particle-particle interactions have not been accounted for. These would result in a higher apparent medium density, which should enhance differences in initial acceleration. Finally, it has been assumed that particles are settling in the Stokes' flow regime. However, jiggling operates in an intermediary regime between Stokes' and Newtonian drag [5]. The implementation of these aspects should be a subject of future work. This current model is, however, sufficient to give an idea of the mechanisms at work during jig operation.

### 3.3 Test Work

Following the work of Yoon and Gupta [4], a study was conducted to scale up the Jig Flotation concept from a 1-inch diameter batch cell to a pilot-scale continuous unit. First, a 2-inch diameter batch cell was constructed to test scale-up. Next, an 8x2-inch continuous cell was constructed to test continuous operation. Finally, a continuous pilot scale unit was constructed, and a conventional jig was modified to demonstrate the operation of Jig Flotation at scale. In the following sections, the tests and their results at each stage will be described.

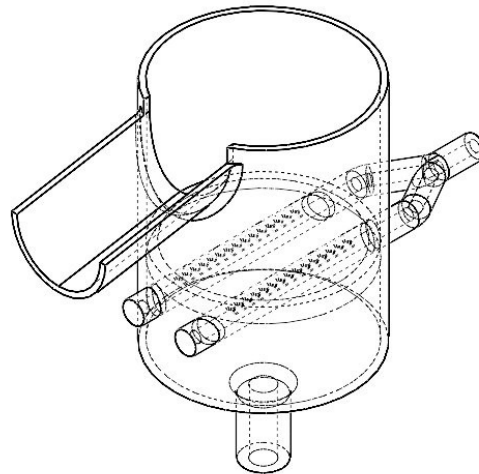


Figure 3.4: Schematic of 2inch batch Jig Flotation cell.

### 3.3.1 Two Inch Jig Flotation Cell

Batch tests were performed using the 2-inch diameter cell shown in Figure 3.4. Material was preloaded on a screen that allowed water but not particles to pass. Jigging action was produced using a modified diaphragm pump, and bubbles produced using a diffuser. Material floating over the top into the chute was taken as cons, and material remaining after 3 minutes was taken as tails.

Figure 3.5 shows the results of batch flotation tests conducted on a porphyry copper ore sample assaying 0.3 %Cu. The sample was wet ground in a rod mill to a d80 of 400  $\mu\text{m}$  and then screened to obtain a -425+210  $\mu\text{m}$  mono-size sample with a 0.2 %Cu grade. Three sets of tests were conducted at different

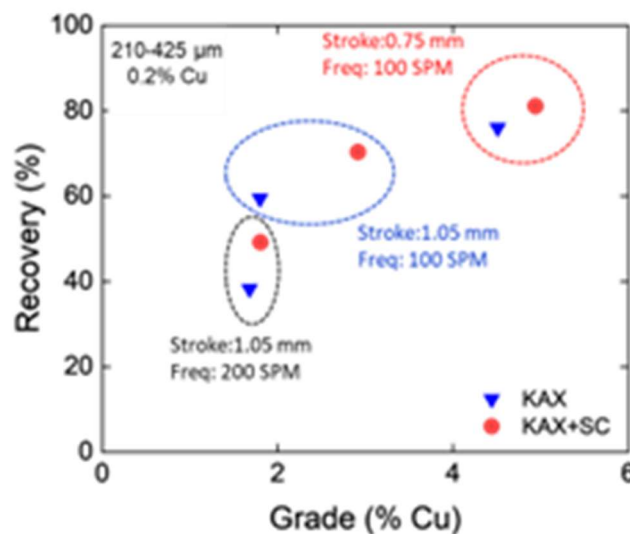


Figure 3.5 Jig Flotation test results based on 210-425  $\mu\text{m}$  copper-quartz composite particles from a copper flotation plant operating in Australia.

amplitudes and frequencies of the jiggling pulsion. In each set, two different extenders were used: diesel and Super Collector (SC), along with KAX to selectively hydrophobize the copper-bearing species. Diesel+KAX gives contact angles in the range of  $80^\circ$ , while KAX+SC gives contact angles above  $150^\circ$  [4]. The work of adhesion increases with contact angle, which should help improve coarse particle flotation by reducing detachment.

According to Gaudin [5], jiggling becomes more efficient at higher frequencies. The results presented in Figure 3.5 show the contrary, which may be attributed to the observation that at higher frequencies, bubbles became smaller, making it difficult for bubble-particle aggregates to cross the pulp-froth interface. Furthermore, the bubble-particle aggregates may be broken at high frequencies due to higher acceleration and turbulence. At lower frequency and stroke, the breakage of bubble-particle aggregates may be minimized. The effect of frequency on flotation efficiency has therefore been observed to be more important than the effect of frequency on jiggling efficiency in these tests. At each set of parameters, tests were performed again with super collector, and therefore, a higher contact angle, showed both higher recovery and product grade. The results presented in Figure 3.5 suggest that control of particle hydrophobicity and control of hydrodynamic force are useful for coarse particle flotation. While some improvement is seen by enhancing the hydrophobicity of particles (i.e., using super collectors), a more significant improvement is seen when the hydrodynamics are controlled. This is in line with the expectation that body forces dominate at coarse particle size.

### 3.3.2 Continuous 8x2 Inch Jig Flotation Cell

Following 2-inch cell batch testing, a continuous 8x2-inch lab scale Jig Flotation cell was constructed, shown in Figure 3.6a. Feed was continuously fed to the cell by gravity using an overhead feed tank as shown in Figure 3.6b. As shown in Figure 3.6c, microbubbles were added via a frother water line. Macrobubbles were added via a diffuser, and jiggling action was produced using pressurized air similar to a Batac jig. In the continuous flotation cell, tails passed through ragging material and were collected from the bottom of the cell. The residence time for this continuous cell was measured as 0.5 minutes.

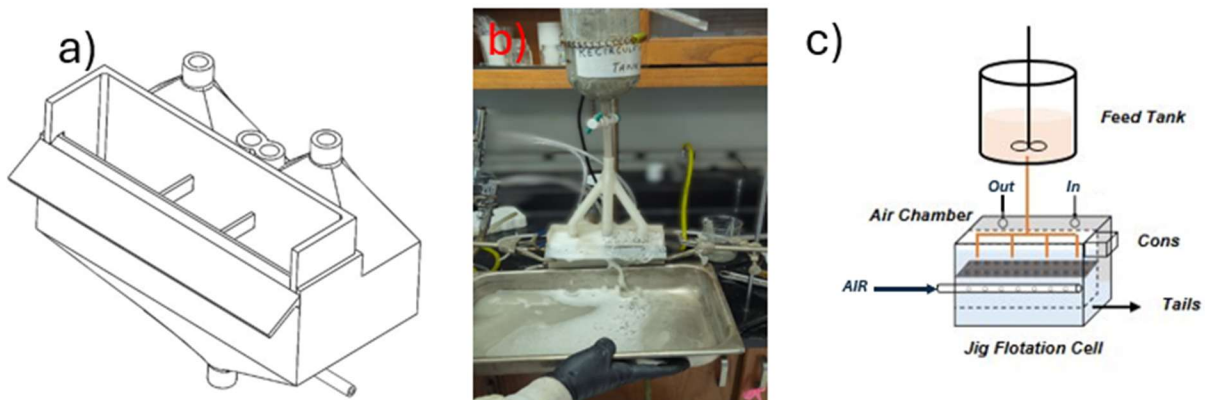


Figure 3.6: a) showing the schematic of an 8x2" continuous Jig Flotation Cell. b) showing a photo of an 8x2" Jig Flotation cell in operation. c) showing the process flow diagram for a continuous Jig Flotation cell.

A test series was performed to compare the effect of the inclusion of fine particles on continuous Jig Flotation. Figure 3.7 shows the grade and recovery across multiple single-stage tests on a porphyry copper sample. Sample was ground to two d80s, 225  $\mu\text{m}$  and 260  $\mu\text{m}$ , and not classified. Feed was prepared with 40 g/t KAX and 30 g/t SC. Frother water was prepared with PPG and MIBC. As compared with the 2 inch batch test the recovery decreased with the presence of fine particles. This may be due to a combination of lower collection efficiency for the fine particles in quiescent conditions and higher entrainment requiring lower mass pull to maintain grade. Additionally, it was observed that the inclusion of fine particles stabilized the froth layer, leading to a deeper froth. This may have resulted in coarse particles struggling to enter the froth and higher detachment. Finally lower recovery is achieved likely due to the lower residence time of the continuous jig compared with the batch tests which were performed for 3 minutes.

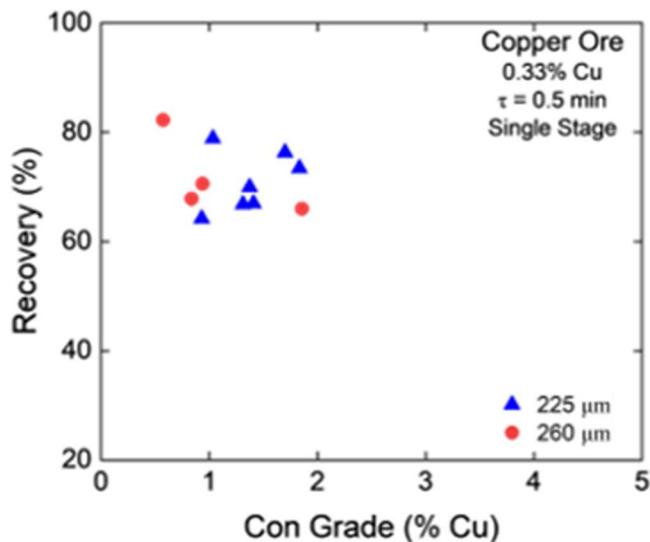


Figure 3.7: Grade vs. recovery for several continuous Jig Flotation tests on by-zero porphyry copper sample.

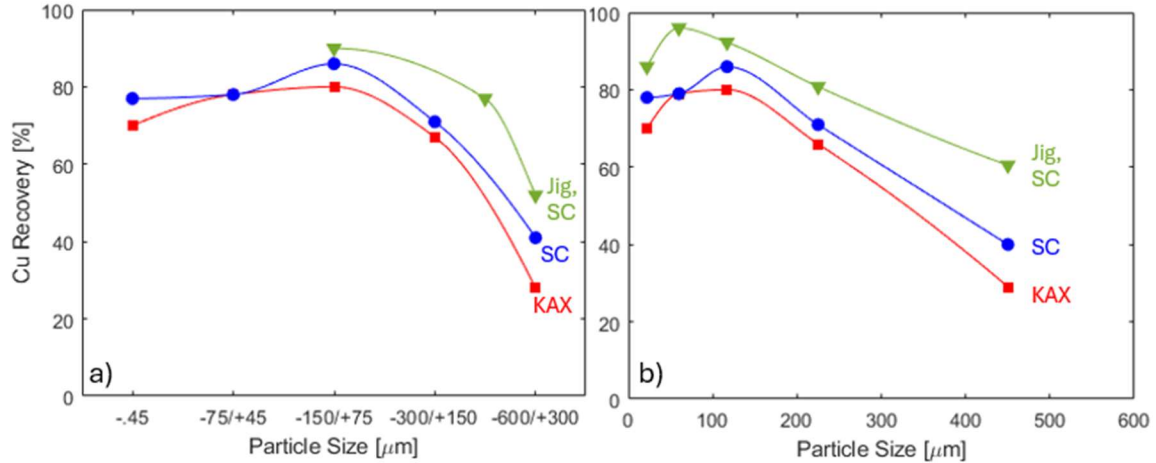


Figure 3.8: a) Recovery by particle size for monosize samples for DenverCell flotation without super collector (red) with super collector (blue), and with super collector and Jig Flotation (green). b) Recovery by particle size with unclassified feed with DenverCell and KAX (red), DenverCell and super collector (blue), and Jig Flotation and super collector (green).

To assess the effect of particle size both with and without desliming, tests were performed with several size fractions independently, and with the full particle size range present in the feed, and the recovery determined for each size class. Figure 3.8a shows recovery using different monosize samples compared with DenverCell tests with and without super collector. Super collector shows an increase in recovery across the board, except for at the ideal size for flotation, likely because there is little room for improvement on the flotation kinetics at this size fraction. The addition of jigging showed a greater increase in recovery. It is important to note that the residence time was lower in Jig Flotation tests as compared to batch Denver Cell tests. In the test results shown in Figure 3.8, the residence time for the continuous Jig Flotation cell was 0.5 minutes, and the residence time for the Denver cell tests was 8 minutes. These results are shown tabularly in Table 3.1, showing that these higher recoveries were achieved at high upgrade ratios. Figure 3.8b shows the size-by-size recovery for a continuous two-stage Jig Flotation test on the full particle size range sample. As compared to the results on monosized samples run independently, the coarse particle recovery in the presence of slimes is higher. This may be due to the stabilizing effect the fine hydrophobic particles have in the froth layer, reducing detachment due to bubble coalescence and increasing froth

Table 3.1: Recovery and upgrade ratio at different particle size ranges using Jig Flotation.

dp (μm)	Recovery (%)	Upgrade Ratio
<150	90.26	4.7
150-425	76.14	11.8
425-600	50.32	15.6

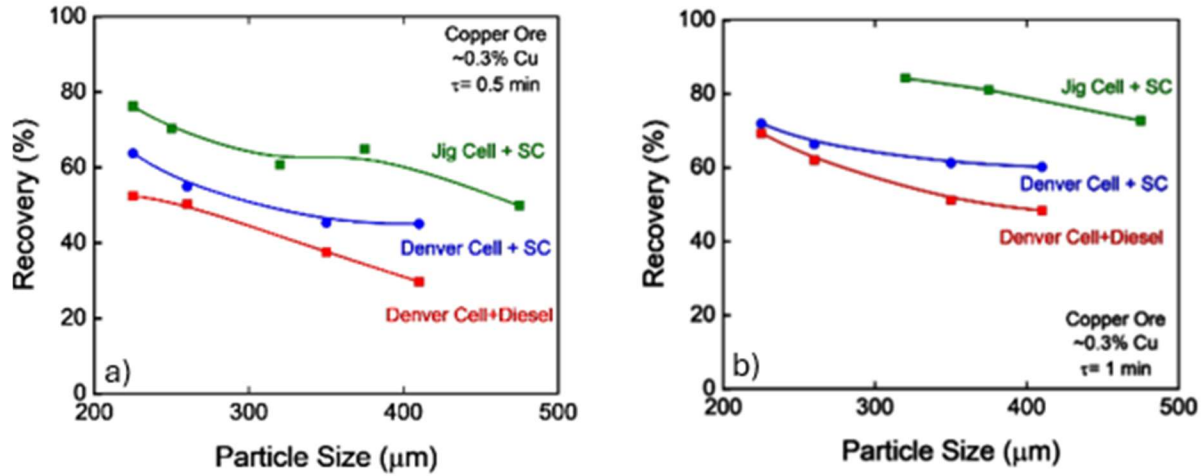


Figure 3.9: a) Copper recovery with Denver cell and single Jig Flotation tests conducted at different grind sizes represented by d80. b) Grade vs. recovery obtained with two stage Jig Flotation and DenverCell at a several grind sizes represented by d80. density, creating sufficient buoyancy for coarse particles to rise in the froth. For comparison, results using DenverCell with and without super collector are shown. There is a greater improvement in recovery with the presence of fines than without. The substantial improvement in flotation recovery stems from enhanced coarse particle flotation, as evidenced by the size-by-size recovery data shown in Table 3.2. By precisely controlling jiggling frequency and amplitude, particles were separated based on their specific gravity (SG), independent of particle size, leading to recovery improvements across the size ranges.

Figure 3.9a shows the results obtained on the feed ground to different d80s without classification in single stage continuous tests as described above. Also shown for comparison are the results obtained using a laboratory Denver flotation cell using KAX + Diesel and KAX+ SC. Similar to the results in Figure 3.8b, Jig Flotation shows markedly higher recovery at coarse d80s as compared to Denver cell flotation at much lower residence times. Figure 3.9b shows the same with a second stage of Jig Flotation performed on Table 3.2: Comparison of size-by-size grade and recovery obtained with Jig Flotation cell and DenverCell both using super collector.

Particle Size (µm)	Feed Grade (%Cu)	Jig Flotation Cell (w/ SC)				Denver Cell (w/ SC)	
		0.5 min		1 min		8 min	
		Recovery (%)	Grade (%Cu)	Recovery (%)	Grade (%Cu)	Recovery (%)	Grade (%Cu)
300-600	0.21	54.9	0.86	60.5	0.82	41.2	2.55
150-300	0.24	57.3	2.75	80.8	0.55	71.2	3.24
75-150	0.41	76.9	3.62	92.3	1.95	86.1	5.92
45-75	0.70	89.7	3.09	96.0	1.93	78.6	6.75
-45	0.54	71.7	0.80	86.0	0.65	77.5	6.73

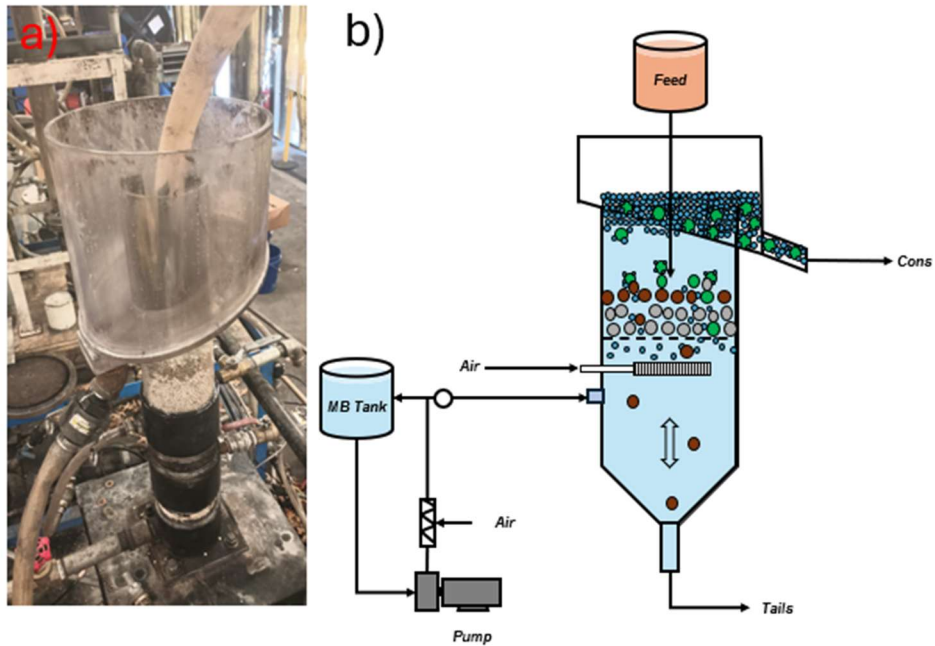


Figure 3.10: a) Modified Jig Morganizer for pilot scale Jig Flotation tests. b) Process flow of continuous pilot scale Jig Flotation tests.

the tails of the first stage for a total residence time of 1 minute. For comparison, the results from DenverCell flotation tests were conducted by taking samples at 0.5, 1, 2, and 8 minutes to obtain kinetic information at the same d80. The results demonstrate that the Jig Flotation cell consistently achieved high Cu recoveries with desirable grades at coarse grind sizes within short retention times. The Jig Flotation Cell achieves better recoveries than the Denver cell in 1/8<sup>th</sup> to 1/4<sup>th</sup> the time.

### 3.3.3 Pilot Scale Jig

Following the success with the lab scale continuous jig, a pilot scale Jig Flotation cell was constructed, shown in Figure 3.10a. The volume and throughput of this unit were much higher compared to the laboratory continuous Jig Flotation cell. Microbubbles can be added both in the feed stream and the microbubble stream. Microbubbles in the feed stream are intended to improve the collision probability for fine particles by preattaching bubbles in a high-turbulence environment. The frother water line is intended to add additional microbubbles to the jig and maintain the level in the jig. Macrobubbles are added via a diffuser installed below the raggging material; these are required to float coarser particles. Baffles divide the

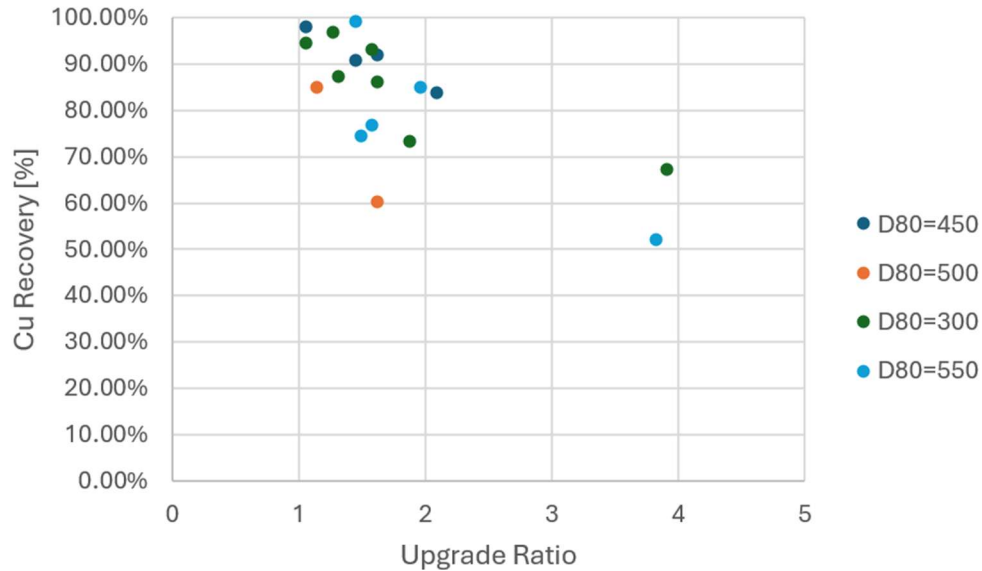


Figure 3.11: Upgrade vs. recovery for several preliminary continuous pilot scale Jig Flotation tests on feed ground to various d80s. This was added after it was observed that a resonance in the cell causes sloshing, which increased entrainment. The residence time for this jig was measured as 45 seconds.

#### Preliminary Tests:

Using the pilot scale Jig Flotation cell, preliminary tests were performed at various d80s. The feed was prepared at 25% solids with 40 g/t KAX and 30 g/t Diesel. The process flow diagram for the setup is shown in Figure 3.10 b). These tests were performed at various strokes and frequencies. These can be found in Appendix A. The results, shown in Figure 3.11, show high recovery regardless of d80. There is, however, a limited increase in grade. This would allow the Jig Flotation cell to be used as a reconcentration step at a larger grind size to reject gangue and reduce the volume going to final grinding by 50%. Following this, batch parameter tests were performed to optimize parameters to increase selectivity.

#### Batch Tests:

A batch test series was performed using the pilot Jig Flotation unit to determine the effect of several parameters (stroke, frequency, and diffuser air flow rate). A screen was placed in the cell to prevent the passage of particles but allow the passage of water. Feed was preloaded on the screen at the start of the test. Water was recycled through the microbubble circuit and reintroduced below the screen. The cell was pre-filled to the same level of frother water with 80 ppm of PPG 400 for each test. Particles reporting to the

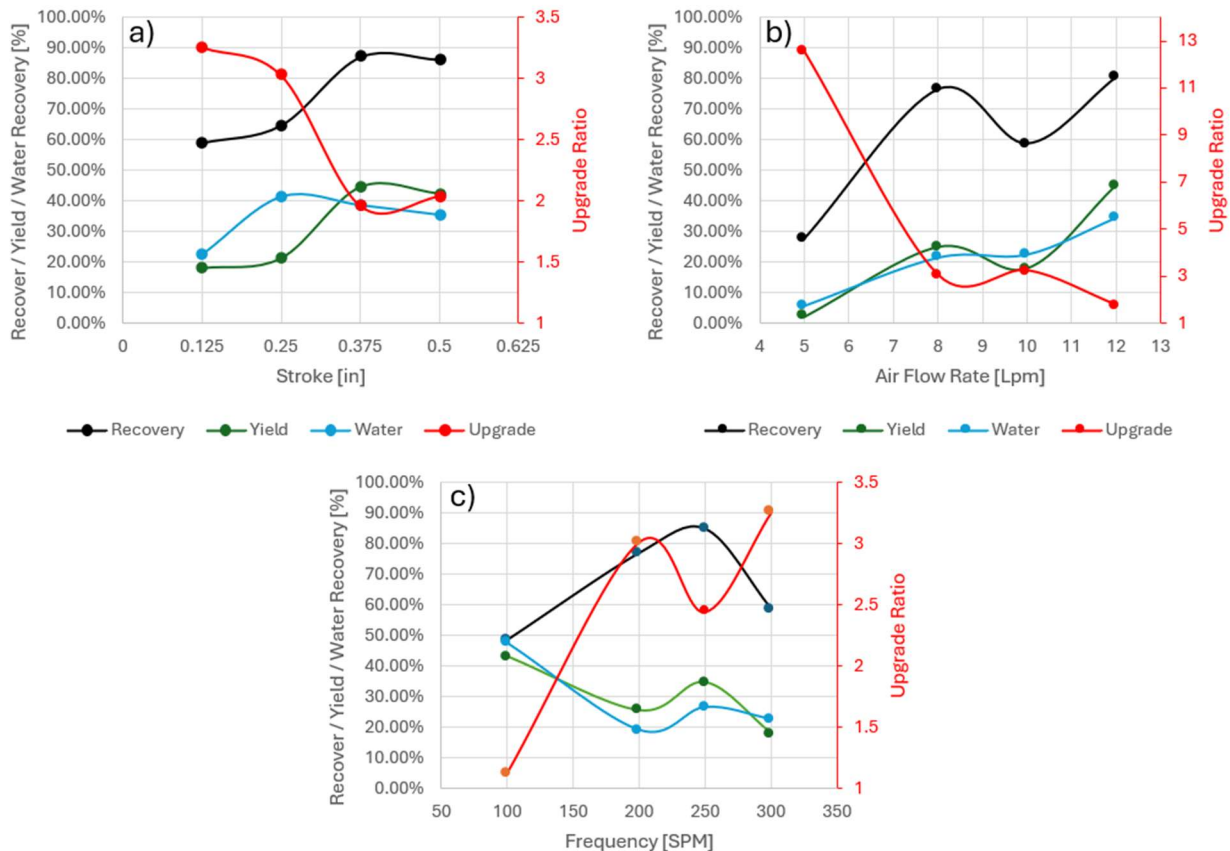


Figure 3.12: Copper recovery, particle yield, water recovery, and upgrade ratio a) with varying stroke, b) with varying diffuser air flow rate, and c) with varying frequencies. Note that the secondary vertical axis b) has a different scale than a) and c). concentrate launder were taken as concentrate samples, and particles remaining in the cell were taken as tails. The volume of water in the tails and concentrate samples was measured along with the mass of solids, and the copper concentration was measured by ICP-MS. The results of this test series are shown in Figure 3.12.

As expected, the mass yield and water recovery follow closely. When varying stroke and air flow rate, the copper recovery follows a similar trend to the product yield, indicating that selectivity is not affected by these parameters. Varying frequency, on the other hand, increases recovery independent of yield. In fact, yield decreased generally with increased frequency. The largest difference is seen at 200 strokes per minute (SPM). At 100 SPM, recovery and yield are very close, indicating the process is very unselective. Indeed, the upgrade ratio is 1.12. As frequency increases, the recovery and grade both generally increase, though there is a drop between 250 and 300 SPM. It may be that above 250 SPM, the higher speed pulsation starts to cause detachment of coarse particles. As expected, water recovery and yield increase with



Figure 3.13: Conventional jig modified for Jig Flotation.

increasing diffuser flow rate and increasing stroke. As a result of increased yield, the grade decreases with air flow rate and stroke, and recovery increases. The results show that frequency is the primary driver of selectivity in Jig Flotation. Interestingly, this shows an opposite trend as seen with the 2-inch batch flotation cell, where lower frequency produced higher selectivity and recovery. This may be due to the inclusion of fines in the tests with the pilot scale unit. According to Gaudin [5], high frequency allows for higher selectivity with a wider size range of particles. It may be that with the inclusion of fines, the importance of jiggling selectivity is greater. Along the same line of reasoning, the higher frequency may improve the collision efficiency for fine particles, and therefore, with the addition of fines, the recovery would improve with higher frequency.

### 3.3.4 Modified Conventional Jig

A conventional jig shown in Figure 3.13a was modified as shown in Figure 3.13b by adding a diffuser and increasing the bed height to accommodate froth. A test produced 70% recovery at an upgrade ratio of 2 at a  $d_{80}$  of  $600\mu\text{m}$ . This shows that only a small modification of existing jigs would be necessary to perform Jig Flotation. In this test, the froth and pulp height was shorter than that of other Jig Flotation cells tested, making it more similar to the hybrid Jig developed by Ito et al. [3]. The exploration of this type of Jig Flotation should be continued in future work.

### 3.4 Conclusion

Jig Flotation is capable of recovering a wider range of particle sizes without the need for classification. This is achieved due to a combination of separation by jiggling, maintaining a froth layer, and quiescent conditions. The jiggling motion preconcentrates particles by density, independent of particle size, and suspends particles while maintaining quiescent conditions. Because fluidization is oscillatory, a froth phase can be maintained, which increases the selectivity for fine particles. Quiescent conditions reduce detachment, the main limitation for coarse particles. In this work, the Jig Flotation concept developed by Yoon and Gupta [4] has been successfully scaled up to pilot-scale testing while maintaining these advantages. High recoveries at desirable upgrade ratios have been achieved in pilot-scale continuous units with retention times as low as 45 seconds with d80s as high as 600 $\mu$ m. This makes Jig Flotation ideal for preconcentration at coarse grind sizes to minimize the energy used in comminution.

## References:

- [1] C O'Connor, "Global Challenges Facing the Minerals Processing Industry," in *IMPC Eurasia*, 2019, pp. 1–10.
- [2] B. A. Wills and J. A. Finch, "Chapter 12 - Froth Flotation," in *Wills' Mineral Processing Technology (Eighth Edition)*, Eighth Edition., B. A. Wills and J. A. Finch, Eds., Boston: Butterworth-Heinemann, 2016, pp. 265–380. doi: <https://doi.org/10.1016/B978-0-08-097053-0.00012-1>.
- [3] M. Ito *et al.*, "Development of suitable product recovery systems of continuous hybrid jig for plastic-plastic separation," *Miner Eng*, vol. 141, p. 105839, Sep. 2019, doi: [10.1016/J.MINENG.2019.105839](https://doi.org/10.1016/J.MINENG.2019.105839).
- [4] M. Gupta and R.-H. Yoon, "IMPROVING COARSE PARTICLE FLOTATION BY CONTROL OF SURFACE AND HYDRODYNAMIC FORCES ," *IMPC*, 2024.
- [5] A. Gaudin, *Principles\_of\_Mineral\_Dressing*. McGraw-Hill Book Company, 1939.
- [6] W. M. Ambrós, "Jigging: A Review of Fundamentals and Future Directions," *Minerals*, vol. 10, no. 11, 2020, doi: [10.3390/min10110998](https://doi.org/10.3390/min10110998).
- [7] S. Janishar Anzoom, G. Bournival, and S. Ata, "Coarse particle flotation: A review," *Miner Eng*, vol. 206, p. 108499, 2024, doi: <https://doi.org/10.1016/j.mineng.2023.108499>.
- [8] V. Chipakwe, R. Jolsterå, and S. C. Chelgani, "Nanobubble-Assisted Flotation of Apatite Tailings: Insights on Beneficiation Options," *ACS Omega*, vol. 6, no. 21, pp. 13888–13894, 2021, doi: [10.1021/acsomega.1c01551](https://doi.org/10.1021/acsomega.1c01551).
- [9] M. FAN, D. TAO, R. HONAKER, and Z. LUO, "Nanobubble generation and its application in froth flotation (part I): nanobubble generation and its effects on properties of microbubble and millimeter scale bubble solutions," *Mining Science and Technology (China)*, vol. 20, no. 1, pp. 1–19, Jan. 2010, doi: [10.1016/S1674-5264\(09\)60154-X](https://doi.org/10.1016/S1674-5264(09)60154-X).
- [10] K. P. Galvin, S. J. Pratten, N. Lambert, A. M. Callen, and J. Lui, "Influence of a jigging action on the gravity separation achieved in a teetered bed separator," *Miner Eng*, vol. 15, no. 12, pp. 1199–1202, Dec. 2002, doi: [10.1016/S0892-6875\(02\)00211-X](https://doi.org/10.1016/S0892-6875(02)00211-X).

- [11] M. Gupta and R. H. Yoon, “Maximizing the recovery and throughput of a rougher flotation bank by improving the recovery of composite particles,” *Miner Eng*, vol. 207, p. 108545, Feb. 2024, doi: 10.1016/J.MINENG.2023.108545.
- [12] H. and N. A. and Y. R.-H. Gupta Mohit and Lim, “Optimizing Flotation Circuit Using a Model that Can Predict Both Grade and Recoveries,” in *12th International Copper Conference*, Cham: Springer Nature Switzerland, 2025, pp. 1669–1674.
- [13] J. and S. A. and Y. R.-H. Gupta Mohit and Leland, “Coarse Particle Recovery by Jig Flotation,” in *12th International Copper Conference*, Cham: Springer Nature Switzerland, 2025, pp. 1281–1287.
- [14] K. Hori, M. Tsunekawa, M. Ueda, N. Hiroyoshi, M. Ito, and H. Okada, “Development of a New Gravity Separator for Plastics —a Hybrid-Jig—,” *Materials Transactions - MATER TRANS*, vol. 50, pp. 2844–2847, Nov. 2009, doi: 10.2320/matertrans.M-M2009825.
- [15] B. K. Mishra and S. P. Mehrotra, “Modelling of particle stratification in jigs by the discrete element method,” *Miner Eng*, vol. 11, no. 6, pp. 511–522, Jun. 1998, doi: 10.1016/S0892-6875(98)00033-8.
- [16] H. J. Steiner, “A contribution to the theory of jigging, Part I: Similarity criteria of the motion of jig layers,” *Miner Eng*, vol. 9, no. 6, pp. 675–686, Jun. 1996, doi: 10.1016/0892-6875(96)00055-6.

## Chapter 4: Continuous Two Liquid Flotation Process Demonstration

### 4.1 Introduction

As discussed in Chapter 1, flotation is inefficient for ultrafine particles ( $\sim 20 \mu\text{m}$ ) due to low collision probabilities. An ultrafine flotation technology capable of recovering these particles would be able to recover high-grade product while reducing the costs and hazards associated with tailings disposal without the need to spend energy on comminution. Such a process has been developed at Virginia Tech. This process is known as hydrophobic-hydrophilic separation (HHS) [1]. HHS is capable of recovering ultrafine coal and producing a dry low-ash product [2], [3]. In this process, particles are collected by oil drops in place of air bubbles, as in traditional flotation. The oil, having a lower specific heat capacity than water, can be easily vaporized and recondensed to be reused. A full-scale HHS plant is currently in operation, treating screen-bowl effluent finer than  $44 \mu\text{m}$  in Alabama. This process is derived from the Two Liquid Flotation process developed by Lai and Fuerstenau (1968), who conducted experiments using oil (iso-octane) droplets in place of air bubbles to recover  $0.1 \mu\text{m}$  alumina particles [4]. This process of forming oil in water emulsions with hydrophobic particles as the emulsifier has practically no lower particle size limit.

The present work describes the development of an ultrafine particle flotation process based on the same principle of collection by a hydrophobic liquid in place of air bubbles used in the HHS process by continuous Two Liquid Flotation (TLF). This process is aimed at extending the effective particle size range as compared to HHS with a simplified process and therefore lower capital and operating costs. This process can treat thickener underflow (TUF), which consists of ultrafine particles not recoverable by traditional flotation. Thickener underflow represents a larger particle size range and a much larger stream volume than screen bowl effluent. Lab testing by Gupta et al. has been performed to confirm the continuous TLF process [5]. The following work outlines the development of a full-scale continuous pilot demonstration unit (PDU) to produce low-ash carbonaceous material using the TLF process.

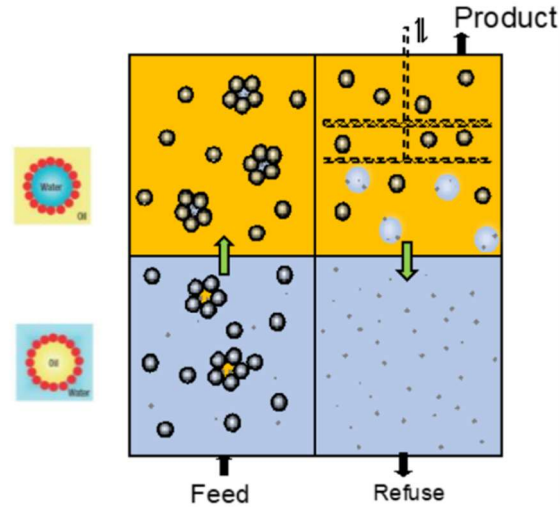


Figure 4.1: Continuous Two Liquid Flotation process shown schematically.

## 4.2 Theory

In the TLF process, oil and feed slurry are mixed in a low-shear environment. This produces loose oil in water emulsions stabilized by solids at the interface. By using oil in place of air bubbles to collect the hydrophobic particles, the vdW forces become attractive. As shown by Huang and Yoon [6], oil droplets form higher contact angles and rupture the thin liquid film faster than air bubbles due to the attractive vdW force. Once formed, the emulsions are fed to a phase separator where they undergo phase inversion, becoming water-in-oil emulsions. The oil phase containing these emulsions is fed to a specially designed Jig Organizer where further phase inversion occurs and the emulsions are broken by jiggling motion in the presence of hydrophilic ragging material [3]. The hydrophobic ragging material pulls the water and entrapped hydrophilic gangue out of the emulsions, leaving only the hydrophobic particles dispersed in the oil phase. The hydrophobic solids can be separated from the oil using a thickener and/or filter, and the oil reused in the process. The product can be further dried with heated nitrogen or steam, and the oil condensed for recycling.

The oil phase keeps out hydrophilic gangue, which effectively prevents entrainment, a major problem for fine, low-inertia particles. This process also produces a dry product with minimal energy input because dewatering by displacement is spontaneous and does not require additional energy. The oil can be vaporized with far less energy than water and at lower temperatures, greatly reducing the cost to produce dry product. In TLF, less energy is used to form and subsequently break strong emulsions than in HHS.

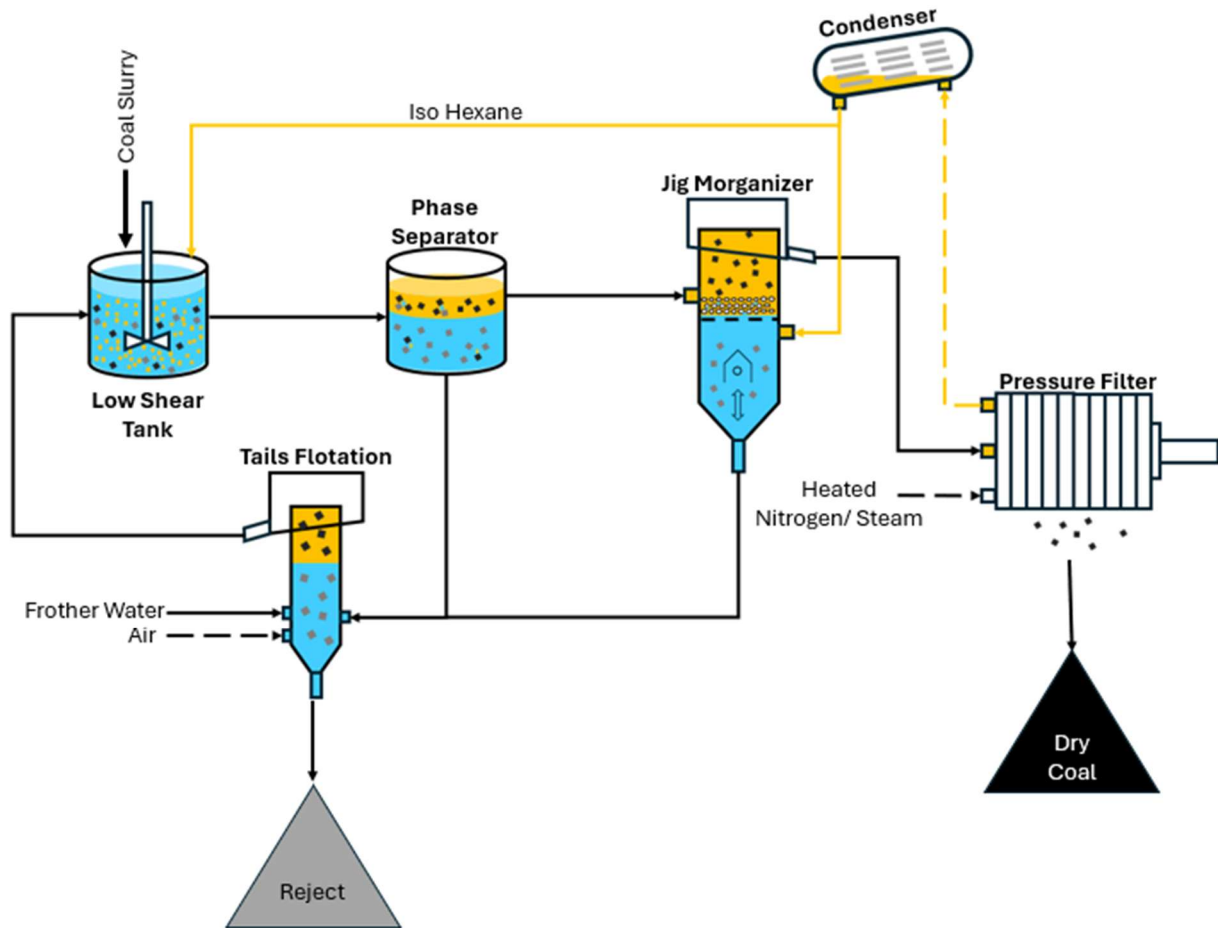


Figure 4.2: Flow sheet of continuous Two-Liquid Flotation process.

The emulsions formed using the TLF process are looser than the HHS process because of the lower amount of shear used to form them. This makes them easier to break. Figure 4.2 shows the flowsheet of the continuous TLF process

Figure 4.3 shows the initial installation of the TLF PDU. From right to left are the low shear tank where coal oil aggregates are formed, the phase separator where pre-concentration and phase inversion occur, the Jig Morganizer where emulsions are broken and water and ash rejected, the thickener where Morganizer product is collected, and the plate and frame filter where iso-hexane is recovered and recycled to the solvent tank. The tails from the Jig Morganizer and phase separator are sent to a flotation column to recover oil and coal, which are recycled to the low shear tank. Solvent and feed are fed to the mixing tank using continuous cavitation pumps to control flow rates precisely.

### 4.3 Experimental



Figure 4.3: Two-Liquid Flotation Process Demonstration Unit.

The PDU was tested on thickener underflow from several coal preparation plants. Results with each are discussed in separate sections below to allow for comparability. Throughout these tests, the flow sheet and parameters were modified in an effort to optimize the process. These modifications and their reasoning will be addressed. For practical reasons, these modifications stretch across multiple feeds; however, the feed samples were not found to have an impact on results, as shown by similarly high recovery and low ash and moisture across the samples tested. Therefore, the results due to changes in flowsheet and operation parameters can be confidently decoupled from changes in the feed sample tested.

#### 4.3.1 UCC Thickener Underflow

Tests were performed on the TUF sample procured from United Coal Company, Grundy, VA. As received, the sample contained 25% solids at 56.1% ash. The feed was diluted to 6-8% solids before each test. Tests were performed with the phase separator at feed and oil flow rates of 1 gpm and 0.6 gpm, respectively, and without the phase separator by feeding agglomerates directly from the low shear tank to the Jig Morganizer at feed and oil flow rates of 0.8 gpm and 0.6 gpm, respectively. Oil was recycled using the pressure filter. After filtration, the product was further dried with pressurized nitrogen. The evaporated oil was then condensed using a heat exchanger. Table 4.1 shows the ash and moisture content of the resulting



Figure 4.4: Phase separator upgrade.

product as well as the dry ash content of the flotation cell tails. These were used along with the feed ash to calculate the combustible recovery. Low moisture <2% was consistently achieved at low product ash as low as <1%. With the phase separator, the recovery was, however, low.

Higher recoveries were achieved without the phase separator than with. Additionally, the product grade was more consistent without the phase separator. This is partly because the process was easier to control in the absence of the phase separator. It is also possible that coarse particles drop out of the oil phase in the phase separator. In the absence of the phase separator, this might be eliminated. This is indicated by the slightly higher ash content in the product produced without the phase separator, as coarse particles in general are composite particles; therefore, the coarse particles recovery should increase the final product

Table 4.1: UCC Bailey TUF results obtained with and without phase separator.

Condition	Ash (%)			Moisture (%)	Yield (%)	Combustible Recovery (%)
	Feed	Product	Refuse			
With Phase Separator	56.10	2.52	71.0	0.95	21.78	48.36
	56.10	6.11	80.9	1.19	33.14	70.88
	56.10	0.63	62.5	0.41	10.32	23.35
Without Phase Separator	56.10	3.37	89.57	4.05	38.83	85.47
	56.10	2.76	85.53	2.50	35.56	78.76
	56.10	7.81	92.23	2.50	42.84	89.94
	56.10	2.60	76.0	1.02	27.11	60.15

ash. The disadvantage of this was that without a preconcentration step, the Jig Morganizer had to process the full flow rate of the system and became the limiting factor for throughput. It was hypothesized that the phase separator was not operating efficiently, and oil and coal were being lost to the phase separator tails. To address this, a taller transparent phase separator was installed, shown in Figure 4.4. This phase separator was expected to operate more efficiently and allow for easier process control.

#### 4.3.2 Itmann TUF Sample

Tests were performed on a feed sample from the Core Resources Itmann plant thickener underflow. The sample consisted of 47.4% ash. Tests were conducted after screening the feed sample to below 250  $\mu\text{m}$  and diluting to 6-8% solids. Table 4.2 shows a summary of results from several tests using the Itmann sample. With the new phase separator, higher recoveries are achieved with more consistent product quality. Before the last run, the height of the Jig Morganizer was increased to increase residence time; additionally, ragging material was added to increase the hydrophilic surface area. With these modifications, a distinct phase separation is visible as shown in Figure 4.5, indicating more efficient demulsification. The modification resulted in an improvement in product grade to 3.8% ash and final moisture content consistently below 2% at high recoveries. Size-by-size analysis was performed on the clean coal obtained from test run 4. Table 4.3 shows the clean coal ash and moisture content of the -250/+150  $\mu\text{m}$  and -150  $\mu\text{m}$  fractions. As shown in Table 4.3, high recovery and grades are achieved at both size fractions.

It was discovered that the previous pressure filter was oversized, which resulted in an inconsistent filter cake that was difficult to dry. A new, smaller, pressure filter was installed to dry the clean coal product. Following this installation, the PDU was run for 3 hours continuously to produce a large sample. This sample was then dried in the new filter press with heated nitrogen maintained at 50 to 60° C and 50 psi for

Table 4.2: Results obtained with TLF pilot plant with Itmann TUF feed - 250 $\mu\text{m}$ .

Run #	Ash (%)			Moisture (%)	Yield (%)	Combustible Recovery (%)
	Feed	Product	Refuse			
1	47.4	5.0	88.6	11.1	49.29	89.01
2	47.4	10.1	88.6	1.3	52.48	89.70
3	47.4	4.6	77.9	-	43.93	77.18
4	45.7	3.8	88.3	1.6	50.41	89.32



Figure 4.5: Extended Jig Morganizer with visible phase separation.

approximately 30 minutes. Due to issues with the nitrogen heating system, the drying time was not consistent; however, the sample was consistently dried to below 2% with no further drying required, and the final product ash was 5.2%.

#### 4.3.3 UCC Wellmore #8

With the modification of the phase separator and Jig Morganizer, the new limitation on throughput was the tails flotation column. A new, larger flotation cell was installed to address this. Tests were performed with as-received coal slurry from the United Coal Company Wellmore #8 thickener underflow. As received, the %solids was 25% and the ash content was 58.7% dry ash. Two tests are shown in Table 4.4 with and without scalping and dilution to determine if the TUF could be fed directly to TLF. In both tests, slurry was fed to the system at 0.4 gpm, and isohaxane was fed at 0.2 gpm.

Table 4.3: Size-by-size coal ash and recovery obtained on Itmann TUF.

Size (µm)	Ash (%)		Comb. Rec. (%)		Product Yield (%)	
	-150	250/150	-150	250/150	-150	250/150
Clean Coal	3.90	3.95	76.2	88.2	38.2	53.4
Tails	81.44	85.31	23.8	11.8		
Feed	85.31	41.89	100.0	100.0		

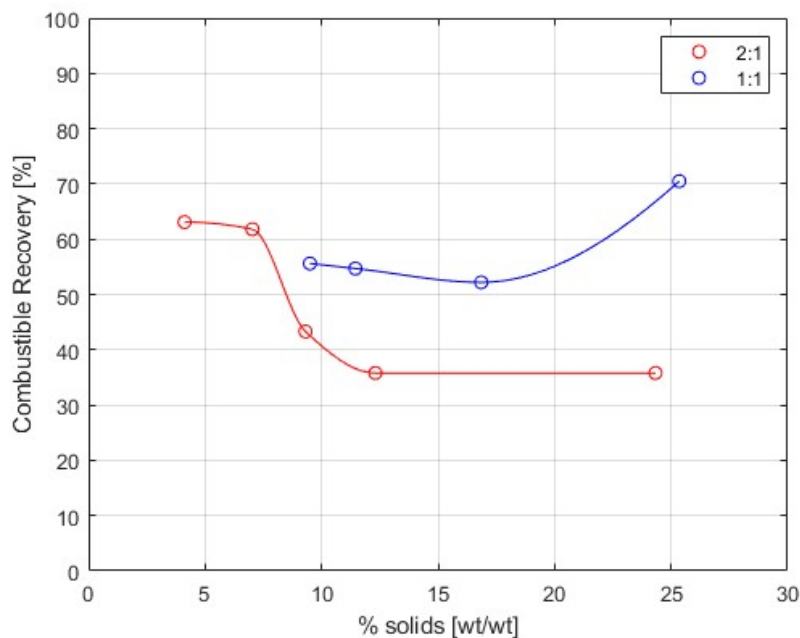


Figure 4.6: Combustible Recovery vs. Feed % solids at two different feed to solvent ratios. 1:1 shown in blue and 2:1 shown in red.

The production rate was increased by over 3 times while maintaining a similar final product ash. The recovery, however, was significantly reduced. It was hypothesized that the low recovery is due to insufficient oil to collect the larger amount of solids. To test this, a test series was performed at different % solids feeds. Feed slurry was added at 0.4 gpm and oil at 0.2 gpm. The emphasis for these tests was to maintain similar conditions between tests, so no adjustments were made to improve recovery during or between tests. Figure 4.6 shows the combustible recovery at different feed slurry %solids. There is a significant jump in recovery between 9.31% solids and 7.03% solids. This is in keeping with previous tests showing high recoveries when diluted to below 8% solids at similar ratios of oil to feed. Next, the proportion of oil was increased while maintaining the same overall flow rate. Feed and isohaxane were added at 0.3 gpm for a ratio of 1:1 feed to oil. As shown in Figure 4.6, this resulted in an increase in the recovery at higher % solids. This finding indicates that the ratio of the oil and feed is an important factor when varying the % solids in the feed.

Table 4.4: Increased throughput obtained on Wellmore #8 sample.

Product Ash%	Feed Rate [lpm]	%Solids	Product rate [kg/min]	Product rate [kg/hr]	Top Size [µm]	Combustible Recovery
2.98	1.134	8%	0.052	2.72	200	86.6
3.73	1.51	25%	0.218	8.76	As-recvd.	67.0

#### 4.4 Conclusion

In this work, a continuous Two-Liquid Flotation process has been successfully developed and demonstrated at scale. The experimental results show the capability of producing high-quality low-moisture product from thickener underflow consisting mainly of ultrafine particles. The process has been demonstrated on several thickener underflow samples consistently producing 2-5% ash product with <2% moisture.

Early on, the phase separator was identified as a source of carbon losses. By redesigning the phase separator to be taller, the recoveries were improved while increasing the potential throughput of the process. The residence time and amount of ragging material were also identified as key factors in the efficiency of demulsification in the Jig Organizer. The process has been proven on as-received thickener underflow without the need for classification or dilution, with the necessity of increasing the solvent dosage to account for increased solids content.

The TLF process demonstrated in this work has the potential to take waste material produced by coal beneficiation plants and recover nearly all of the carbonaceous material as high-quality carbon. This can be used to produce carbon products such as graphene for electric vehicle batteries or construction materials with significantly higher value than typical coal products. This is achieved while minimizing the waste sent to tailings impoundments. The TLF process has low energy and capital requirements due to the formation of weak emulsions and the simplicity of the process, making it easier to implement.

## References:

- [1] R.-H. Yoon, "Method of separating and de-watering fine particles," US9518241B2, 2016
- [2] N. Gupta *et al.*, "HHS Process: A New Approach for Recovering Fine Illinois Basin Coals," Nov. 2016.
- [3] B. Li, G. H. Luttrell, C. A. Noble, and N. Gupta, "Hydrophobic-Hydrophilic Separation Process for the Recovery of Ultrafine Particles," 2019.
- [4] R. Lai and D. Fuerstenau, "Liquid-liquid extraction of ultrafine particles," *Trans. AIME*, vol. 241, pp. 549–556, Nov. 1968.
- [5] M. Gupta, K. Huang, N. Youmans, B. Li, A. Noble, and R.-H. Yoon, "WO-LIQUID FLOTATION FOR THE RECOVERY OF ULTRAFINE PARTICLES ," *IMPC*, 2024.
- [6] K. Huang and R.-H. Yoon, "Surface Forces in the Thin Liquid Films (TLFs) of Water Confined between n-Alkane Drops and Hydrophobic Gold Surfaces," *Langmuir*, vol. 35, no. 48, pp. 15681–15691, Dec. 2019, doi: 10.1021/acs.langmuir.9b02102.
- [7] H. and N. A. and Y. R.-H. Gupta Mohit and Lim, "Optimizing Flotation Circuit Using a Model that Can Predict Both Grade and Recoveries," in *12th International Copper Conference*, Cham: Springer Nature Switzerland, 2025, pp. 1669–1674.
- [8] G. J. Jameson, "Advances in Fine and Coarse Particle Flotation," *Canadian Metallurgical Quarterly*, vol. 49, no. 4, pp. 325–330, Oct. 2010, doi: 10.1179/cmqr.2010.49.4.325.
- [9] G. J. Jameson, "New directions in flotation machine design," *Miner. Eng.*, vol. 23, no. 11–13, pp. 835–841, Oct. 2010, doi: 10.1016/J.MINENG.2010.04.001.
- [10] Mike Mankosa, "A New Paradigm in Sulphide Processing," *Engineering and Mining Journal*, pp. 56–61, 2017.
- [11] M. J. Mankosa, J. N. Kohmuench, L. Christodoulou, and E. S. Yan, "Improving fine particle flotation using the StackCell™ (raising the tail of the elephant curve)," *Miner. Eng.*, vol. 121, pp. 83–89, Jun. 2018, doi: 10.1016/J.MINENG.2018.03.012.

- [12] Eric Bain Wasmund, "Flotation technology for coarse and fine particle recovery," *I Congreso Internacional De Flotacion De Minerales*, 2014.
- [13] E. Wingate and J. Kohmuench, "An optimized approach to phosphate recovery," *Beneficiation of Phosphates: Comprehensive Extraction, Technology Innovations, Advanced Reagents*, vol. 43, 2016.

## Chapter 5: Conclusion

### 5.1 Introduction

Flotation is only effective in a narrow size range, typically 20-150  $\mu\text{m}$  [1]. Because of this, particles outside of this range are lost to tailings. In the case of ultrafine particles, this is due to low collision probability; this leads to a large amount of well-liberated particles that cannot be separated from process water in the tailings stream. This increases the volume of waste streams. As primary ore grades decrease, the grade of these tailings becomes higher than that of primary ore bodies; however, these particles cannot be recovered economically due to their low floatability [2]. An ultrafine particle recovery technology capable of recovering such material could take advantage of this higher-grade source without the need for further comminution. Such a technology needs to increase the flotation kinetics sufficiently to overcome low collision efficiency. One such technology, HHS, exists and is capable of treating -44 $\mu\text{m}$  coal tailing and producing low ash, low moisture carbonaceous product [3]. This process operates using high shear to form strong oil-in-water emulsions and subsequently breaks those emulsions after phase separation. This process is, however, limited in that high energy is used to form and break these emulsions, and the particle size is limited such that the wider size ranges in thickener underflow, which represents a larger source of tailings, cannot be treated.

In the case of coarse particles, low recovery is due to high detachment probability. The need to grind particles below this size leads to higher energy requirements in the comminution circuit. As ore grades decline this is exacerbated because ores become finer grained, requiring ores to be ground still further to achieve the same liberation, and as a higher percentage of these ores is made up of gangue, the majority of the energy is spent needlessly reducing the size of gangue particles [4]. A coarse particle separation technology would allow for the rejection of gangue particles at coarser grind sizes, thus reducing the volume through the grinding circuit. Several such technologies exist for this purpose, as discussed in Chapter 2. These have excelled at recovering coarse particles as large as 850  $\mu\text{m}$  employing various methods of reducing turbulence and therefore detachment in the cell; however, these mechanisms often lead to reduced selectivity at the fine fractions, requiring the use of classification. There is an opportunity to improve the

selectivity of fine particles. Jigging is a coarse particle separation technology that can operate selectively at wide size ranges and is the inspiration for the CPF technology presented in this work.

This work presents two technologies to address the need for separation technologies at extreme particle sizes that flotation cannot effectively separate. Jig Flotation for coarse particles and Two-Liquid Flotation for ultrafine and fine particle flotation. Jig Flotation takes advantage of volumetric properties that grow in importance with particle size, along with the surface properties that flotation employs by combining jigging and flotation. Additionally, because this technology uses an intermittent fluidized bed in the form of jigging motion, turbulence is minimized, and detachment due to centrifugal force is minimized. Jig Flotation has demonstrated the ability to recover coarse particles with grind sizes as large as 600  $\mu\text{m}$  while treating the entire size range selectively, all with an extremely low residence time and high throughput. In a plant, this means reduced footprint and capital costs. Two liquid flotation is capable of producing low-ash low-moisture product from ultrafine coal beneficiation plant tailings while recovering over 90% of coal. This is achieved by increasing the rate of flotation using higher contact angles due to the attractive vdW force between a hydrophobic particle and an oil drop [5], and dewatering by displacement, which occurs spontaneously. The continuous TLF process developed is simple and therefore has lower capital costs for implementation. The process also requires low energy due to the low shear used to produce and break aggregates, and the low energy required to vaporize and recycle oil, reducing operating costs. These two technologies are very promising for addressing the increasing demand for minerals in the face of declining ore grades. While reducing emissions by reducing energy consumption and reducing environmental impacts by reducing the volume of waste streams.

## **5.2 Future Work**

Though great strides have been made, these two technologies are in very early stages of development. Similar technologies mentioned in this work (HydroFloat™, HHS) have been in development for much longer and have seen successful demonstrations at the plant scale. Further work is recommended to optimize them further and prepare for full-scale demonstrations.

### 5.2.1 Jig Flotation

As discussed in Chapter 3, a simple analytical and numerical model for the movement of a bubble particle aggregate in Jig Flotation has been developed. This model does not, however, consider particle-particle interaction, horizontal mixing, and flow regimes beyond Stokes' drag. In a future work, a model that accounts for these should be developed. Discrete element modelling (DEM) could be used most directly to model particle-particle interaction in the jig. This would allow for the modelling of the bed of solids itself. A simpler method would be to model particle-particle interaction as an increased apparent density of the medium. This could be treated as a gradient throughout the height of the jig, calculated by the density of particles at a given height. This treatment has the advantage of being simpler; however, it would not model a bed of solids. The model of motion in Jig Flotation could be combined with flotation models to predict grade and recovery in Jig Flotation. The movement of various sizes of particles, bubbles, and bubble particle aggregates could be simulated in the jig using a Monte Carlo scheme. The calculated movement of the particles and bubbles could be used to calculate the probabilities of each subprocess of flotation as described in Chapter 1. For example, the detachment forces between bubble and particle could be tracked in the simulation and used to calculate the probability of detachment. The treatment of particle movement through the ragging material poses an interesting problem, as the jiggling motion in the presence of ragging material serves to selectively increase the residence time of low SG species and reduce the residence time of high SG species. This residence time could be used with the calculated rate constant to calculate recovery. Another treatment would be an additional probability term in Equation 1.1, given as the probability that the particle remains in the jig.

Further optimization and scale-up of the pilot-scale Jig Flotation cell would be beneficial. A larger prototype may be able to increase the residence time without the need for several stages. Increasing the residence time would prove that the high selectivity and recovery achieved with batch tests can be achieved with the same residence time in a continuous unit. The modification of a conventional jig for Jig Flotation showed promising results. This arrangement with concentrate flowing laterally through the cell may be a way to achieve higher residence times. The residence time in this jig was not measured, though it is

anticipated to be higher due to the multiple stages and higher volume. Additionally, the shorter pulp depth in this cell may emphasize the jiggling separation method, which should be more effective for separating coarse particles over recovery by flotation.

Finally, Jig Flotation has only been applied to chalcopyrite ores. Testing Jig Flotation on other types of ores should be undertaken to prove its universal applicability. Jig flotation on low SG minerals such as coal could be highly effective as the SG difference between product and gangue is favourable for the jiggling mechanism before the addition of bubbles.

### 5.2.2 Two Liquid Flotation

In lab testing, Two Liquid Flotation has been demonstrated to work on copper-bearing minerals [6]. Pilot-scale testing would demonstrate the universality of the Two Liquid Flotation process to be used for any ore type. The application of Two Liquid Flotation to higher SG minerals poses some interesting considerations. It is possible that due to the higher density of these minerals, they could be lost due to settling out of the hydrophobic phase. The use of fluorinated hydrocarbons offers a potential solution to this problem. Many of these have SG significantly higher than water. This would allow for the TLF process to be flipped, taking the concentrate product out of the bottom of the phase separator and Jig Organizer. In this way, gravity would act in favour of high SG mineral recovery; however, this could result in the reverse problem in which gangue is “entrained” by settling into the hydrophobic phase. Fluorinated hydrocarbons also offer several other advantages. They are less flammable than typical hydrocarbons; this could enhance the safety of the TLF process and reduce capital costs by reducing the number of controls required. Fluorinated hydrocarbons are also more hydrophobic than hydrocarbons, potentially increasing the kinetics of TLF. Fluorinated hydrocarbons do, however, pose an emissions risk as they are greenhouse gases. Lab testing of the TLF process using fluorinated hydrocarbons could assess these advantages.

## 5.3 Final thoughts

Extending the effective range of flotation is necessary in the face of increasing demand and decreasing ore grades to reduce the amount of material lost to tailings and decrease the energy consumption. Two technologies have been developed and demonstrated at continuous pilot scale in this work. Two liquid

flotation in the case of ultrafine particles, and Jig Flotation in the case of coarse particles. Both of these technologies improve upon alternatives in their selectivity at wide particle sizes, and combined, they allow for the recovery of the full range of particle sizes.

## References:

- [1] B. A. Wills and J. A. Finch, “Chapter 12 - Froth Flotation,” in *Wills’ Mineral Processing Technology (Eighth Edition)*, Eighth Edition., B. A. Wills and J. A. Finch, Eds., Boston: Butterworth-Heinemann, 2016, pp. 265–380. doi: <https://doi.org/10.1016/B978-0-08-097053-0.00012-1>.
- [2] R. B. Gordon, “Production residues in copper technological cycles,” *Resour. Conserv. Recycl.*, vol. 36, no. 2, pp. 87–106, Aug. 2002, doi: 10.1016/S0921-3449(02)00019-8.
- [3] N. Gupta *et al.*, “HHS Process: A New Approach for Recovering Fine Illinois Basin Coals,” Nov. 2016.
- [4] S. Northey, S. Mohr, G. M. Mudd, Z. Weng, and D. Giurco, “Modelling future copper ore grade decline based on a detailed assessment of copper resources and mining,” *Resour. Conserv. Recycl.*, vol. 83, pp. 190–201, Feb. 2014, doi: 10.1016/J.RESCONREC.2013.10.005.
- [5] K. Huang and R.-H. Yoon, “Surface Forces in the Thin Liquid Films (TLFs) of Water Confined between n-Alkane Drops and Hydrophobic Gold Surfaces,” *Langmuir*, vol. 35, no. 48, pp. 15681–15691, Dec. 2019, doi: 10.1021/acs.langmuir.9b02102.
- [6] M. Gupta, K. Huang, N. Youmans, B. Li, A. Noble, and R.-H. Yoon, “WO-LIQUID FLOTATION FOR THE RECOVERY OF ULTRAFINE PARTICLES ,” *IMPC*, 2024.

## Appendix A: Jig Flotation Data

Table A.1 Raw data for 2-inch circular jig.

Parameters						Collector	Extender		Frother			Results							
JF#	max d	min d	Freq [spm]	Stroke [% or lpm]	Diffuser Air [lmp]	PAX [g/ton]	Diesel [g/ton]	SC [g/ton]	MIBC [drops/uL]	Time [min]	Feed mass [g]	Con mass [g]	Tails Mass [g]	Yield	Con Grade	Tails Grade	Feed Grade	Recovery	Upgrade Ratio
30	425	250	150	70	2	20	20		4	2	4.29	0.73	3.56	17.0%	1.37	0.13	0.34	68%	4.01
31	425	250	150	70	2	20	20		4	2	7.2	0.87	6.33	12.1%	1.36	0.15	0.30	55%	4.59
32	425	250	150	70	2	20	20		4	2	8.26	0.93	7.33	11.3%	1.56	0.19	0.34	51%	4.55
33	425	250	150	80	2	20	20		4	2	4.75	0.38	4.37	8.0%	1.49	0.15	0.26	46%	5.80
39	425	250	200	60	2	20	20		4	3	15.13	1.15	13.98	92.4%	1.35	0.18	0.27	38%	4.95
40	425	250	200	70	2	20	20		4	3	13.58	0.44	13.14	96.8%	2.24	0.20	0.27	27%	8.32
41 C1	425	250	150	70	2	20	20		4	0.5		0.2	-0.2		0.22	0.18	0.18	2%	1.21
41 C2	425	250	150	70	2	20	20		4	0.5		0.17	-0.17		0.30				
41 C3	425	250	150	70	2	20	20		4	3		0.41	13.26		0.15				
41 C1 Net	425	250	150	70	2	20	20		4	0.5	13.58	0.2	13.38	1.5%					
41 C2 Net	425	250	150	70	2	20	20		4	1	13.58	0.37	13.21	2.7%					
41 C3 Net	425	250	150	70	2	20	20		4	4	13.58	0.78	12.8	5.7%					
42	425	250	150	70	2	20	20		4	2	14.71	1.17	13.54	8.0%	0.35	0.22	0.23	12%	1.53
43	425	250	150	60	2	20	20		4	2	13.2	0.38	12.82	2.9%	2.06	0.19	0.24	25%	8.62
44	425	250	200	60	2	20	20		4	2	12.24	1.25	10.99	10.2%	0.06	0.11	0.11	6%	0.60
50	425	210	150	70	1	20	20		4	3	14.85	0.75	14.1	5.1%	1.41	0.08	0.15	48%	9.59
51	425	210	150	60	1	20	20		4	3	7.44	0.88	6.56	11.8%	0.72	0.05	0.13	65%	5.51
52	425	210	200	60	2	20	20		4	3	11.23	0.36	10.87	3.2%	2.45	0.10	0.17	46%	14.32
53	425	210	150	60	2	20	20		4	3	11.01	0.54	10.47	4.9%	1.43	0.08	0.14	49%	9.99
54	425	210	100	60	2	20	20		4	3	10.3	0.44	9.86	4.3%	0.55	0.14	0.16	15%	3.45
55	425	210	200	70	1	20	20		4	3	14.55	0.46	14.09	3.2%	1.46	0.13	0.18	26%	8.31
56	425	210	150	70	1	20	20		4	3	10.07	0.88	9.19	8.7%	1.18	0.08	0.18	57%	6.54
57	425	210	200	70	3	20	20		4	3	7.57	1.87	5.7	24.7%	0.51	0.12	0.22	59%	2.38
58	425	210	100	70	1	20	20		4	3	14.15	0.62	13.53	4.4%	2.53	0.08	0.19	58%	13.32
59	425	210	100	60	3	20	20		4	3	6.42	0.6	5.82	9.3%	0.72	0.15	0.20	33%	3.58
60	425	210	150	60	1	20	20		4	3	8.87	1.52	7.35	17.1%	0.52	0.11	0.18	50%	2.92
61	425	210	200	80	3	20	20		4	3	9.96	0.98	8.98	9.8%	1.10	0.08	0.18	61%	6.22
62	425	210	100	80	3	20	20		4	3	5.7	0.54	5.16	9.5%	0.49	0.15	0.18	26%	2.75
63	425	210	100	60	2	20	20		4	3	5.11	0.19	4.92	3.7%	2.01	0.11	0.18	42%	11.19

64	425	210	100	60	2	20	20		4	3	7.86	0.6	7.26	7.6%	1.04	0.10	0.17	47%	6.21
65	425	210	100	70	3	20	20		4	3	3.04	0.3	2.74	9.9%	0.46	0.15	0.18	25%	2.56
66		425	150	70	1	20	20		4	3	8.76	0.3	8.46	3.4%	0.47	0.17	0.18	9%	2.62
67		425	150	60	1	20	20		4	3	9.91	0.58	9.33	5.9%	0.53	0.15	0.17	18%	3.13
68		425	200	60	2	20	20		4	3	9.48	0.19	9.29	2.0%	1.30	0.17	0.19	14%	6.79
69		425	150	60	2	20	20		4	3	9.61	0.29	9.32	3.0%	1.04	0.13	0.15	20%	6.71
70		425	100	60	2	20	20		4	3	9.26	0.31	8.95	3.3%	0.53	0.17	0.18	10%	2.94
71		425	200	70	1	20	20		4	3	9.57	0.23	9.34	2.4%	0.98	0.13	0.15	16%	6.53
72		425	150	70	1	20	20		4	3	9.28	0.3	8.98	3.2%	0.96	0.14	0.16	19%	5.83
73	425	210	200	40	3	40	20		4	3	6.78	0.37	6.41	5.5%	0.25	0.17	0.17	8%	1.46
74	425	210	200	50	3	40	20		4	3	9.28	0.5	8.78	5.4%	0.86	0.16	0.19	24%	4.42
75	425	210	150	60	3	40	20		4	3	8.08	0.79	7.29	9.8%	1.27	0.11	0.23	55%	5.66
76	425	210	150	70	3	40	20		4	3	7.64	0.42	7.22	5.5%	2.03	0.10	0.21	54%	9.76
77	425	210	100	70	3	40	20		4	3	9.57	0.67	8.9	7.0%	1.80	0.09	0.21	59%	8.49
78	425	210	150	40	3	40	20		4	3	9.59	0.9	8.69	9.4%	1.49	0.07	0.20	69%	7.40
79	425	210	150	50	3	40	20		4	3	8.82	0.57	8.25	6.5%	2.19	0.06	0.20	71%	11.05
80	425	210	200	60	3	40	20		4	3	10.26	0.52	9.74	5.1%	2.62	0.06	0.19	69%	13.54
81	425	210	200	70	3	40	20		4	3	9.02	0.35	8.67	3.9%	1.68	0.11	0.17	38%	9.86
82	425	210	100	50	3	40	20		4	3	10.12	0.48	9.64	4.7%	4.51	0.07	0.28	76%	16.02
83	425	210	200	40	3	40		30	4	3	9.82	0.68	9.14	6.9%	1.44	0.15	0.24	42%	6.09
84	425	210	200	50	3	40		30	4	3	8.46	0.74	7.72	8.7%	1.87	0.11	0.26	62%	7.07
85	425	210	150	60	3	40		30	4	3	8.46	0.45	8.01	5.3%	3.16	0.14	0.30	56%	10.47
86	425	210	150	70	3	40		30	4	3	7.66	0.69	6.97	9.0%	1.52	0.13	0.26	53%	5.89
87	425	210	100	70	3	40		30	4	3	8.7	0.54	8.16	6.2%	2.92	0.08	0.26	70%	11.33
88	425	210	150	40	3	40		30	4	3	9.67	0.84	8.83	8.7%	2.18	0.09	0.27	70%	8.01
89	425	210	150	50	3	40		30	4	3	8.81	0.55	8.26	6.2%	2.34	0.09	0.23	65%	10.35
90	425	210	200	60	3	40		30	4	3	8.12	0.53	7.59	6.5%	2.24	0.10	0.24	62%	9.45
91	425	210	200	70	3	40		30	4	3	7.38	0.55	6.83	7.5%	1.80	0.15	0.27	49%	6.60
92	425	210	100	50	3	40		30	4	3	8.3	0.48	7.82	5.8%	4.94	0.07	0.35	81%	14.02
93		425	200	70	3	40		30	4	3	7.19	0.67	6.52	9.3%	0.51	0.19	0.22	21%	2.28
94		425	200	70	3	40		30	4	3	7.57	0.27	7.3	3.6%	1.41	0.18	0.22	23%	6.40
95		425	200	70	3	40		30	4	3	8.77	1.12	7.65	12.8%	0.62	0.14	0.20	40%	3.11
96		425	200	70	3	40		30	4	3	8.47	0.69	7.78	8.1%	1.27	0.12	0.21	49%	6.01
97		425	200	80	3	40		30	4	3	8.86	0.24	8.62	2.7%	2.01	0.16	0.21	26%	9.78
98		425	200	90	3	40		30	4	3	7.59	0.7	6.89	9.2%	1.24	0.14	0.25	47%	5.06
99		425	200	100	3	40		30	4	3	8.21	0.9	7.31	11.0%	0.95	0.13	0.22	47%	4.26
100			100	50	3	40		30	4	3	12.45	0.45	12	3.6%	1.34	0.19	0.23	21%	5.86
101			200	50	3	40		30	4	3	12.96	1.56	11.4	12.0%	2.64	0.13	0.44	73%	6.06
102			200	70	3	40		30	4	3	13.75	1.76	11.99	12.8%	1.68	0.10	0.31	71%	5.51

103			100	70	3	40		30	4	3	9.54	1.41	8.13	14.8%	2.20	0.11	0.42	77%	5.23
104			150	60	3	40		30	4	3	7.3	1.96	5.34	26.8%	0.82	0.17	0.34	64%	2.38
105			150	50	3	40		30	4	3	9.06	1.72	7.34	19.0%	0.91	0.12	0.27	64%	3.38
106			150	70	3	40		30	4	3	9.13	1.79	7.34	19.6%	1.02	0.16	0.33	61%	3.12
107			200	60	3	40		30	4	3	12.14	4.57	7.57	37.6%	0.92	0.14	0.43	80%	2.12
108			100	60	3	40		30	4	3	11.03	1.68	9.35	15.2%	1.49	0.11	0.32	71%	4.65
115 c1			100	50	3	40		30	4	0.5	7.29	1.05	6.24	14.4%	1.04	0.16	0.29	53%	3.65
115 c2			100	50	3	40		30	4	0.5	6.24	0.66	5.58	10.6%	0.18	0.16	0.16	12%	1.14
115 c3			100	50	3	40		30	4	1	5.58	0.18	5.4	3.2%	0.12	0.16	0.16	2%	0.77
115 c4			100	50	3	40		30	4	2	5.4	0.07	5.33	1.3%	2.14	0.13	0.16	18%	13.65
115 c1 net			100	50	3	40		30	4	0.5	7.29	1.05	6.24	14.4%	1.04	0.16	0.29	53%	3.65
115 c2 net			100	50	3	40		30	4	1	7.29	1.71	5.58	23.5%	0.71	0.16	0.29	58%	2.48
115 c3 net			100	50	3	40		30	4	2	7.29	1.89	5.4	25.9%	0.65	0.16	0.29	59%	2.29
115 c4 net			100	50	3	40		30	4	4	7.29	1.96	5.33	26.9%	0.71	0.13	0.29	66%	2.47
116 c1			100	50	3	40		30	4	0.5	6.24	0.14	6.1	2.2%	3.86	0.23	0.31	28%	12.42
116 c2			100	50	3	40		30	4	0.5	6.1	0.31	5.79	5.1%	1.43	0.17	0.23	32%	6.24
116 c3			100	50	3	40		30	4	1	5.79	1.24	4.55	21.4%	0.24	0.15	0.17	31%	1.44
116 c4			100	50	3	40		30	4	2	4.55	0.72	3.83	15.8%	0.17	0.14	0.15	19%	1.17
116 c1 net			100	50	3	40		30	4	0.5	6.24	0.14	6.1	2.2%	3.86	0.23	0.31	28%	12.42
116 c2 net			100	50	3	40		30	4	1	6.24	0.45	5.79	7.2%	2.19	0.17	0.31	51%	7.04
116 c3 net			100	50	3	40		30	4	2	6.24	1.69	4.55	27.1%	0.76	0.15	0.31	66%	2.43
115 c4 net			100	50	3	40		30	4	4	6.24	2.41	3.83	38.6%	0.58	0.14	0.31	72%	1.87
117 c1			100	50	3	40	30		4	0.5	6.67	0.04	6.64	0.6%	4.15	0.32	0.35	7%	12.00
117 c2			100	50	3	40	30		4	0.5	6.64	0.12	6.52	1.8%	4.21	0.25	0.32	24%	13.06
117 c3			100	50	3	40	30		4	1	6.52	0.08	6.44	1.2%	2.23	0.23	0.25	11%	8.89
117 c4			100	50	3	40	30		4	2	6.44	0.12	6.32	1.9%	0.56	0.22	0.23	5%	2.47
117 c1 net			100	50	3	40	30		4	0.5	6.67	0.04	6.64	0.6%	4.15	0.32	0.35	7%	12.00
117 c2 net			100	50	3	40	30		4	1	6.67	0.16	6.52	2.4%	4.20	0.25	0.35	29%	12.13
117 c3 net			100	50	3	40	30		4	2	6.67	0.24	6.44	3.6%	3.54	0.23	0.35	37%	10.23
117 c4 net			100	50	3	40	30		4	4	6.67	0.36	6.32	5.4%	2.55	0.22	0.35	40%	7.36
118 c1			100	50	3	40	30		4	0.5	5.96	1.03	4.93	17.3%	0.88	0.16	0.29	53%	3.07
118 c2			100	50	3	40	30		4	0.5	4.93	0.16	4.77	3.2%	0.57	0.15	0.16	11%	3.50
118 c3			100	50	3	40	30		4	1	4.77	0.03	4.74	0.6%	3.99	0.12	0.15	17%	26.78
118 c4			100	50	3	40	30		4	2	4.74	0.41	4.33	8.6%	0.28	0.11	0.12	19%	2.25
118 c1 net			100	50	3	40	30		4	0.5	5.96	1.03	4.93	17.3%	0.88	0.16	0.29	53%	3.07
118 c2 net			100	50	3	40	30		4	1	5.96	1.19	4.77	20.0%	0.84	0.15	0.29	58%	2.92
118 c3 net			100	50	3	40	30		4	2	5.96	1.22	4.74	20.5%	0.92	0.12	0.29	65%	3.19
118 c4 net			100	50	3	40	30		4	4	5.96	1.63	4.33	27.3%	0.76	0.11	0.29	72%	2.64
119 c1			100	50	3	40		30	4	0.5	6.52	2.27	4.25	34.8%	0.87	0.22	0.45	68%	1.95

119 c2			100	50	3	40		30	4	0.5	4.25	0.02	4.23	0.5%	1.21	0.22	0.22	3%	5.47
119 c3			100	50	3	40		30	4	1	4.23	0.01	4.22	0.2%	1.65	0.21	0.22	2%	7.62
119 c4			100	50	3	40		30	4	2	4.22	0.29	3.93	6.9%	0.39	0.20	0.21	13%	1.83
119 c1 net			100	50	3	40		30	4	0.5	6.52	2.27	4.25	34.8%	0.87	0.22	0.45	68%	1.95
119 c2 net			100	50	3	40		30	4	1	6.52	2.29	4.23	35.1%	0.87	0.22	0.45	69%	1.95
119 c3 net			100	50	3	40		30	4	2	6.52	2.3	4.22	35.3%	0.88	0.21	0.45	69%	1.96
119 c4 net			100	50	3	40		30	4	4	6.52	2.59	3.93	39.7%	0.82	0.20	0.45	73%	1.84
120 c1			100	50	3	40		30	4	0.5	11.18	0.71	10.47	6.4%	5.11	0.16	0.47	69%	10.79
120 c2			100	50	3	40		30	4	0.5	10.47	0.14	10.33	1.3%	0.74	0.15	0.16	6%	4.65
120 c3			100	50	3	40		30	4	1	10.33	1.21	9.12	11.7%	0.24	0.14	0.15	19%	1.59
120 c4			100	50	3	40		30	4	2	9.12	1.9	7.22	20.8%	0.10	0.15	0.14	15%	0.72
120 c1 net			100	50	3	40		30	4	0.5	11.18	0.71	10.47	6.4%	5.11	0.16	0.47	69%	10.79
120 c2 net			100	50	3	40		30	4	1	11.18	0.85	10.33	7.6%	4.39	0.15	0.47	70%	9.27
120 c3 net			100	50	3	40		30	4	2	11.18	2.06	9.12	18.4%	1.95	0.14	0.47	76%	4.12
120 c4 net			100	50	3	40		30	4	4	11.18	3.96	7.22	35.4%	1.06	0.15	0.47	80%	2.25
121 c1			100	50	3	40	30		4	0.5	7.17	0.15	7.02	2.1%	9.93	0.20	0.40	52%	24.62
121 c2			100	50	3	40	30		4	0.5	7.02	0.21	6.81	3.0%	1.13	0.17	0.20	17%	5.66
121 c3			100	50	3	40	30		4	1	6.81	0.26	6.55	3.8%	0.49	0.16	0.17	11%	2.86
121 c4			100	50	3	40	30		4	2	6.55	0.55	6	8.4%	0.25	0.15	0.16	13%	1.58
121 c1 net			100	50	3	40	30		4	0.5	7.17	0.15	7.02	2.1%	9.93	0.20	0.40	52%	24.62
121 c2 net			100	50	3	40	30		4	1	7.17	0.36	6.81	5.0%	4.80	0.17	0.40	60%	11.89
121 c3 net			100	50	3	40	30		4	2	7.17	0.62	6.55	8.6%	2.99	0.16	0.40	64%	7.42
121 c4 net			100	50	3	40	30		4	4	7.17	1.17	6	16.3%	1.70	0.15	0.40	69%	4.22
122 c1			100	50	3	40	30		4	0.5	8.94	0.51	8.43	5.7%	4.89	0.21	0.48	58%	10.24
122 c2			100	50	3	40	30		4	0.5	8.43	0.37	8.06	4.4%	1.06	0.17	0.21	22%	5.04
122 c3			100	50	3	40	30		4	1	8.06	0.69	7.37	8.6%	0.37	0.15	0.17	18%	2.16
122 c4			100	50	3	40	30		4	2	7.37	1.18	6.19	16.0%	0.22	0.14	0.15	23%	1.44
122 c1 net			100	50	3	40	30		4	0.5	8.94	0.51	8.43	5.7%	4.89	0.21	0.48	58%	10.24
122 c2 net			100	50	3	40	30		4	1	8.94	0.88	8.06	9.8%	3.28	0.17	0.48	68%	6.87
122 c3 net			100	50	3	40	30		4	2	8.94	1.57	7.37	17.6%	2.00	0.15	0.48	74%	4.19
122 c4 net			100	50	3	40	30		4	4	8.94	2.75	6.19	30.8%	1.24	0.14	0.48	80%	2.59

Table A.2 8x2 inch Jig Flotation tests raw data.

Parameters				Collector	Extender	Results								
JF#	d80	Freq [spm]	Stroke [% or [pm]	PAX [g/ton]	SC [g/ton]	Feed mass [g]	Con mass [g]	Tails Mass [g]	Yield	Con Grade	Tails Grade	Feed Grade	Recovery	Upgrade Ratio
192	225	200	2	40	30	67.55	10.41	57.14	15.41%	1.83	0.12	0.38	73%	4.76
193	225	200	4	40	30	64.29	11.14	53.15	17.33%	1.41	0.15	0.36	67%	3.87
194	225	200	6	40	30	69.3	23.3	46	33.62%	1.03	0.14	0.44	79%	2.35
195	225	100	2	40	30	62.19	9.37	52.82	15.07%	1.37	0.10	0.30	70%	4.64
196	225	100	4	40	30	51.5	5.1	46.4	9.90%	1.70	0.06	0.22	76%	7.70
197	225	100	6	40	30	69.43	10.62	58.81	15.30%	1.31	0.12	0.30	67%	4.37
198	225	-	0	40	30	61.62	12.62	49	20.48%	0.93	0.13	0.30	64%	3.13
199	250	200	2	40	30	42.87	11.01	31.86	25.68%	0.94	0.14	0.34	71%	2.75
200	250	200	2	40	30	11.16	1.29	9.87	11.56%	1.86	0.12	0.32	66%	5.71
201	250	200	4	40	30	9.71	1.11	8.6	11.43%	1.27	0.18	0.30	48%	4.20
202	250	200	6	40	30	8.76	1.49	7.27	17.01%	0.84	0.08	0.21	68%	3.99
203	250	100	4	40	30	26.07	10.48	15.59	40.20%	0.57	0.08	0.28	82%	2.05
204 stage 1		200	2	40	30	112.36	32.18	80.18	28.64%	0.72	0.15	0.40	79%	1.80
204 stage 2		200	2	40	30	80.18	18.37	61.81	22.91%	0.40	0.08	0.15	58%	2.67
204 net		200	2	40	30	112.36	50.55	61.81	44.99%	0.60	0.08	0.40	92%	1.51
205 stage 1	475	200	6	40	30	95.85	37.05	29.4	38.65%	0.53	0.18	0.26	47%	2.04
205 stage 2	475	200	6	40	30	29.4	7.9	21.5	26.87%	0.35	0.12	0.18	51%	1.94
205 net	475	200	6	40	30	95.85	44.95	21.5	46.90%	0.50	0.12	0.26	71%	1.92
206	375	200	2	40	30	41.69996368	11.48	30.21996368	27.53%	0.99	0.12	0.36	76%	2.75
207	375	200	2	40	30	5.9	1.94	3.96	32.88%	0.72	0.10	0.30	77%	2.40
206&207	375	200	2	40	30								95%	
208	375	200	3	40	30	2.39	1.33	1.06	55.65%	0.24	0.03	0.15	91%	1.60
209	375	200	3	40	30	48.84	20.99	27.85	42.98%	2.51	0.14	0.36	65%	6.97
210	375	200	3	40	30	27.85	6.21	21.64	22.30%	0.29	0.09	0.14	52%	2.07
209&210	375	200	3	40	30								83%	
211	165	300	2	40	30	28.46	3.88	24.58	13.63%	0.83	0.18	0.27	42%	3.10
212	165	200	2	40	30	61.49	10.33	51.16	16.80%	0.91	0.12	0.25	61%	3.61
213	310	200	1	40	30	40.55	7.91	32.64	19.51%	0.95	0.14	0.30	62%	3.19

214	310	300	1	40	30	34.79	2.85	31.94	8.19%	1.54	0.27	0.37	34%	4.15
215	350	150	4	40	30	22.6	2.45	20.15	10.84%	1.18	0.17	0.28	46%	4.25
216	350	250	4	40	30	6.8	2.01	4.79	29.56%	1.08	0.13	0.41	78%	2.62
217	350	250	4	40	30	5.77	1.37	4.4	23.74%	0.70	0.23	0.34	49%	2.05
218	350	250	2	40	30	3.29	1.39	1.9	42.25%	0.41	0.28	0.33	51%	1.21
219	350	250	2	40	30	20.74	1.27	19.47	6.12%	3.27	0.17	0.36	56%	9.12
220	350	150	2	40	30	14.84	0.81	14.03	5.46%	4.48	0.15	0.39	63%	11.62
221	350	250	3	40	30	10.4	1.83	8.57	17.60%	1.90	0.19	0.49	68%	3.87
223	350	150	3	40	30	6.22	2.33	3.89	37.46%	0.55	0.29	0.38	53%	1.42
224		250	7	40	30	29.55	1.91	27.64	6.46%	3.31	0.18	0.38	56%	8.70
225		150	4	40	30	18.24	2.26	15.98	12.39%	1.50	0.21	0.37	50%	4.04
226		250	1.5	40	30	1.67	0.63	1.04	37.72%	3.37	0.26	1.43	89%	2.35
227		150	1	40	30	3.41	2.57	0.84	75.37%	0.38	0.15	0.33	89%	1.17

Table A.3: Pilot scale continuous Jig Flotation preliminary tests.

JM#	d80	Freq [spm]	Stroke [in]	Diffuser Air [lmp]	Micro Bubbles Flow Rate [lpm]	PAX [g/ton]	SC [g/ton]	PPG 400 [ppm]	Feed mass [g]	Con mass [g]	Tails Mass [g]	Yield	Con Grade	Tails Grade	Feed Grade	Feed Grade (Calculated)	Recovery (known Feed)	Recovery (Calculated Feed)	Upgrade Ratio (Known Feed)	Upgrade Ratio (Calculated Feed)
1	450	Low	High	20		40	0	20	16.16	10.3	5.9	63.6%	1.90	0.33	1.21	1.33	88.2%	91.1%	1.57	1.43
2	450	High	High	20		40	0	20	59.16	54.3	4.9	91.8%	1.42	0.36	1.21	1.34	94.1%	97.8%	1.18	1.07
3	450	High	High	20		40	0	20	20.80	11.8	10.3	56.9%	1.96	0.21	1.21	1.21	92.4%	92.4%	1.62	1.62
4	450	High	High	20		40	0	20	129.35	52.0	77.4	40.2%	2.61	0.33	1.21	1.25	83.0%	84.0%	2.16	2.09
4	-150								0			62.2%	2.69	0.36	1.81	1.81	92.4%	92.4%	1.49	1.49
4	+150								0			47.5%	1.48	0.22	0.82	0.82	85.8%	85.8%	1.81	1.81
5	500	300	Low	18		40	0	20	23.32	17.3	6.1	74.1%	1.02	0.54		0.90		84.5%		1.14
6	500	300	Low	18		40	0	20	78.13	29.2	49.0	37.3%	1.95	0.78		1.22		59.9%		1.61
7	300	300	0.25	20	4.5	40	0	80	38.8	35.2	3.6	90.7%	1.13	0.62	0.37	1.08		94.7%	3.05	1.04
8	300	200	0.375	20	4.5	40	0	80	70.7	47.2	23.6	66.7%	0.58	0.16	0.37	0.44	78.4%	87.9%	1.57	1.32
9	300	200	0.25	20	4.5	40	0	80	61.13	46.8	14.3	76.6%	1.78	0.18	0.37	1.40	57.1%	97.0%	4.81	1.27
10	300	200	0.125	20	4.5	40	0	80	35.64	13.9	21.8	38.9%	0.81	0.19	0.53	0.43	83.8%	73.1%	1.53	1.88
11	300	300	0.125	20	4.5	40	0	80	29.66	16.1	13.6	54.2%	0.99	0.18	0.53	0.62	80.7%	86.7%	1.87	1.60
12	300	100	0.125	20	4.5	40	0	80	17.45	3.0	14.5	17.1%	2.55	0.26	0.53	0.65	56.7%	66.9%	4.81	3.92
13	300	200	0.125	15	4.5	40	0	80	25.17	14.9	10.3	59.1%	2.16	0.21	0.53	1.36	66.9%	93.7%	4.08	1.59
14	300	200	0.125	10	4.5	40	0	80	58.97	2.9	56.0	5.0%	8.95	0.15	0.53	0.59	72.9%		16.89	
15	550	100	0.125	15	4.5	40	30	80	100.35	48.2	52.1	48.1%	0.94	0.27	0.50	0.59	64.5%	76.3%	1.88	1.59
16	550	100	0.125	10	4.5	40	30	80	34.43	17.3	17.1	50.2%	1.33	0.47	0.50	0.90	9.3%	74.1%	2.66	1.47
17	550	100	0.125	12.5	4.5	40	30	80	22.31	9.6	12.7	43.0%	3.02	0.39	0.50	1.52	25.3%	85.4%	6.05	1.99
18	550	200	0.125	12.5	4.5	40	30	80	53.38	36.9	16.5	69.1%	1.24	0.01	0.50	0.86	98.8%	99.6%	2.48	1.44
19	550	50	0.125	12.5	4.5	40	30	80	29.55	4.1	25.5	13.7%	3.10	0.45	0.50	0.81	11.7%	52.3%	6.20	3.81

Table A.4: Pilot scale continuous Jig Flotation batch tests.

JM#	d80	Freq [spm]	Stroke [in]	Diffuser Air [lmp]	PAX [g/ton]	Diesel [g/ton]	PPG 400 [ppm]	Time [min]	Feed mass [g]	Con mass [g]	Tails Mass [g]	Yield	Con Grade	Tails Grade	Feed Grade (Calculated)	Recovery (Calculated Feed)	Upgrade Ratio (Calculated)	Tails Water [mL]	Cons Water [mL]	Water recovery
28	325	250	0.125	8	20	20	100	0.25	1375.91	4.04			2.49%							
	325	250	0.125	8	20	20	100	0.75		10.02			3.55%							
	325	250	0.125	8	20	20	100	1.5		13.16			0.96%							
	325	250	0.125	8	20	20	100	3		9.66			4.16%							
	325	250	0.125	8	20	20	100	5		30.83			1.28%							
	325	250	0.125	8	20	20	100	7		5.76			2.58%							
	325	250	0.125	8	20	20	100	10.5		62.09	1240.35		1.44%	0.30%						
	325	250	0.125					0.25	1375.91	4.04	1371.87	0.29%	2.49%	0.44%	0.44%	1.65%	5.61			
	325	250	0.125					0.75	1375.91	14.06	1361.85	1.02%	3.24%	0.42%	0.44%	7.46%	7.30			
	325	250	0.125					1.5	1375.91	27.22	1348.69	1.98%	2.14%	0.41%	0.44%	9.53%	4.82			
	325	250	0.125					3	1375.91	36.88	1339.03	2.68%	2.67%	0.38%	0.44%	16.11%	6.01			
	325	250	0.125					5	1375.91	67.71	1308.2	4.92%	2.04%	0.36%	0.44%	22.58%	4.59			
325	250	0.125					7	1375.91	73.47	1302.44	5.34%	2.08%	0.35%	0.44%	25.01%	4.68				
325	250	0.125					10.5	1375.91	135.56	1240.35	9.85%	1.79%	0.30%	0.44%	39.60%	4.02				
29		250	0.125	8	40	30				33.6			0.47%							
		250	0.125	8	40	30				74.37			0.61%							
		250	0.125	8	40	30				58.96			0.37%							
		250	0.125	8	40	30				106.54			0.58%							
		250	0.125	8	40	30				106.3			0.79%	0.21%						
		250	0.125					0.25	649.97	33.6	616.37	5.17%	0.47%	0.44%	0.44%	5.55%	1.07			
		250	0.125					0.75	649.97	107.97	542	16.61%	0.57%	0.41%	0.44%	21.46%	1.29			
		250	0.125					1.5	649.97	166.93	483.04	25.68%	0.50%	0.42%	0.44%	29.07%	1.13			
		250	0.125					3	649.97	273.47	376.5	42.07%	0.53%	0.37%	0.44%	50.79%	1.21			
							5.5	649.97	379.77	270.2	58.43%	0.60%	0.21%	0.44%	79.95%	1.37				
30	300	250	0.125	10	40	30	60	3	49.84	17.33	32.51	34.77%	1.87%	0.18%	0.76%	84.97%	2.44	3991	1436	26.46%
31	300	300	0.125	5	40	30	60	3	54.59	1.2	53.39	2.20%	5.11%	0.30%	0.41%	27.61%	12.56	4500	271	5.68%
32	300	300	0.375	10	40	30	60	3	140.33	62.39	77.94	44.46%	1.21%	0.14%	0.62%	87.07%	1.96	3433	2159	38.60%
33	300	200	0.125	10	40	30	60	3	66.15	16.91	49.24	25.56%	2.65%	0.27%	0.88%	77.05%	3.01	4743	1110	18.96%

34	300	300	0.5	10	40	30	60	3	92.49	39.12	53.37	42.30%	1.45%	0.17%	0.71%	86.21%	2.04	3837	2107	35.45%
35	300	300	0.125	8	40	30	60	3	75.99	19.02	56.97	25.03%	2.39%	0.24%	0.78%	76.55%	3.06	4610	1262	21.49%
36	300	300	0.125	12	40	30	60	3	83.66	37.9	45.76	45.30%	1.57%	0.31%	0.88%	80.59%	1.78	3865	2043	34.57%
37	300	100	0.125	10	40	30	60	3	102.63	44.43	58.2	43.29%	0.53%	0.43%	0.47%	48.55%	1.12	3155	2852	47.48%
38	300	300	0.125	10	40	30	60	3	87.99	15.88	72.11	18.05%	2.18%	0.34%	0.67%	58.78%	3.26	4271	1240	22.50%
39	300	300	0.25	10	40	30	60	3	116.23	24.8	91.43	21.34%	1.50%	0.22%	0.50%	64.57%	3.03	3441	2428	41.37%

## Appendix B: TLF Data

Table B.1: TLF pilot plant raw data.

Notes		Ash			Ash Mineral			Carbon (%)			Carbon (Mineral Ash) (%)			Moisture (%)	Yield (%)	Combustible Recovery (%)	Organic Recovery (%)
		Feed	Product	Refuse	Feed	Product	Refuse	Feed	Product	Refuse	Feed	Product	Refuse				
With Phase separator	UCC TUF	56.10	2.52	71.02	60.03	2.70	75.99	43.90	97.48	28.98	39.97	97.30	24.01	1.3	21.78	48.4%	53.0%
		56.10	6.10	80.88	60.03	6.53	86.54	43.90	93.90	19.12	39.97	93.47	13.46	1.6	33.14	70.9%	77.5%
		56.10	0.63	62.48	60.03	0.67	66.85	43.90	99.37	37.52	39.97	99.33	33.15	0.4	10.32	23.3%	25.6%
Without Phase separator	UCC TUF	56.10	3.37	89.57	60.03	3.61	95.84	43.90	96.63	10.43	39.97	96.39	4.16	4.05	38.83	85.5%	93.6%
		56.10	2.76	85.53	60.03	2.95	91.52	43.90	97.24	14.47	39.97	97.05	8.48	2.5	35.56	78.8%	86.3%
		56.10	2.60	76.00	60.03	2.78	81.32	43.90	97.40	24.00	39.97	97.22	18.68	1.02	27.11	60.2%	65.9%
	Itmann TUF	49.41	1.10	91.51	52.87	1.18	97.92	50.59	98.90	8.49	47.13	98.82	2.08	3.1	46.57	91.0%	97.6%
		49.41	5.68	83.20	52.87	6.08	89.02	50.59	94.32	16.80	47.13	93.92	10.98	3.1	43.59	81.3%	86.9%
Phase Separator Installed		48.31	3.89	88.02	51.69	4.16	94.18	51.69	96.11	11.98	48.31	95.84	5.82	1.07	47.20	87.8%	93.6%
		48.31	3.64	83.92	51.69	3.89	89.79	51.69	96.36	16.08	48.31	96.11	10.21	1.7	44.36	82.7%	88.2%
		48.31	3.89	85.36	51.69	4.16	91.34	51.69	96.11	14.64	48.31	95.84	8.66	1.13	45.48	84.6%	90.2%
		48.31	2.98	87.11	51.69	3.19	93.21	51.69	97.02	12.89	48.31	96.81	6.79	1.49	46.12	86.6%	92.4%
		48.31	5.28	84.62	51.69	5.65	90.54	51.69	94.72	15.38	48.31	94.35	9.46	1.93	45.77	83.9%	89.4%
		47.40	4.96	88.60	50.72	5.31	94.80	52.60	95.04	11.40	49.28	94.69	5.20	11	49.26	89.0%	94.6%
		47.40	10.06	88.60	50.72	10.76	94.80	52.60	89.94	11.40	49.28	89.24	5.20	1.27	52.46	89.7%	95.0%
		47.40	8.13	88.63	50.72	8.70	94.83	52.60	91.87	11.37	49.28	91.30	5.17	1.92	51.22	89.5%	94.9%
		47.40	11.97	90.92	50.72	12.81	97.28	52.60	88.03	9.08	49.28	87.19	2.72	2.11	55.12	92.3%	97.5%
		47.40	4.97	91.71	50.72	5.32	98.13	52.60	95.03	8.29	49.28	94.68	1.87	-	51.08	92.3%	98.1%
0.2GPM solvent 0.4 GPM feed		47.40	3.73	93.73	50.72	3.99	100.29	52.60	96.27	6.27	49.28	96.01	-0.29	1.65	51.48	94.2%	100.3%

	Wellmore #8	58.87	6.73	88.92	62.99	7.20	95.14	41.13	93.27	11.08	37.01	92.80	4.86	-	36.56	82.9%	91.7%	
High Throughput 25% solids		58.87	3.16	78.10	62.99	3.38	83.57	41.13	96.84	21.90	37.01	96.62	16.43	-	25.66	60.4%	67.0%	
% solids																		
4.12		58.87	6.72	78.96	62.99	7.19	84.49	41.13	93.28	21.04	37.01	92.81	15.51	-	27.81	63.1%	69.7%	
7.03		58.87	2.44	78.74	62.99	2.61	84.25	41.13	97.56	21.26	37.01	97.39	15.75	-	26.04	61.8%	68.5%	
9.31		58.87	4.55	71.33	62.99	4.87	76.32	41.13	95.45	28.67	37.01	95.13	23.68	-	18.65	43.3%	48.0%	
12.31		58.87	12.33	68.27	62.99	13.19	73.05	41.13	87.67	31.73	37.01	86.81	26.95	-	16.80	35.8%	39.4%	
24.33		58.87	4.15	68.80	62.99	4.44	73.62	41.13	95.85	31.20	37.01	95.56	26.38	-	15.36	35.8%	39.7%	
25.35		58.87	4.59	82.59	62.99	4.91	88.37	41.13	95.41	17.41	37.01	95.09	11.63	-	30.41	70.5%	78.1%	
16.85		58.87	7.04	74.44	62.99	7.53	79.65	41.13	92.96	25.56	37.01	92.47	20.35	-	23.10	52.2%	57.7%	
11.45		58.87	16.60	74.49	62.99	17.76	79.70	41.13	83.40	25.51	37.01	82.24	20.30	-	26.98	54.7%	60.0%	
9.5		58.87	11.08	75.40	62.99	11.86	80.68	41.13	88.92	24.60	37.01	88.14	19.32	-	25.70	55.6%	61.2%	
With microbubbles		58.87	2.39	66.64	62.99	2.56	71.30	41.13	97.61	33.36	37.01	97.44	28.70	-	12.09	28.7%	31.8%	
		58.87	2.41	76.24	62.99	2.58	81.58	41.13	97.59	23.76	37.01	97.42	18.42	-	23.52	55.8%	61.9%	